Modelling Fischer Tropsch Synthesis in two-phase, continuous, well-mixed slurry reactors

By:

Bongani Mthombeni

Submitted in partial fulfillment of the requirements for the degree of
Master of Science in Engineering (Chemical)

August 2009

Process Modelling and Optimisation Research Group
Department of Chemical Engineering
University of Cape Town
Rondebosch, 7701
Republic of South Africa

Abstract

Fischer Tropsch Synthesis (FTS) is the conversion of syngas (CO and H_2) to cleaner liquid transportation fuels. The modelling of such a supercritical, highly non-ideal, multi-component system requires the detailed knowledge of the reaction mechanism, reaction kinetics, phase-equilibrium and reactor technology. The objectives of this work were to: develop a complete Fischer Tropsch model, predict the hydrocarbon product distribution, determine what effect Vapour-Liquid Equilibrium (VLE) has on the product distribution, selectivity and kinetics, and determine whether the deviations from the 'ideal' Anderson-Schulz Flory (ASF) distribution can be attributed to VLE.

Two models were developed for FTS in a well-mixed, continuous slurry reactor: a single-phase model and a two-phase model. In the two-phase model, a different approach to the conventional product distribution model was taken whereby the Fischer Tropsch model was developed by considering the phase equilibrium and reaction kinetics of the system simultaneously. The kinetic model was developed using elementary reaction steps for the olefins and paraffins based on the species' activities, a function of the species' partial molar fugacities. The fugacities were evaluated using the Peng-Robinson Equation of state (PREOS) with a modification to heavier hydrocarbons as done by Twu et al. (1995). At phase equilibrium, the fugacities are equal in both phases, making the kinetic model independent of the number of phases present in the system. For the single-phase model, the activity was considered as the ratio of the species partial pressure to the standard pressure.

The reactor is assumed to behave as an ideal, well-mixed, continuous flow reactor with no heat or mass transfer limitations. The purpose of this assumption is to assess only the influence of VLE without the complications of heat and mass transfer limitations. The cobalt catalyst at low temperature and pressure conditions (240°C and 20 bar) is used, allowing the water-gas-shift reaction to be neglected.

The dynamic, transient, continuous mass balances were written for all species and their intermediates, leading to a system of (7N+10) Differential Algebraic Equations (DAE's) for the two-phase system that considered VLE, and (5N+7) DAE's for the single-phase system that didn't consider VLE, where N is the maximum carbon number, $N = 60$. The initial conditions were obtained by equilibriating an equimolar mixture of syngas and water (at a mole fraction of 0.1 each), and an ASF distributed mixture of paraffins and olefins (at a chain-growth probability factor, $\alpha = 0.7$) in an isothermal flash calculation. The system's response to changes in operating conditions and kinetic rate constants was studied for both models.

The product distribution, selectivity, kinetics, ratio of olefin:paraffin reaction rates $\left(\frac{r_o}{r_p}\right)$ and steady state results of the two models were compared, where the operating conditions and kinetic parameters for both models were the same. The only difference between the two models was the formulation of the activity.

For the two-phase model, two different distributions were observed, corresponding to two different chain growth probability factors $\alpha_1 = 0.82$ and $\alpha_2 = 0.63$, in comparison to a single distribution in the single phase model with $\alpha = 0.62$. VLE increased the probability of forming longer hydrocarbon chains, as it caused a movement of hydrocarbon species from a predominantly vapour-rich phase to a predominantly liquid rich phase.

A higher methane selectivity than the rest of the hydrocarbons was observed for both models, where the C_1:C_2 molar ratio $\left(\frac{z_{C_1}}{z_{C_2}}\right)$ was higher in the single-phase model at 36.3, than the two-phase model, at 31.9. The combined kinetic and equilibrium effect increased the overall hydrocarbon selectivity in the two-phase model, compared to the single-phase model. This was observed by the higher mole fraction (z_i) in the two-phase model. VLE decreased the olefin:paraffin selectivity ratio $\left(\frac{z_{Ol_i}}{z_{Pn_i}}\right)$ due to the effect of the olefin:paraffin partial molar fugacity ratio.

VLE has a small (almost no) effect on the kinetics in the two phase model, with

$$\left(\frac{r_o}{r_p}\right)_{\text{single-phase}} \approx \left(\frac{r_o}{r_p}\right)_{\text{two-phase}}$$

This is because the kinetics are driven primarily by the activities of CO and H_2 ($\bar{a}_{CO}$ and $\bar{a}_{H_2}$) which are very similar at the operating conditions. The reason there's a deviation from the classical ASF distribution in the two-phase model, even though the kinetic models are similar, is due to a distortion factor, D, a function of the relative rates in the reactor, which differ as a result of VLE. The resulting Differential Algebraic Equations (DAE) systems for both models are significantly different, thus the product distributions are different. At steady state, the CO conversion for both models is 0.82, and it takes $\approx 870\times$ longer to reach steady state in the two-phase model than in the single-phase model. This is due to the slow dynamics of the liquid phase.

From varying the process conditions and catalyst loading, it was concluded that α is not solely dependent on CO conversion, but dependent on a combination of the process parameters (catalyst loading and pressure) and the kinetic parameters. In order to have a high CO conversion (X_{CO}), with a longer chain-growth probability factor (α), as in the event of maximising on wax yield, the system must operate at a high pressure $P \geq 20$bar with an increase in the CO adsorption and chain-growth reaction rate constants (k_1 and k_5 respectively). An increase in the chain-growth rate encourages the formation of longer chains. If it is desired to have a high X_{CO} and low α, as in the event of maximising on shorter-chain hydrocarbon yield, it is recommended that the catalyst loading (M_{cat}) and the hydrogen surface reaction constant be

increased k_2.

There are numerous studies that can be performed in this work. Both models are setup such that it is easy to observe the behaviour of the FTS system with modifications on the either process parameters, kinetic parameters or both. The model can be improved by fitting FTS plant data for the system to the model to determine the actual kinetic constants and apply the findings from this work for model optimisation. A statistical sensitivity analysis can be conducted to study the responses to combined kinetic parameter effects.

Acknowledgements

I would like to thank SASOL, for their continual support, financially and otherwise. Their belief in me and my abilities is greatly appreciated. Thank you to the Process Modelling and Optimisation Research Group and the Centre for Catalysis Research for constantly enriching my mind and interest in this line of work. Special thanks go to Eric van Steen, Michael Claeys and Jack Fletcher, for always giving me their technical input whenever I needed it (typically at the spur of the moment). Thank you also to Walter Böhringer for always having an open door.

I extend my most sincere appreciation and gratitude to my research associate and friend, Professor Klaus Möller. Klaus, thank you for your wisdom, quirkiness, guidance and unexplainable intelligence. Above all, thank you for understanding how important closing this chapter of my life was. You are my role model and you never cease to amaze me! Danke Klaus-Peter!!

I would then like to extend my gratitude to my immediate family: Mphahlele (Dada), Tshoniswa (Daisy), Bonisile (Kono) and Bathandile (Bathafly) Mthombeni, for their continual love and support. To my girls: I hope this work inspires you and urges you to do even more. The sky is NOT EVEN the limit. Thank you for being my joy and for bringing sunshine on the cloudy days. I love you both so much. To my parents: You've seen me through it all. Dada, thank you for being there to remind me that I am indeed ***BONGZ1***. Daisy, thank you for your gentleness, compassion, matchless loyalty and encouragement. I love you both immeasurably. Thank you also to my close friends and spiritual family. Special thanks go to Nydean Stamboul, Natalie Green, Pastor Michel Nlandu, Pastor Nic Kruyer, Rhona Kruyer, Tina George, Yudeshnee Perumal, and Oluwaseun Oyekola. You are the people that stand out to me the most. I thank you. To my late cousins, Sandile and Fezile Hlanganiso, I will always remember you and your wise words: 'O bale Bongi'. This goes out to you.

Lastly, but most certainly not least, I would like to giving all the praise, glory, honour and eternal gratitude to my Lord and Saviour, Jesus Christ, without Whom I would not have been able to achieve this and come this far in my life. You put me back together when I was broken, believed in me when I stopped believing in myself, and saw me through it all, right to the very end. I dedicate to You, my work, my soul, my heart and my life. **1 Chronicles 28:20 -** "'Be strong and of good courage and do it. Do not be afraid, nor be dismayed, for the Lord, your God will be with you. He will never leave you, nor forsake you. Until you have finished all the work, for the service of the house of the Lord." Khensani.

Contents

I Introduction and Literature Review **1**

1 Introduction **2**

1.1 Background to Fischer Tropsch Synthesis 2

1.1.1 Fischer Tropsch Reactions 2

1.1.2 Reactors and catalysts 3

1.2 Modelling in FTS 4

1.3 Research Objectives 6

2 Modelling FTS **7**

2.1 Kinetic modelling of FTS 7

2.1.1 Approach 1: Modelling the syngas consumption rates and product selectivity models 8

2.1.2 Approach 2: Detailed reaction kinetic models 14

2.1.3 Parameter estimation and optimisation 19

2.2 Modelling the Vapour-Liquid- Equilibrium (VLE) 20

2.2.1 Phase equilibrium theory 20

2.2.2 Modelling VLE in FTS 21

2.3 Reactor modelling 22

II Model Development and Numerical Simulation **23**

3 Model Development **24**

3.1 Introduction 24

3.2 The system 27

3.3 Modelling the VLE 29

3.4 Transient reactor model with VLE 29

3.5 Transient reactor model without VLE 31

3.6 Obtaining consistent initial conditions 32

3.7 Reaction scheme 33

3.8 Model parameters 35

4 Numerical Simulation **36**

III Results and Discussion 39

5 Results and Discussion 40

5.1 Start-up . . . 40
5.2 Model parameters . . . 41
5.3 Comparative model results . . . 42
5.3.1 Product distribution . . . 42
5.3.2 Selectivity . . . 44
5.3.3 Ratio of olefin reaction rate to paraffin reaction rate . . . 47
5.3.4 The difference in product distributions . . . 48
5.3.5 Steady state results . . . 51
5.3.6 Overall VLE effect: base case . . . 53
5.4 Profile sensitivity to process parameters . . . 54
5.4.1 Variation in catalyst loading . . . 54
5.4.2 Variation in pressure . . . 57
5.4.3 Relationship between α and conversion . . . 58
5.5 Profiles sensitivity to kinetic constants in the VLE model . . . 58
5.5.1 Effect of reaction rate constant k_1 on FTS product distribution . . . 58
5.5.2 Effect of reaction rate constant k_2 on FTS product distribution . . . 62
5.5.3 Effect of reaction rate constant k_3 on FTS product distribution . . . 64
5.5.4 Effect of reaction rate constant k_4 on FTS product distribution . . . 66
5.5.5 Effect of reaction rate constant k_5 on FTS product distribution . . . 68
5.5.6 Effect of reaction rate constant k_{6f} on FTS product distribution . . . 70
5.5.7 Effect of olefin reverse reaction rate constant k_{6r} on FTS product distribution . . . 72
5.5.8 Effect of paraffin reaction rate constant k_7 on FTS product distribution . 75
5.6 Overall parameter analysis . . . 77

6 Conclusions and Recommendations 80

6.1 Conclusions . . . 80
6.1.1 Developing the complete Fischer Tropsch models . . . 80
6.1.2 The effect of VLE on product distribution, selectivity and kinetics . . . 81
6.1.3 Effect of process parameters on FTS chain growth probability and conversion . . . 81
6.1.4 Effect of kinetic parameters on FTS chain growth probability and conversion 82
6.1.5 Relationship between α and conversion . . . 82
6.2 Recommendations . . . 83

A Correlation of critical values to higher carbon numbers 88

B Thermodynamic calculations **90**
B.0.1 Pure component thermodynamics 90
B.0.2 Mixture thermodynamics 92

C Reactor Initialisation and Start-up process models **96**
C.1 Initialisation 97
C.2 Isothermal Flash calculation 101

D Transient process models **104**
D.1 Transient two-phase model (with VLE) 104
D.2 Transient single-phase model (no VLE) 114

E Isothermal Flash results **121**

F Equilibrium *K-value* as a function of carbon number **125**

G Hydrocarbon liquid fraction at steady state **126**

List of Tables

1.1 Main Reactions in Fischer Tropsch Synthesis (van der Laan and Beenackers, 1999b) 3

3.1 Proposed Fischer Tropsch Reaction Mechanism and corresponding rate equations 34

5.1 Calculated values from Rachford-Rice Isothermal Flash calculation 41
5.2 Model variables for the single- and two- phase models 42
5.3 Kinetic rate constants corresponding to proposed mechanism 42
5.4 Comparison of α values and CO conversion (X_{CO}) from the two models 42
5.5 Variables to explain $\left(\frac{r_6}{r_7}\right)$ for the two models 47
5.6 Steady state results for both models 52
5.7 Conversion and alpha as a function of catalyst loading 54
5.8 Conversion and α as a function of pressure for the single-phase model 57
5.9 Conversion and α as a fuction of pressure for the two-phase model 58
5.10 Conversion and α as a function of k_1 59
5.11 Conversion and α as a function of k_2 62
5.12 Conversion and alpha as a function of k_3 65
5.13 Conversion and alpha as a function of k_4 67
5.14 Conversion and alpha as a function of k_5 68
5.15 Conversion and alpha as a function of k_{6f} 70
5.16 Conversion and alpha as a function of k_{6r} 72
5.17 Conversion and alpha as a function of k_7 75
5.18 Summary of the effects of increasing kinetic parameters 77

A.1 Correlated constants for critical pressure and accentric factor 88

G.1 Hydrocarbon liquid fraction (ψ) vs. of Carbon number C_N 126

List of Figures

2.1 A typical ASF distribution of FT products at $\alpha = 0.85$, (Vessia, 2002) 10
2.2 Scheme of the reaction network of the Olefin Readsorption Product Distribution Model ,van der Laan and Beenackers (1999b) 10
2.3 a. Classical Anderson-Schulz-Flory distribution os all products. b. Distribution graph with two different chain growth probabilities van der Laan and Beenackers (1999b) 12
2.4 Schematic diagram of experimentally observed trends in hydrocarbon selectivity plots, modified from Raje and Davis (1996) 12
2.5 a.Classical Anderson-Schulz-Flory distribution of all products. b.Classical distribution with abnormalities at C_1 and C_2 products, van der Laan and Beenackers (1999b) 13
2.6 Observed and postulated chemisorbed species during FTS (van der Laan and Beenackers, 1999b) 15
2.7 Carbide mechanism for the Fischer-Tropsch Synthesis, (van der Laan and Beenackers, 1999b) 16
2.8 Kinetic scheme of FTS, secondary hydrogenation reaction and WGS on Fe-Cu-K-SiO2 catalyst, adapted from Chang et al. (2007) 18

3.1 Relationship between reactor and kinetic models, adapted from Wang et al. (2004) 25
3.2 Proposed novell FTS model 26
3.3 Representation of the continuous flow system 27
3.4 Schematic diagram of a continuous, well-mixed, transient, slurry reactor used for model development 28

4.1 FTS block flow diagram of model development procedure 36

5.1 Initial hydrocarbon distribution fed into isothermal flash, at $\alpha = 0.7$ 40
5.2 Modified hydrocarbon distribution after satisfying the volume constraints. . . . 41
5.3 a. Hydrocarbon product distribution for single phase model, b. Hydrocarbon product distribution for two-phase model 43
5.4 Fraction of component i in the liquid phase as a function of carbon number . . . 44

5.5 Product distribution curve illustrating the equilibrium effect on hydrocarbon selectivity, single-phase ('Paraffins', 'Olefins'), two-phase ('Paraffins VLE', 'Olefins VLE') . . . 45
5.6 Identifying 2 regions in the hydrocarbon product distribution: two-phase model 46
5.7 Hydrocarbon surface species ($C_nH_{2n+1}\theta$) distribution for both models . . . 48
5.8 Olefin activities, $\bar{a}_{CnH2n}$, as a function of carbon number . . . 49
5.9 Hydrocarbon product distribution plots for single-phase and two-phase models for variations in catalyst mass . . . 54
5.10 α and X_{CO} as a function of the relative change in catalyst mass . . . 55
5.11 α as a function of pressure for both models . . . 57
5.12 α as a function of CO conversion with a variation in M_{cat} and pressure (P) . . . 59
5.13 Hydrocarbon product distribution for single-phase and two-phase models, with a variation in kinetic parameter k_1 . . . 61
5.14 Hydrocarbon product distribution for single-phase and two-phase models, with a variation in kinetic parameter k_2 . . . 63
5.15 Hydrocarbon product distribution for single-phase and two-phase models, with a variation in kinetic parameter k_3 . . . 64
5.16 Hydrocarbon product distribution for single-phase and two-phase models, with a variation in kinetic parameter k_4 . . . 66
5.17 Hydrocarbon product distribution for single-phase and two-phase models, with a variation in kinetic parameter k_5 . . . 69
5.18 Hydrocarbon product distribution for single-phase and two-phase models, with a variation in kinetic parameter k_{6f} . . . 71
5.19 Hydrocarbon product distribution for single-phase and two-phase models, with a variation in kinetic parameter k_{6r} . . . 74
5.20 Hydrocarbon product distribution for single-phase and two-phase models, with a variation in kinetic parameter k_7 . . . 76
5.21 α as a function of conversion for the 3 parameter groups for the single-phase model 78
5.22 α_1 as a function of conversion for the 3 parameter groups in the two-phase model 78
5.23 α_2 as a function of conversion for the 3 parameter groups in the two-phase model 79

A.1 Actual (×) and Correlated(–) corresponding states' values for paraffins . . . 89
A.2 Actual (×) and Correlated (–) corresponding states' values for olefins . . . 89

C.1 FTS block flow diagram of model development procedure . . . 96

F.1 *K-value* as a function of carbon number for the 2-phase model . . . 125

Nomenclature

α The chain-growth prabability factor

$\bar{a_i}$ Activity of species i

$\bar{f_i}(T, P, z)$ Partial molar fugacity of species i in a phase, Pa

$\bar{V}$ Molar volume, $[m^3 mol^{-1}]$

$\dot{f}_i^L$ The molar flowrate of species i flowing out in the liquid stream, $[mol.s^{-1}]$

$\dot{f}_i^V$ The molar flowrate of species i flowing out in the vapour stream, $[mol.s^{-1}]$

$\dot{F}^L$ Liquid Flow, $[mol.s^{-1}]$

$\dot{F}^V$ Vapour Flow, $[mol.s^{-1}]$

$\dot{f}_{i,in}$ The molar flowrate of species i flowing into the system, $[mol.s^{-1}]$

$\dot{F}_{in}$ Flow into the system, $[mol.s^{-1}]$

$\nu_{i,k}$ The stoichiometric coefficient of species i in reaction mechanistic step k

ω Accentric factor

ρ^L Liquid molar density, $[mol.m^{-3}]$

ρ^V Vapour molar density, $[mol.m^{-3}]$

ρ^L Liquid molar density,$[mol.m^{-3}]$

ρ^V Vapour molar density,$[mol.m^{-3}]$

θ_{j*} Fraction of catalyst site occupied by intermediate j

θ_v Fraction of vacant catalyst site

a Peng Robinson Equation of State parameter, a

b Peng Robinson Equation of State parameter, b

D ASF distortion factor

$f_i(T,P)$ Pure component fugacity of species i in a phase

K_i Phase distribution ratio, or K-value

M_{cat} Catalyst loading, $g.m^3$

N_0^F Total number of moles in the feed initially,$[mol]$

$N_{i,0}^F$ Number of moles of species i in the feed initially,$[mol]$

N_0^L Total number of moles in the liquid phase initially,$[mol]$

$N_{i,0}^L$ Number of moles of species i in the liquid phase initially,$[mol]$

N_0^V Total number of moles in the vapour phase initially,$[mol]$

$N_{i,0}^V$ Number of moles of species i in the vapour phase initially,$[mol]$

N^L Number of moles in the liquid phase, $[mol]$

N^V Number of moles in the vapour phase, $[mol]$

$Ni_{i,0}^L$ Initial number of moles in the liquid phase, mol

$Ni_{i,0}^V$ Initial number of moles in the vapour phase, mol

P Pressure, Pa

q_i Number of moles of species i, $[mol]$

q_j Number of moles of reaction intermediate j

R Ideal gas constant, $[J.(mol.K)^-1]$

R_p Rate of propagation

R_t Rate of termination

S_R Selectivity ratio

T Temperature, K

T_r Reduced Temperature, [K]

V Volume, $[m^3]$

V^L Liquid volume, $[m^3]$

V^V Vapour volume, $[m^3]$

x_i Liquid mole fraction of species i

$x_{i,0}$ Liquid mole fraction of species i initially

y_i Vapour mole fraction of species i

$y_{i,0}$ Vapour mole fraction of species i initially

Z Compressibility factor

z General mole fraction

Part I

Introduction and Literature Review

Chapter 1

Introduction

1.1 Background to Fischer Tropsch Synthesis

Fischer Tropsch Synthesis (FTS) is the catalysed polymerisation and conversion of syngas (carbon monoxide and hydrogen) to liquid transportation fuels and other valuable products. The fluctuating price of crude oil has increased the global demand for an alternative way to develop cleaner and less expensive fuels, and FTS has shown to be a lucrative alternative. The fuels produced from FTS are cleaner and of high performance and quality, due to their low aromaticity and lack of sulphur, (van der Laan and Beenackers, 1999b). In particular, considering the depleting coal reserves, FTS through Gas-to-Liquid technology (GTL) has shown to be a good alternative. In South Africa, Fischer Tropsch technology is used extensively by petrochemical companies SASOL and PETROSA.

The process modelling of FTS is significant to this industry, as it effectively predicts the hydrocarbon product selectivity by considering all possible factors. These factors include: the reaction mechanism, reaction kinetics, phase equilibrium, catalyst activity, mass transfer characteristics and reactor characteristics, just to name a few. It is through the modelling of such processes that industrial operations can be improved and optimised.

1.1.1 Fischer Tropsch Reactions

During FTS, reactants (CO and H_2) adsorb and dissociate at the catalyst surface, and react through a series of steps to form the methylene monomer (CH_2), chain initiator (CH_3) and water. The hydrocarbons are formed by CH_2 insertion into metal-alkyl bonds and subsequent dehydrogenation or hydrogenation to yield predominantly straight chain α-olefins or paraffins respectively (van der Laan and Beenackers, 1999b). The main chemical reactions that take place in FTS are summarized in Table 1.1, where n denotes the carbon number.

The resulting non-ideal, multicomponent mixture is made up of syngas, carbon dioxide, water and a wide range of hydrocarbons, including oxygenates and linear to branched paraffins and olefins. At industrial operating conditions, large water concentrations are present. The presence of water in the FT reaction mixture has been a matter of discussion for a long time, as

Table 1.1: Main Reactions in Fischer Tropsch Synthesis (van der Laan and Beenackers, 1999b)

Main Reactions			
1. Paraffins	$nCO + (2n+1)H_2$	$\rightarrow$	$C_nH_{2n+2} + nH_2O$
2. Olefins	$nCO + 2nH_2$	$\rightarrow$	$C_nH_{2n} + nH_2O$
3. Water Gas Shift	$CO + H_2O$	$\rightleftharpoons$	$CO_2 + H_2$
Side Reactions			
4. Alcohols	$nCO + 2nH_2$	$\rightarrow$	$C_nH_{2n+2}O + (n-1)H_2O$

it increases the non-ideality of the multi-component mixture, and affects the selectivity of C_{5+} hydrocarbons (Krishnamoorthy et al., 2002). At the operating conditions, phase equilibrium is unavoidable and needs to be considered. However, there has been debate whether the FT reactions are kinetically- or thermodynamically-controlled. The study of the effect of phase equilibrium on product selectivity and reactivity is rarely found in literature, and it is yet to be determined whether phase equilibrium influences the kinetics.

There are two modes of operation for FT:

- a high temperature (300-350°C) FT process (HTFT) with iron-based catalysts, predominantly used for the production of gasoline and linear low-molecular mass olefins, and
- a low temperature (200-240°C) FT process (LTFT) with either iron or cobalt catalysts, used for the production of high molecular mass linear waxes (Dry, 2002).

HTFT is significantly influenced by the water-gas shift (WGS) reaction. The H_2:CO ratio for HTFT has to be below 2, because an excess of CO is converted with water to form carbon dioxide and hydrogen, allowing for the H_2:CO ratio to increase to the stoichimetric requirements for FTS (van der Laan and Beenackers, 1999b). The LTFT process has insignificant WGS activity, and therefore the feedstock has to have a H_2:CO ratio of 2.

1.1.2 Reactors and catalysts

Many reactor configurations have been proposed since FTS was commercialised in the 1950's. Some of these reactors include fixed-bed reactors with gas recycle, slurry three-phase reactors and three-phased fluidized bed reactors. The preferred reactor type for the FTS of high molecular weight products is a slurry bubble column reactor, as it exhibits excellent heat transfer characteristics providing near isothermal operations (van der Laan and Beenackers, 1999b). In addition to the large number of products that are to be considered in FTS, another important aspect is the high heat of reaction. Near isothermal operation of the slurry reactor allows operation at higher average temperatures, resulting in higher conversions and product selectivity. Slurry reactor-types are also preferred due to the low pressure drop across the reactor and improved mass transfer due to smaller catalyst particles(Dry, 2002). For optimum FT product yield in slurry reactor systems, the reactor temperature is typically between 210°C and 240°C, and a pressure of 20bar (Withers et al., 1990).

Fischer Tropsch Synthesis is catalysed by cobalt, iron or ruthenium, with cobalt and iron being most extensively used. Cobalt-based catalysts have been successfully applied in the industrial processes due to their high FT activity and low selectivity for oxygenates, in comparison to their iron counterpart (Teng et al., 2007). Iron-based catalysts are less expensive than cobalt-based catalysts, which is an important economic factor. However, iron-based catalysts have a high selectivity for carbon-monoxide polymerisation in combination with the water gas shift reaction (WGS), increasing the complexity of the resulting mixture, for example, the measurable quantity of oxygenates and loss of catalyst activity. In slurry reactor systems, constant overall catalytic activity can be maintained through the addition of small amounts of catalyst, to compensate for catalyst attrition. In cobalt catalyst-based slurry reactor systems, the total oxygen-containing substances (alcohols, aldehydes, ketones, acids, etc.) do not amount to more than about 1 percent of the whole product range (Hall, 1949). It was suggested by Hall (1949) that these substances arise as the result of side reactions and play no part in the main reaction mechanism. Cobalt catalyst particles (having a mean average diameter of approximately 75μm (Visconti et al., 2007)) have the added advantage, in the slurry systems, of reducing intra-particular diffusion effects and the deposition of heavy product on the catalyst (Krishna and Sie, 2000). This, therefore, allows for the valid assumption that diffusion effects are negligible in this system.

1.2 Modelling in FTS

The modelling of such reaction systems needs to consider the multiphase behaviour, which has generally been ignored to date. The nature of the slurry system with small catalyst particles is that diffusion limitations are minimised. Thus, adsorption onto the active site occurs from the bulk liquid phase. The simplest rate model taking into account the multiphase nature comprises of an equilibrium across the gas-liquid phase, with adsorption on the surface of the catalyst particles. This will be the approach taken in this work.

The kinetics of FTS have been a matter of controversy for many years, with relatively few studies aimed at understanding and modelling the complete FT reaction mechanism. The complexity of the reaction and the large number of species in the system make it very difficult to develop reliable kinetic expressions. There have been many attempts to model Fischer Tropsch product distributions. Researchers are in agreement that FTS is a polymerisation reaction with a molar product yield that decreases exponentially with increasing chain length. Two approaches are generally taken in describing kinetics of the FTS reactions:

Approach 1: Rate laws are postulated, empirically or otherwise, for the conversion of the reactants, CO and H_2. Thereafter, the distribution of the polymerisation products are described by a product selectivity model (such as the Anderson-Schulz-Flory (ASF) distribution model).

Approach 2: A reaction mechanism is proposed considering all the mechanistic steps by which CO and H_2 are consumed, to form the FT reaction products. Afterwhich, kinetic expres-

sions are developed to mathematically determine the product formation (Visconti et al., 2007).

Numerous researchers have derived Langmuir-Hinshelwood-Hougen-Watson (LHHW) or Eley-Rideal type of rate expressions, based on partial pressures of species, for the reactant consumption and have proposed quantitative formulations to describe the product distribution of alcohols and of linear and branched paraffins and olefins (van der Laan and Beenackers, 1999b). Most kinetic studies in literature take *Approach 1* and assume the Anderson-Schulz-Flory (ASF) distribution to model the product selectivity. The effect of phase equilibrium on product selectivity, and the consideration of equilibrium in product selectivity model development is rarely studied in literature, yet it is often debated whether phase equilibrium influences the kinetics.

Some researchers have taken *Approach 2*, whereby kinetic equations were derived based on an elementary reaction mechanisms and the postulation of a rate determining step. The effect of phase equilibrium is rarely accounted for in the kinetic model development but rather in explaining the equilibrium state of the bulk fluid. The way in which the species behave across the two phases, as they are formed or consumed is not generally considered. Some models incorporate phase equilibrium as part of the reactor model. That is, the bulk effects (the flow patterns, phase equilibrium, solubility and diffusity) are incorporated in the reactor model development, and the kinetic model developed separately.

This research project proposes a different approach, whereby the thermodynamic and kinetic models are coupled and dependent on each other. This is done such by following kinetic *Approach 2*, whereby elementary reaction rate equations are developed for every mechanistic step. The reaction rate equations are written in terms of species' activities, a concentration-like measure of species' deviation from the standard state. Activity is defined as the ratio of the fugacity of a species in a mixture to the fugacity of that species at the standard pressure. Phase equilibrium requires the equality of the partial molar fugacities of a species i in both phases. By writing the reaction rate equations in terms of fugacities, the equilibrium criterion can be included in the kinetics. This is an important consideration due to the supercritical and non-ideal nature of the Fischer Tropsch system. This method is followed in order to integrate the kinetics and the thermodynamics, and to bridge the gap between the liquid and the vapour phases.

In this model development, it is assumed that the reactor behaves as an ideal well-mixed, two phase, continuous flow reactor with no heat or mass transfer limitations. The purpose of this assumption is to assess only the influence of VLE without the complications of heat and mass transfer limitations.

1.3 Research Objectives

This research project was motivated by the literature review, which demosntrated that there is a lack of an accurate and complete Fischer Tropsch model in slurry reactor systems, that integrates elementary kinetics, vapour-liquid equilibrium and reactor technology. On the basis of what other researchers had done, it was clear that generally too many assumptions were made in order to simplify the system, and consequently process relevant factors were neglected. This work was aimed at taking an integrated and fundamental approach more consistent with physical phenomena of the process, where every species (including reaction intermediates) was accounted for. The objectives of this work were to:

- develop a complete two-phase Fischer Tropsch model,
- predict the hydrocarbon product distribution,
- determine what effect Vapour-Liquid Equilibrium (VLE) has on the product distribution, selectivity and kinetics and
- determine whether the deviations from the "ideal" Anderson-Schulz Flory (ASF) distribution can be described by VLE.

By investigating the basic building blocks and the way in which the 'blocks' are mathematically related, a complete FT model is developed. The development of this model results in a broader understanding of what happens within a slurry phase reactor, predicts what parameters to change in order to optimise the system and determines the hydrocarbon product distribution and the effect equilibrium has on the distribution.

Chapter 2

Modelling Fischer Tropsch Synthesis: A Literature Review

2.1 Kinetic modelling of FTS

In modelling the kinetics of FTS, as mentioned in chapter 1, one of two approaches are generally taken in literature:

1. In the first approach, expressions are postulated to describe the reactant consumption rates, often empirically or through the derivation of Langmuir-Hinshelwood-Hougen-Watson (LHHW) or Eley- Rideal (ER) type of rate expressions. Thereafter, models are developed to describe the FT product selectivity. In most cases, product selectivities are described by the 'ideal' "Anderson-Schulz-Flory" (ASF) model, or an extended/modified form of the ASF model to account for deviations from the 'ideal' distribution. In the ASF model, the formation of hydrocarbon chains was assumed as a stepwise polymerisation process, and the chain growth probability, α, assumed independent of carbon number, (Yang et al., 2003). In product selectivity models, the hydrocarbon products are lumped according to the carbon number of hydrocarbon molecules. This method is theoretically justified, based on the assumption that the reaction products do not affect or participate in the monomer formation mechanism (Visconti et al., 2007).

2. In the second, a more realistic approach, models are developed on the basis of a proposed reaction mechanism. All the steps in which CO and H_2 are consumed to lead to the final products of FTS are accounted for. The kinetic expressions are typically developed by considering elementary surface reaction rate equations for each step in a proposed reaction mechanism. LHHW-type expressions have been developed for the rate expressions by many researchers, on the basis of a number of mechanistic assumptions.

2.1.1 Approach 1: Modelling the syngas consumption rates and product selectivity models

Syngas consumption rates

The rate of synthesis gas consumption only differs from the FT reaction rate, by the reaction stoichiometry, that is $R_{CO+H_2} = -R_{CO} - R_{H_2} = (2 + m/2n)\, R_{FT}$, where n is the average carbon number and m the average number of hydrogen atoms of the hydrocarbon products, (van der Laan and Beenackers, 1999b). Therefore, many researchers have postulated rate expressions for syngas consumption rates, in order to stoichiometrically relate them to overall FTS reaction rates. The rate of syngas consumption (or CO consumption) is typically correlated with the gas-phase concentrations of CO, hydrogen and/or water.

Most of these rate expressions are derived by taking the LHHW approach. van Steen and Schulz (1999) developed a model describing the rate of CO consumption in FTS by developing the rate equation considering a simplified mechanistic scheme, first order with respect to surface species, following a polymerisation principle. It was assumed that the formation of the monomer (chain starter) was the rate limiting step, and that all the reaction steps following the monomer formation were in equilibrium. The work followed a kinetically-controlled product distribution approach, on the basis of experimental observations. The work showed that the consumption rate of CO was given by equation 2.1.

$$r_{CO} = \frac{aP_{CO}\left(P_{H_2}\right)^{3/2}/P_{H_2O}}{\left[1 + bP_{CO}P_{H_2}/P_{H_2O}\right]^2} \tag{2.1}$$

Ledakowicz et al. (1985) proposed a syngas consumption rate law given by equation 2.2 which takes the CO_2 concentration into account. This is due to the chemisorption of water having a significant effect on the syngas rate, and the formation of CO_2 through the WGS reaction. Compared to iron, cobalt is much more resistant to oxidation by water vapour, implying that the adsorption of water is much weaker on cobalt. Most kinetic expressions over cobalt catalysts do not contain a water partial pressure term, (Dry, 1996).

$$-r_{CO+H_2} = 1.4 \times 10^{10} e^{-12407/T} \frac{C_{H_2}}{1 + 0.115\dfrac{C_{CO_2}}{C_{CO}}} \tag{2.2}$$

van der Laan et al. (1999) proposed equation 2.3 for the overall FT reaction rate,

$$r_{FT} = \frac{kP_{CO}P_{H_2}^{1/2}}{\left(1 + aP_{CO} + bP_{CO_2}\right)^2} \tag{2.3}$$

and Ahon et al. (2005) proposed equation 2.4 in terms of fugacities to take high pressure systems into account.

$$r_{FT} = \frac{k_{FT}\bar{f}_{CO}^{1/2}\bar{f}_{H_2}^{1/2}}{1 + c\bar{f}_{CO}^{1/2}d\bar{f}_{H_2}^{1/2}} \tag{2.4}$$

For the slurry phase system, the catalyst particles are very small. Since they are suspended in a large amount of wax, syngas consumption rate equations are assumed to be limited by the diffusion of the reactants from the gas bubbles through the wax, to the catalyst particles (Dry, 1996). Interestingly, a lot of these derived rate expressions simplify to the same or similar kinetic expressions, even though several different surface reactions may be assumed to be that rate limiting step, (Dry, 1996).

Product Selectivity Models

The best known product selectivity model was developed in the early years of FTS. This model is called the Anderson-Schultz-Flory (ASF) product distribution model, and it describes the entire product range by a single parameter, α, the probability of adding a carbon intermediate to a chain (van der Laan and Beenackers, 1999a). Models for the hydrocarbon selectivity of products obtained from FTS are usually based on the ASF distribution. This distribution, however, is only valid when there is a constant probability of chain growth.

The ASF distribution model was developed by assuming that the FT reaction is a polymerisation reaction, wherein C_1 monomer units are added stepwise to a growing hydrocarbon chain on the catalyst surface. The model defines the mole fraction, x_i, of a hydrocarbon possessing i carbon atoms by equation 2.5, which represents the stepwise addition of monomer to species $i-1$, (x_{i-1}), to form the next heavier species i, (x_i) with a probability of α_{i-1}.

$$x_i = \alpha_{i-1} x_{i-1} \tag{2.5}$$

α is defined by equation 2.6,

$$\alpha_i = \frac{R_{p,i}}{R_{p,i} + R_{t,i}} \tag{2.6}$$

where $R_{p,i}$ and $R_{t,i}$ are the first order rate of propagation and rate of termination of species i respectively (van der Laan and Beenackers, 1999b). In the case where α is a constant, the sequential application of equation 2.5 leads to equation 2.7, (Raje and Davis, 1996).

$$x_i = (1-\alpha)\alpha^{i-1} \tag{2.7}$$

According to equation 2.7, from plotting the logarithm of the hydrocarbons' mole fraction versus the carbon number, should yield a straight line with a slope given by α (see Figure 2.5a). A typical ASF distribution plot of hydrocarbon molar and mass fraction vs. carbon number is given in Figure 2.1, at an α value of 0.85. However, many researchers have shown that experimentally-obtained hydrocarbon selectivities deviate from those predicted from the ASF distribution model. Olefin readsorption is one of the possible reasons given for the deviations from the ASF product distribution model. These are known as Olefin Readsorption Product Distribution Models (ORPDM's) which combine olefin readsorption with chain growth and termination on the same catalytic site. A scheme of a possible reaction network demonstrating

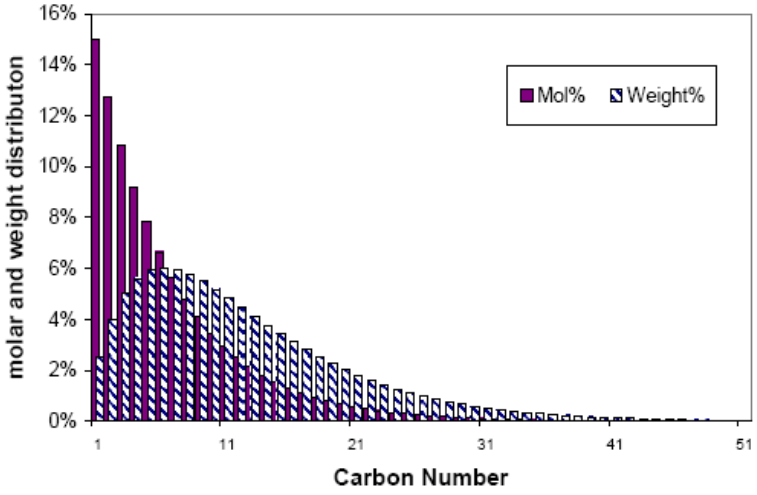

Figure 2.1: A typical ASF distribution of FT products at $\alpha = 0.85$, (Vessia, 2002)

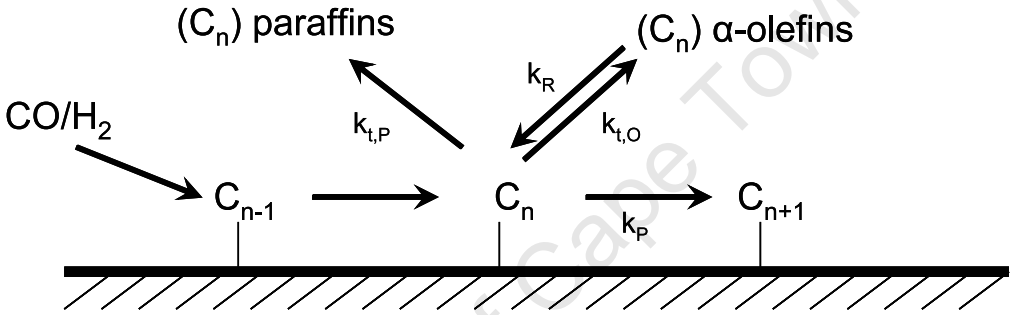

Figure 2.2: Scheme of the reaction network of the Olefin Readsorption Product Distribution Model ,van der Laan and Beenackers (1999b)

olefin readsorption is shown in Figure 2.2. $k_{t,P}$ and $k_{t,O}$ are the paraffin and olefin termination rate constants respectively, k_R the olefin readsorption constant and k_P the propagation rate constant. The olefin readsorption rate depends on the chain length due to increasing physisorption strength and increasing solubility in FT-wax with increasing chain length, (van der Laan and Beenackers, 1999b). On the basis of observed experimental trends, researchers have attempted to develop similar distribution models that take observed deviations from ideal distribution into account.

Schulz and Claeys (1999) proposed a model which was an extension of the 'ideal' ASF product selectivity model. The work obtained the hydrocarbon formation rates as functions of the probability of chain growth and desorption. The steady state model showed that the sum of the formation rates of all the organic compounds on a carbon basis, was equal to the rate of CO consumption. The model incorporated olefin readsorption (demonstrating how it can affect the product carbon number distribution), hydrogenation, isomerisation and chain-length dependent solubility in the liquid FT product. This was done on the basis of kinetic experiments, for a continuously operated and well-mixed slurry reactor. Vapour-Liquid-Equilibrium is included in the kinetic model development by assuming that the vapour and liquid streams leaving the CSTR are in thermodynamic equilibrium, and that their concentrations are related by a

carbon dependent partition coefficient K_N. The total liquid and vapour flows are included in the selectivity model development, but are not explicitly formulated.

Ahon et al. (2005) also developed a product selectivity model to describe the kinetics of the slurry reactor system. The model is a generalization of the steady-state model developed by Schulz and Claeys (1999), where the overall FT reaction rate was written as a function of the syngas fugacities, as shown in equation 2.4. The hydrocarbons were lumped according to the number of carbon atoms in their molecules, for the paraffin and 1-olefin families. This model incorporated 1-olefin readsorption with secondary reactions and the possible existence of two chain growth mechanisms (or sites) with different propagation possibilities. The reaction rates involving the surface species were assumed to be first order for both the Schulz and Claeys (1999) and the Ahon et al. (2005) models. In contrast to Schulz and Claeys (1999), Ahon et al. (2005) did not incorporate the gas and liquid flow rates in the selectivity model development, but rather in the transient reactor model development. In addition to that, Schulz and Claeys (1999) incorporated the VLE in the selectivity model, whereas Ahon et al. (2005) described the VLE in the reactor model, using an equation of state approach.

Anfray et al. (2007) developed a similar ORPDM for the same reactor system as Schulz and Claeys (1999) expressing the reaction rate expressions as functions of liquid concentrations. The CO consumption rates were taken from the works of van Steen and Schulz (1999) and Yates and Satterfield (1991). Anfray et al. (2007) further stated that CO consumption and hydrocarbon distribution are partially decoupled processes, considering the CO dissociation mechanism and the $CH_2\theta$ polymerisation mechanism as independent. The presence and role of water in the reactor is not addressed or incorporated in the model, which is unrealistic, as water is one of the most abundant products in the FT reactor.

However, even though these extended models paint a clearer picture of what happens in the complex FT environment, there are a number of over-simplifications in the model development, leaving room for discrepancy.

Deviations from ASF product distribution

As mentioned earlier, there have been observed deviations from ideal ASF product distribution. The observed deviations have been classified in four categories, namely: more than one α distribution, anomalies in C_1 and C_2 hydrocarbons, positive deviations from ASF distribution, and negative deviations from ASF distribution.

More than one α distribution: Experimental work conducted by many researchers has shown the prospects of more than one α value in FT product selectivity. The range of α is dependent on the process conditions and the catalyst type, (van der Laan and Beenackers, 1999b), and most product distributions show lines with varying slopes. A comparison of the classical ASF distrubution and that with two chain growth probabilities is shown in Figure 2.3. Figure 2.4 shows 3 different α values for an experimentally obtained hydrocarbon selectivity plot, for an FT slurry reactor. One chain growth probability is identified in region 1, α_1, as shown by the dashed line, as the slope wouldn't change, to give the

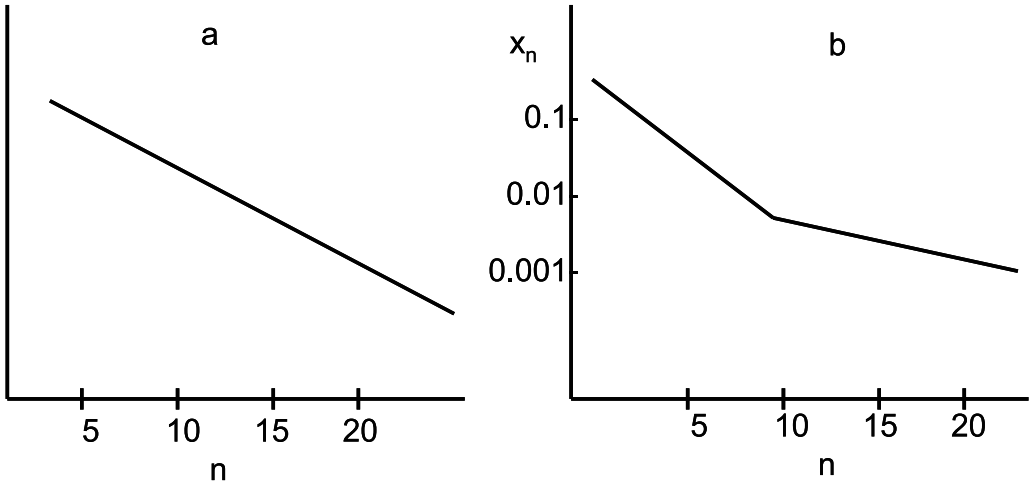

Figure 2.3: a. Classical Anderson-Schulz-Flory distribution os all products. b. Distribution graph with two different chain growth probabilities van der Laan and Beenackers (1999b)

classical ASF distribution. A smaller slope is identified in region 2, α_2, exhibited for hydrocarbons possessing 12-25 carbon atoms, (Raje and Davis, 1996). This is a so-called positive deviation from ASF distribution. As the slope decreases, the α value increases. If α increases (as in $\alpha_2 > \alpha_1$), the probability of forming heavy hydrocarbons is high. Thus, as the hydrocarbons get heavier, the chance of chain growth increases. What is observed in region 3 is a so-called negative deviation from ASF distribution, for hydrocarbons with carbon atoms exceeding 25, that is $\alpha_3 < \alpha_2$, due to an increased slope. This means that long chain formation is reduced.

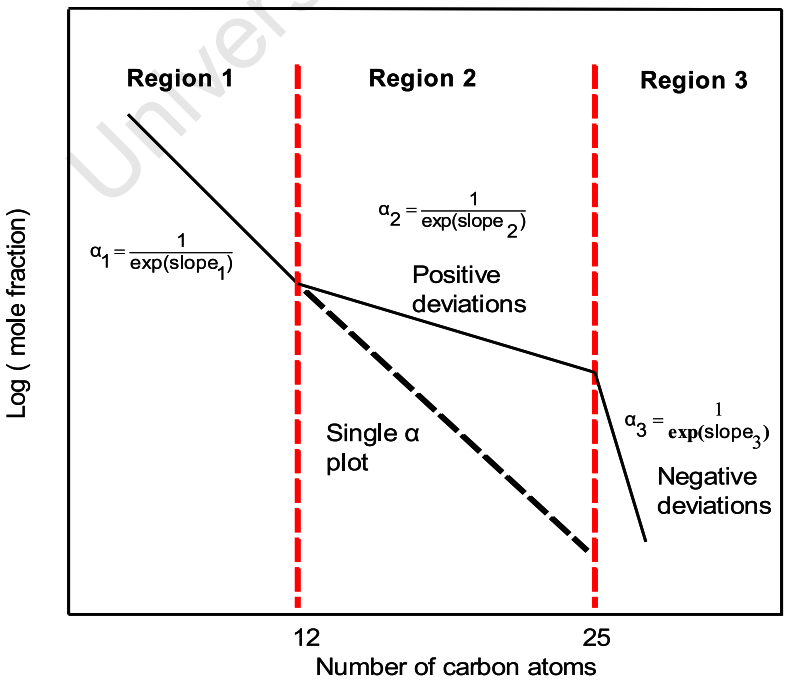

Figure 2.4: Schematic diagram of experimentally observed trends in hydrocarbon selectivity plots, modified from Raje and Davis (1996)

Donnelly et al. (1988) showed that a single-α product selectivity model was inadequate, as the deviations from the 'straight line' began to appear around C_{14}, where a potassium-promoted iron catalyst was shown to significantly influence the second chain growth probability. The presence of two chain growth probabilities is also emphasized in the work of Patzlaff et al. (1999), expanding on the model developed by Donnelly et al. (1988), for both cobalt and iron catalysts, where the mole fraction of species i would be determined by equation 2.8.

$$x_i = A\alpha_1^{i-1} + B\alpha_2^{i-1} \tag{2.8}$$

The determination of the probabilities α_1 and α_2 is based on hydrocarbons with carbon numbers $i > 2$, based on anomalies observed for C_1 and C_2 hydrocarbons.

Anomalies of C_1 and C_2 hydrocarbons: The usual deviations observed are a higher selectivity to methane, a relatively lower selectivity to ethane, and an increase in the chain growth probability with increasing molecular size in comparison to the ASF distribution (Yang et al., 2003). The fraction of methane does not obey the ASF equation due to several routes of formation, (Patzlaff et al., 1999). van der Laan and Beenackers (1999a) showed that the deviations of short-chain hydrocarbons from ideal ASF product distribution are accounted to the higher surface mobility or the reactivity of C_1 and C_2 precursors and rapid ethene readsorption. The C_1 and C_2 deviation is shown in Figure 2.5. According

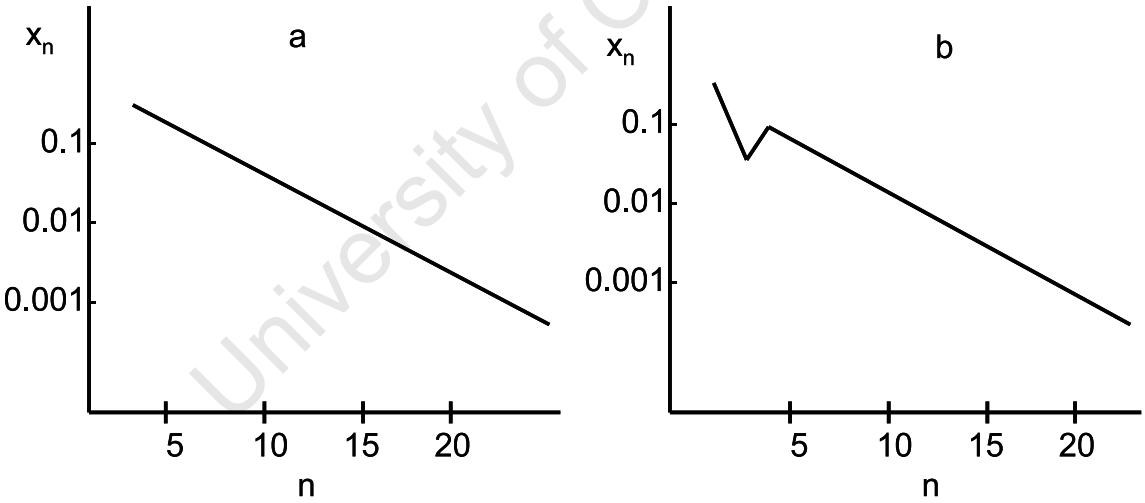

Figure 2.5: a.Classical Anderson-Schulz-Flory distribution of all products. b.Classical distribution with abnormalities at C_1 and C_2 products, van der Laan and Beenackers (1999b)

to Dry (1982) mass transfer limitations are possible reasons for high methane yield. The methane is usually more than predicted, particularly over Co and Ru catalysts. Puskas and Hurlbut (2003) attributed this to hydrogenolytic cleavage of the 1-olefins in secondary reactions.

Negative deviations from ASF distribution: As shown in Figure 2.4, negative deviations occur when the formation of long chains is reduced. It has been suggested by Dictor and Bell (1983) that this occurs due to the transient holdup of higher molecular weight

products in the oil phase surrounding the catalyst, in slurry reactor systems. Negative deviations have also been accounted to the cracking of higher molecular weight products by Puskas and Hurlbut (2003). Dictor and Bell (1983) proposed the reduction of negative deviations by the reduction of the oil volume surrounding the catalyst, and the increase of the syngas flowrate.

Positive deviations from ASF distribution: Positive deviations are identifiable by concave curvature in the ASF plots, or by a break in the C_{10} to C_{13} range, (Puskas and Hurlbut, 2003). These deviations have been firmly established and extensively studied in literature much more than other deviations. In positive deviations, it means that the formation of long-chain hydrocarbons is favoured. Raje and Davis (1996) observed positive deviations to Vapour Liquid Equilibrium (VLE) phenomena during catalyst deactivations, and to diffusion limitations or olefin readsorption. However, Zhan and Davis (2000) argued that as long as catalyst activity is maintained constant, deviations from ASF distibution could not be accounted for by the accumulation of products and/or VLE behaviour, without the consideration of olefin products' reactivity.

It is evident that the ASF distribution does not accurately model the FT product distribution, and evidently there are postulated models that try and take these deviations into account. However, these models are based on simplifications and assumptions. Even so, the reasons behind these deviations is a matter of controversy. These factors suggest that product selectivity models are not a viable approach for modelling Fischer Tropsch Synthesis kinetics accurately.

2.1.2 Approach 2: Detailed reaction kinetic models

Detailed reaction kinetic models are developed on the basis of a proposed reaction mechanism, whereby elementary reaction rate equations are written for every mechanistic step. Seeing that the development of the kinetics rate expressions is so dependent on the proposed mechanism, this is the first thing to look into.

Fischer Tropsch mechanisms

The mechanistic details of FTS have been a matter of controversy for many years, with the common agreement being the stepwise addition of single carbon monomers, ($CH_2\theta$, where θ is the catalyst site) (Ahon et al., 2005). The process is chain-building, where the hydrocarbon chain either gains length by adsorbing another alkyl-surface species group, or terminates and leaves the catalyst as either a paraffin or an olefin, through the addition or removal of a hydrogen intermediate respectively. The FTS polymerisation reaction mechanism has the following steps:

- Reactant adsorption and formation of surface species by dissociation,
- Chain initiation (that is formation of $CH_2\theta$ and $CH_3\theta$),
- Chain growth (the addition of $CH_2\theta$ to C_nH_{2n+1}, for n = 1 to N-1),

- Chain termination,
- Product desorption, and
- Readsorption and further reaction (van der Laan and Beenackers, 1999b)

There have been many mechanisms proposed in literature trying to explain the distribution of products from different viewpoints. Lox and Froment (1993) proposed a detailed mechanistic kinetic model which included traditional syngas consumption information and detailed product distribution information. With reference to Figure 2.6, an overview of observed and postulated species on the catalyst surface during FTS is given. Reactants in the mechanisms are shown

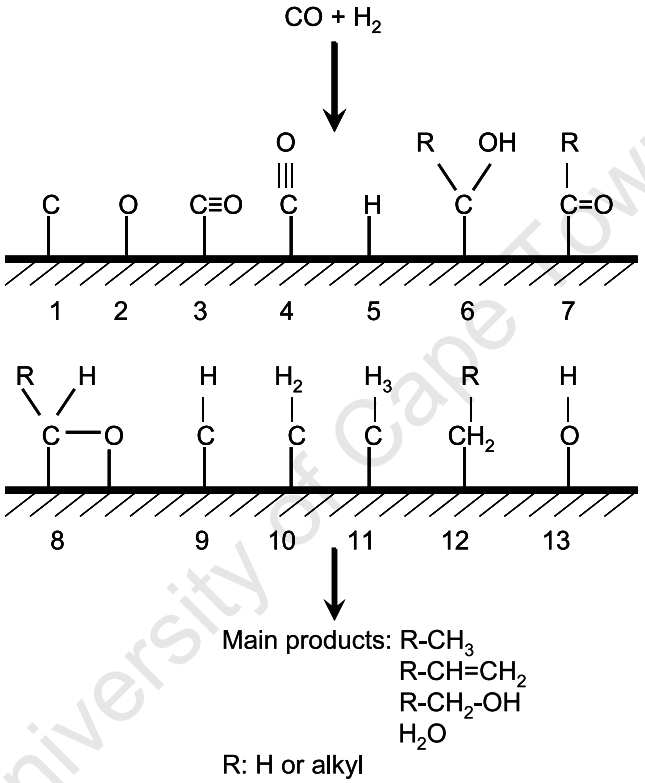

Figure 2.6: Observed and postulated chemisorbed species during FTS (van der Laan and Beenackers, 1999b)

by species **1,2,3,4,5**, oxygen-containing intermediate species by **6,7,8** and the hydrocarbon intermediates by **9,10,11,12**. Several compounds are possible monomers for chain growth to occur in Fischer Tropsch Synthesis. In proposing mechanistic steps for FTS, single-site mechanisms, and mechanisms involving two or more sites have been reported.

Single-site mechanisms: The carbide mechanism by CH_2 insertion is the most plausible mechanism for the formation of hydrocarbons on ruthenium, cobalt and iron (van der Laan and Beenackers, 1999b). With reference to Figures 2.6 and 2.7, the initiation, growth and termination of the chains according to this mechanism are presented. As observed, CO and H_2 are shown to adsorb dissociatively, forming several species such as CH (species **9**), CH_2 (**10**) , which is the monomer in the mechanism, and CH_3 (**11**). There is still

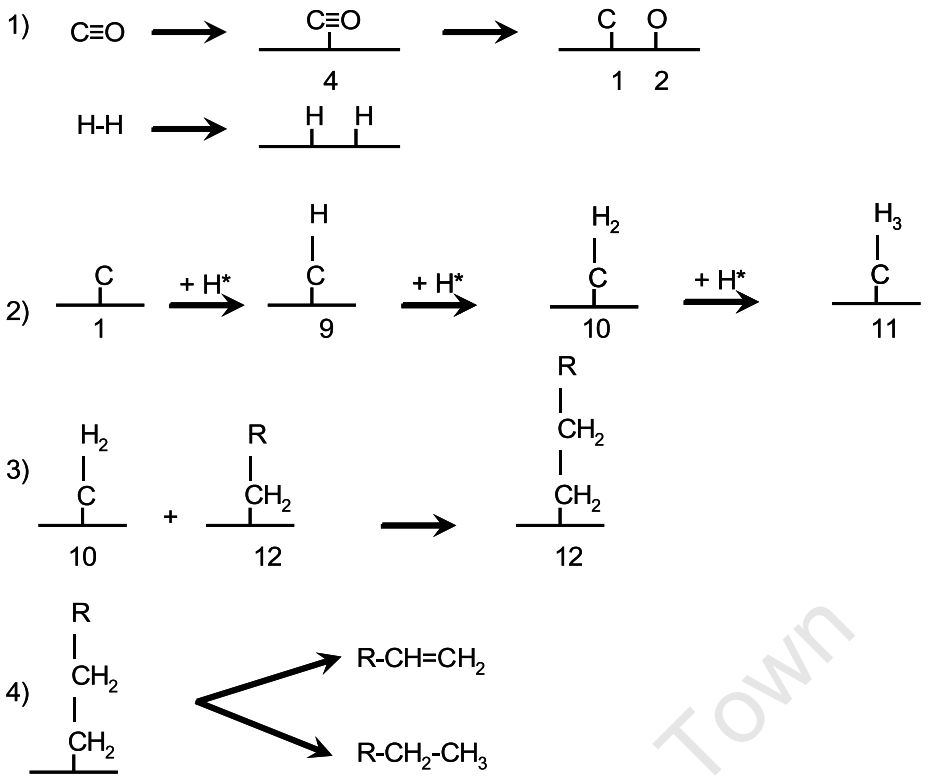

Figure 2.7: Carbide mechanism for the Fischer-Tropsch Synthesis, (van der Laan and Beenackers, 1999b)

controversy about the chain-growth mechanism in FTS, but the alkyl-insertion mechanism is the most widely used. Chain growth occurs by the insertion of the methylene molecule (CH_2) on a growing alkyl species. Termination can take place by the dehydrogenation of the alkyl species to the formation of an olefin, or the hydrogenation of the alkyl species (or the addition of CH_3) to form a paraffin (van der Laan and Beenackers, 1999b).

There is another mechanism which assumes that chain growth is initiated by the adsorption of CO on the active sites already containing a hydrocarbon intermediate, and then by a sequence of hydrogenation, (Yang et al., 2003). Yang et al. (2003) investigated various single-site mechanisms for FTS in order to see which mechanism produced rates which could be fitted accurately to experimental data. The most accurate mechanism, which yielded the least Mean Absolute Relative Residual (MARR) was identical to that proposed by van der Laan and Beenackers (1999b). Visconti et al. (2007) proposed an alkyl-insertion mechanism (similar to that by van der Laan and Beenackers (1999b)) with the reaction steps leading to the formation of methylene species (CH_2) and water assumed to occur very fast. Water was assumed to form via two consecutive steps involving the reaction between surface oxygen($O\theta$) and surface hydrogen (θ), and thereafter a reaction between $OH\theta$ and $H\theta$. An overall rate for the 'initiation' steps leading to the formation of $CH_2\theta$ was described by the CO adsorption reaction.

The work of Lozano-Blanco et al. (2008) is an example of a single-site mechanism that classifies the different pathways by which alkanes and alkenes can be formed in terms of

reaction families. The initiation steps, for the formation of methylene are identical to that proposed by van der Laan and Beenackers (1999b), Yang et al. (2003) and Visconti et al. (2007). This shows uniformity in literature with respect to the initiation steps of FTS.

Mechanisms involving two or more catalytic sites: The models proposed by Zimmerman et al. (1992) and Schulz and Claeys (1999) assumed that there were two different types of catalyst sites existing on the catalyst, one for the formation of primary products (including n-paraffns and 1-olefins) and the other site for the formation of olefins formed via secondary reactions. Secondary reactions occured when primary products desorbed from a site and interacted with another catalytic site before leaving the reactor. These secondary reactions can influence the type and molecular weight of the hydrocarbon products (van der Laan and Beenackers, 1999b), and result in an increase in the net chain growth probability (Kuipers et al., 1996). Bukur et al. (2005) proposed a dual-site mechanism, one site for FTS and another for the WGS reaction. Chang et al. (2007) also proposed a mechanism with three different catalytic sites, for modelling FT over iron catalyst in a slurry reactor. This was chosen on the basis of three kinds of reactions occuring in FTS, namely:

1. The formation of primary hydrocarbons (assumed to take place on active site θ),
2. Secondary reactions of primary 1-olefins (taking place on active site σ), and
3. The WGS reaction (taking place on active site ψ)

This proposed mechanism is shown in Figure 2.8, whereby the primary olefins are considered to be able to readsorb on the catalyst surface, and then re-enter the reaction chains on site θ. Chang et al. (2007) proposed 6 different mechanistic possibilities for reactions on the θ sites, a mechanistic possibility for the secondary hydrogenation reactions (on the σ sites) and two mechanistic possibilities for the WGS shift reaction on the ψ sites. The best combination of reaction mechanisms was determined by the combination that resulted in the least mean absolute relative residual (MARR), when fitting the data to the proposed model.

Deriving the reaction rate equations

Elementary reaction rates can be represented in their simplest form as:

$$\text{rate} \propto \text{f(T)}(\text{concentration})^n$$

where n is the order of the reaction. A power law expression is also sometimes used for explaining the rate of a reaction, due to its simplicity and its property that it frequently fits the data rather easily, (Berger et al., 2001). The concentration-measure in the reaction rates is typically in the form of vapour-phase partial pressures, liquid-phase concentrations or mole fractions.

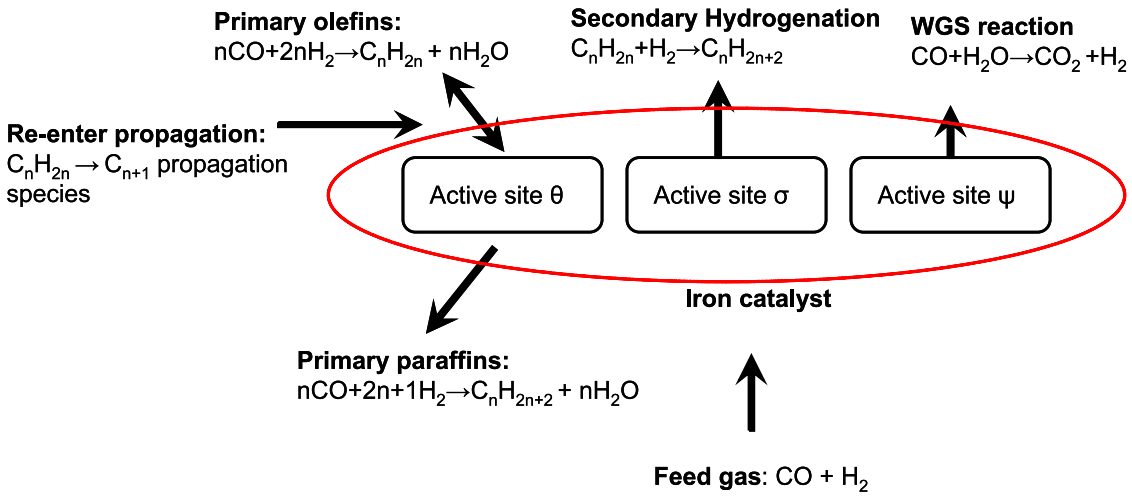

Figure 2.8: Kinetic scheme of FTS, secondary hydrogenation reaction and WGS on Fe-Cu-K-SiO2 catalyst, adapted from Chang et al. (2007)

Visconti et al. (2007) expressed elementary reaction rate equations for every step in the proposed mechanism, except for a power law expression for the hydrogen adsorption reaction, which was based on experimental observations. The reaction rates were a function of the liquid-phase concentrations, with the syngas surface reaction rates as a function of the CO and H_2 partial pressures.

A number of researchers take the Langmuir-Hinshelwood-Hougen-Watson (LHHW) approach in deriving kinetic expressions, for example in the works of Bukur et al. (2005), Yang et al. (2003), Chang et al. (2007) and Lox and Froment (1993). Once the reaction mechanism is proposed, elementary rate equations are written for the individual steps, typically assuming the steps are reversible or in quasi-equilibrium. The rate limiting step(s) (that is, the slowest step(s) in the product formation in FTS) is (are) assumed in the mechanistic schemes and the steps that are not rate limiting are used to eliminate all coverage-dependent terms, (Fogler, 1999). In this approach, it is assumed that there are uniformly energetic adsorption sites and that mono-layer coverage occurs. This model makes assumptions about desorption and adsorption on the catalyst surface, assuming that the species adsorb before reaction occurs on the surface, yielding a kinetic expression of the form:

$$\text{rate} \propto \frac{(\text{kinetic factor})(\text{driving force})}{(\text{adsorption term})^n}$$

Chang et al. (2007) and Bukur et al. (2005) took the LHHW approach to derive the FT rate equations. Bukur et al. (2005) used the kinetic model developed by Lox and Froment (1993) where two rate determining steps were assumed: the adsorption of CO (onto a site occupied by a hydrocarbon intermediate) and the desorption of paraffins and olefins respectively. The reaction rates were expressed in terms of liquid concentrations. Chang et al. (2007) assumed that the propagation step was rate limiting and expressed the rates as a function of both liquid concentrations and vapour partial pressures, related by a carbon-number dependent Henry's constant.

Lozano-Blanco et al. (2008) developed a single-event microkinetic (SEMK) model for FTS, by constructing a reaction network in terms of elementary steps, by means of an algorithm. SEMK models use a limited number of adjustable kinetic parameters and still preserve the fundamental nature of the FT model. These models separate the symmetry aspects of the kinetic coefficients, leading to a single-event kinetic coefficient, unique to a particular reaction family, where a reaction family is a proposed chain growth pathway.

Expressing the overall FTS reaction rate as a function of species fugacities was observed in the work of Ahon et al. (2005), so as to allow usage at high pressures. This, however was not applied to a detailed mechanistic approach. The kinetic model developed by Yang et al. (2003) also expressed the reaction rates in terms of partial molar fugacities, taking the LHHW approach to derive the kinetic expressions. By using fugacities as a variable in determining the reaction rate, the kinetics and the VLE can be integrated, thereby bridging the gap between the liquid and the vapour phases.

2.1.3 Parameter estimation and optimisation

The parameters in kinetic models are usually obtained by fitting experimental data to the proposed models, and applying regression techniques to solve for the unknown kinetic variables. This is typically done by optimising an objective function by minimising the sum of the squares of the residuals. van der Laan and Beenackers (1999b) uses the Levenberg-Marquardt method to minimise a function given by:

$$S = \sum \frac{(x_i^{\text{exp}} - x_i^{\text{mod}})^2}{\sigma^2} \tag{2.9}$$

where σ is the relative variance of the experimental data point and x_i^{exp} and x_i^{mod} are the experimental and model value of the selectivity or the reaction rate respectively. The accuracy of the fitted model relative to the experimental data was obtained from the Mean Absolute Relative Residual (MARR) function,

$$MARR = \sum \left| \frac{x_i^{\text{exp}} - x_i^{\text{mod}}}{x_i^{\text{exp}}} \right| \frac{1}{n} \times 100 \tag{2.10}$$

where n is the total number of optimised data points, (van der Laan and Beenackers, 1999b). Bukur et al. (2005) estimated parameters by optimising an objective function similar to equation 2.9, that also considered an error covariance matrix. The common assumption that is made concerning the specific reaction rate constants in the FTS mechanism, is that they are not carbon number dependent, thereby reducing the number of kinetic parameters to solve for.

2.2 Modelling the Vapour-Liquid- Equilibrium (VLE)

The thermodynamic understanding of this multi-component FT system relies on the extension from binary mixing data to multicomponent mixing data through the application of mixing rules. The accuracy of the results depend on the pure component properties and on the thermodynamic model that is chosen to describe the behaviour of each phase. What has been observed in literature is the independent development of a thermodynamic model to describe the resulting mixture phase behaviour.

2.2.1 Phase equilibrium theory

There are two methods that exist in order to determine or compute fluid phase equilibria, namely:

The application of different models to each phase: In this method, the Liquid-phase partial molar fugacities are calculated from a reference state characterised by the pure component in the same conditions of physical state, temperature and pressure. Ideal laws are corrected by using a Gibbs free energy model or an activity coefficients model such as NRTL, UNIQUAC or UNIFAC. Vapour-phase fugacities are calculated using an equation of state (EOS) such as the Peng Robinson EOS or the Soave-Redlich-Kwong EOS, depending on the system. This method is commonly referred to as the gamma-phi method ($\gamma - \phi$), where γ indicates that an activity coefficient method is used for the liquid-phase, and ϕ indicates that an EOS is used to compute for the vapour-phase fugacity coefficient (Orbey and Sandler, 1997). The two-phase FT system that is investigated here exhibits strong non-idealities, greater than that describable by regular solution theory, which has traditionally described the liquid by an activity coefficient model and the vapour phase by an EOS. These methods are called heterogenous methods and are used in order to represent the heterogeneity of the system. It has been shown by Twu and Coon (2000a) that the use of an activity coefficient model for the liquid phase and an EOS for the vapour phase is very inaccurate near and above the critical conditions. It is therefore not applicable to the FT reaction system.

The application of the same model to each phase: This method involves applying the same model, typically an EOS, to both liquid and vapour phases, commonly known as the phi-phi method ($\phi - \phi$). This is done to allow continuity at the critical point. Equations of State and the relations between pressure, molar volume and absolute temperature, have played a central role in the thermodynamic modelling of the VLE of hydrocarbon fluids, especially at high and moderate temperatures (Orbey and Sandler, 1997). This homogenous method is typically used for moderate to high pressure systems (Ahon et al., 2005), typical of FTS systems.

The starting point and criterion for equilibrium in a closed, isothermal and isobaric system, involves the minimisation of the Gibbs free energy. The condition which has to be satisfied

to have equilibrium, is for the partial molar fugacity of component i in phase I, at the system temperature T and a pressure P, to be equal to that in phase II, as shown in equation 2.11. In this case, the two phases are the Liquid phase (L) and the Vapour phase (V).

$$\bar{f}_i^V(y_i, T, P) = \bar{f}_i^L(x_i, T, P) \tag{2.11}$$

Equation 2.11 can be expanded to:

$$y_i \bar{\phi}_i^{\,V}(y_i, T, P) = x_i \bar{\phi}_i^{\,L}(x_i, T, P) \tag{2.12}$$

$$y_i = \frac{\bar{\phi}_i^{\,L}}{\bar{\phi}_i^{\,V}} \cdot x_i = K_i x_i \tag{2.13}$$

This gives the relationship between the vapour and liquid compositions of a species i, across both phases, as a function of the species' partial molar fugacity coefficients in each phase (Smith et al., 2001), and consequently the so-called *K-value*, (K_i). The calculation of the partial molar fugacity coefficients is given in Appendix B.

2.2.2 Modelling VLE in FTS

It is rare to find the simultaneous consideration of an equilibrium model with a kinetic model. In the work of Visconti et al. (2007), the liquid-phase concentrations that were used in the kinetic model were obtained from an external VLE calculation using the Soave-Redlich-Kwong equation of state (SRK-EOS). Ahon et al. (2005) also took an equation of state approach, in developing the phase equilibrium considering Van der Waal's mixing rules and the SRK-EOS. The Van der Waals' mixing rules are inadequate to describe the mixture properties of this system. Mixing rules are explained in Appendix B.

Chang et al. (2007) described the relation between the olefinic partial pressure and the concentration at the catalyst surface by a carbon number dependent Henry's constant. Schulz and Claeys (1999) also based the solubilities in the product selectivity model on Henry's law, equation 2.14.

$$p_N = \gamma_N \cdot x_N \cdot p_N^{sat} \tag{2.14}$$

Wang et al. (2004) calculated the Henry's coefficients through extrapolation using saturated vapour pressures of pure components and Dictor and Bell (1983) assumed that VLE was established instantaneously, with the distribution was represented by the Henry's law constant. The problem with these approaches is that Henry's law is only valid for highly diluted solutions, which is not a true representation of the FTS system. In addition to that, it has been established in literature, (see section 2.2.1) that the activity coefficient model is inadequate to describe the phase equilibrium in FTS systems.

2.3 Reactor modelling

The reactor system of choice is a well-mixed, continous slurry reactor, and there has been a lot of experimental work carried out in this reactor type, shown in the works of van Steen and Schulz (1999), Schulz and Claeys (1999), Ledakowicz et al. (1985), Dictor and Bell (1983) and Ahon et al. (2005) just to name a few. This is because the continuously operated slurry reactor is best suited to study hydrocarbon product selectivites in FTS, (Patzlaff et al., 1999). When it comes to modelling these reactor types, the common assumptions made are that:

1. the gas and liquid phases are perfectly mixed, due to turbulence caused by the impeller,
2. the catalyst particles are uniformly distributed in the reactor,
3. reactions only take place in the liquid phase,
4. the reactor is operated isobarically and isothermally, and
5. diffusion limitations in the catalyst pores are negligible. (Wang et al. (2004); Ahon et al. (2005)).

From the literature review it is clear that the FTS system is extremely complex. There is strong coupling between the two phases and any modelling of this reaction system needs to address this. Although considerable experimental work has been carried out for more than 50 years, attempts to model the system have mainly focused on interpretations based on the ASF distribution. More recently, authors have tried to address a more complete multi-phase model. However, these models are not yet fully developed and there is the need for a complete reactor model. This research addresses these issues.

Part II

Model Development and Numerical Simulation

Chapter 3

Model Development

3.1 Introduction:A novel complete Fischer Tropsch Synthesis model

In modelling FTS from the viewpoint of chemical reaction engineering, researchers take the approach of considering the bulk effects of the system (that is eg. solubility, diffusivity, equilibrium) in the reactor model, and the reaction details intrinsically in the kinetic model, shown in the works of Ahon et al. (2005), Visconti et al. (2007) and Wang et al. (2004). This idea is illustrated in Figure 3.1. The development of the novell FTS model considers all effects simultaneously. That is, the kinetic and the thermodynamic models are coupled, within the transient reactor model developed, as shown in Figure 3.2.

Modelling the kinetics

From the literature review, it is without a doubt that the most accurate way of modelling the kinetics of FTS is the detailed mechanistic approach. Product selectivity models assume that all product species form in parallel, and the selectivity is independent of conversion. The FT reactions are best represented by a series-parallel scheme, in which case, the selectivity depends on the relative concentration of the intermediates, which cannot be accounted for by the ASF distribution. Therefore, a model of this type cannot be used to study the influence of the phase equilibrium on reactivity and selectivity. However, a lot of important considerations can be taken from product selectivity models. This work does not agree with the simplification of first order kinetics for the surface reactions, nor does it agree with the assumption of steady state kinetic model development. The reaction rates themselves change with time, as the concentrations of all the species, including reaction intermediates, change with time, until such time that steady state is reached. These lumped consumption kinetic models are not able to describe the whole FTS reaction performance, (Chang et al., 2007).

In as much as the detailed mechanistic approach is the most accurate way in describing what happens within the FT reactor, there are a lot of considerations to take in proposing an accurate mechanism. A single-site mechanism modified from van der Laan and Beenackers

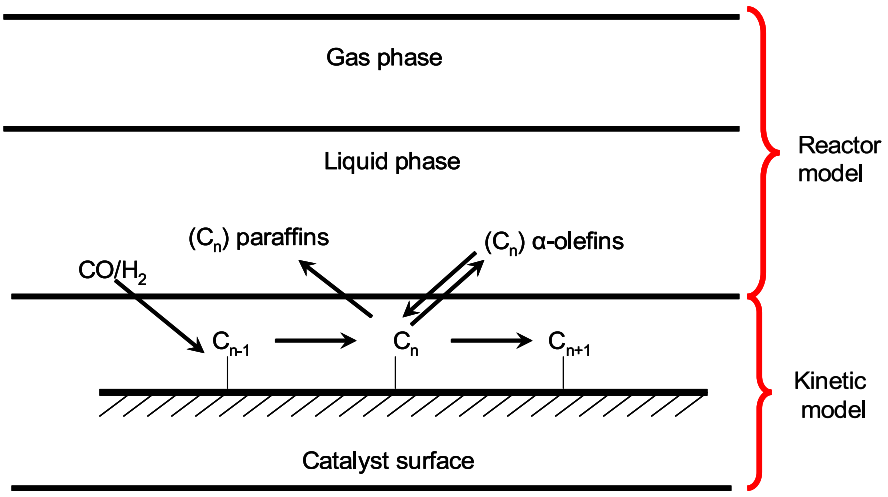

Figure 3.1: Relationship between reactor and kinetic models, adapted from Wang et al. (2004)

(1999b) is proposed. There is no need to propose another type of catalyst site for other reactions. For the cobalt-catalysed FTS, as for this reactor system, the WGS reaction is negligible. A fundamental approach is taken where what adsorbs onto a catalyst site is available for surface reaction. Olefin readsorption is taken into account by considering the olefin formation reaction as reversible, with all the other reaction steps as irreversible. A modification to van der Laan and Beenackers (1999b)'s mechanism is the agreement with the assumption made by Visconti et al. (2007), to have a net reaction rate for the initiation steps of FTS, limited to the CO adsorption rate. This is further elaborated on in chapter 3.

The concentration measure that is rarely used in literature, which is employed in this work, is that of species' activities, $\bar{a_i}$. Activity is a concentration-like measure of a species' deviation from the standard state, (Elliot and Lira, 1999). It is defined as the ratio of the partial molar fugacity of a species i in a mixture, to the fugacity of that pure species at the standard pressure, (Sandler, 1999). This is given in equation 3.1, where $\bar{f_i}(T, P, z)$ is the partial molar fugacity of species i in a phase and $f_i(T, P = 1bar)$ is the pure component fugacity at temperate T, and at pressure P= 1bar, (Elliot and Lira, 1999).

$$\bar{a_i} = \frac{\bar{f_i}(T, P, z)}{f_i(T, P = 1bar)} \tag{3.1}$$

It is believed that the development of the elementary reaction rates as functions of the species activities' is the most accurate way in directly incorporating the effect of Vapour-Liquid Equilibrium into the reaction kinetics. This work does not agree with considering the equilibrium as a separate entity to the kinetics. This is the most feasible way in which to settle the controversy of whether FTS is influenced by phase equilibrium.

Modelling the VLE

This work agrees with the incorporation of the VLE in the kinetic model, so as to include the equilibrium effect in the reaction kinetics, introduced in the work of Schulz and Claeys (1999),

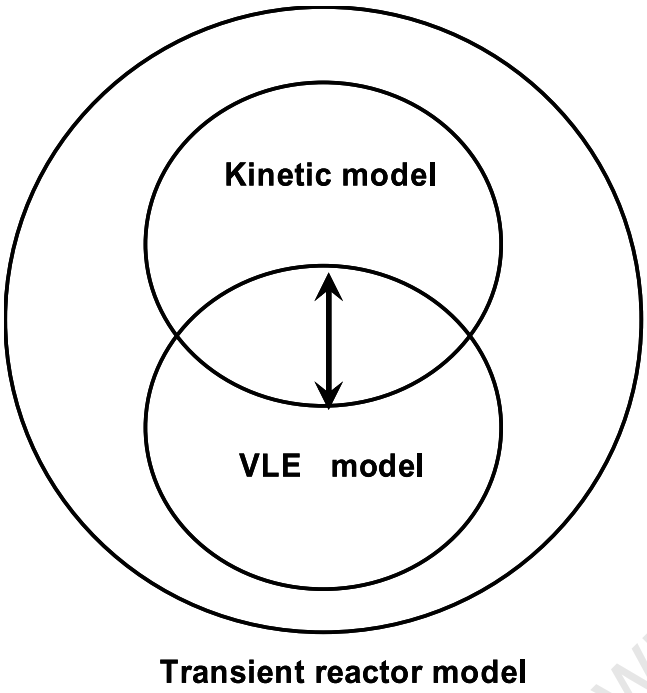

Figure 3.2: Proposed novell FTS model

even though as a product selectivity model. What this work does differently is not to assume a constant (or carbon number dependent) 'partition coefficient', based on Henry's law. The Henry's coefficient, even with the incorporation of an exponential and temperature dependent increase with carbon number (shown by Chang et al. (2007)), is inadequate to describe the VLE of this non-ideal, multi-component hydrocarbon mixture. The interaction of all the species is to be simultaneously considered, and the presence of water in the FT reaction significantly influences the thermodynamics of the system. Obtaining the Henry's coefficients through the extrapolation of pure component vapour pressures, as done by Wang et al. (2004) is inaccurate.

The equation of state approach is taken in this work to describe the VLE, similar to the work of Ahon et al. (2005), but the difference now is that the elementary reaction rate equations for every mechanistic step are functions of the species' fugacities, effectively modelling the VLE in both the kinetics and the dynamics of the transient reactor model. The partial molar fugacity coefficients of the generic species, which determine the K value, are themselves a function of the compositions. Taking the $\phi - \phi$ approach is the most accurate way for describing the VLE of the system, and is further emphasised by the work of Twu and Coon (2000b). The resulting hydrocarbon mixture is highly non-ideal, due to the large concentration of water in the mixture resulting from the FTS reactions.

Modelling the transient reactor

The development of a transient reactor model similar to that developed by Ahon et al. (2005) is the correct approach in solving this dynamic system, and a system of differential algrebraic equations was developed for this system. Dictor and Bell (1983) developed a transient balance for the same reactor system where it was assumed that the gas volume, liquid volume, liquid

density and molecular weight were constant with time. This simplified the resulting system of equations, but did not improve the accuracy of the model.

By taking a fundamental approach in developing a complete FTS model, the hydrocarbon product selectivity was predicted, and the effect that VLE has on the product distribution was accurately determined. The schematic representation of the slurry reactor system is shown in Figure 3.3 and can be considered as a continuous-stirred-tank-reactor (CSTR). The modelling

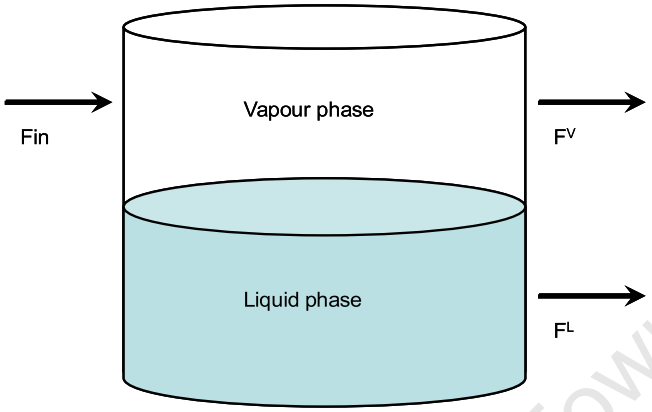

Figure 3.3: Representation of the continuous flow system

of this reactor model is a challenging task as it requires the solving of a system of Differential Algebraic Equations (DAE's) that considers the material balance of every species, the equilibrium, the volume of the liquid and vapour, among other things. Ahon et al. (2005) developed a transient reactor model for a well-mixed, continuous slurry reactor in which syngas was fed continuously at a constant rate and composition. The gas phase products were continuously removed and liquid phase products either accumulated in the reactor or continuously drained. A system of differential algebraic equations was developed consisting of:

- transient material balances for each species i,
- the equilibrium equation for each species, (equation 2.13),
- a volume balance, and
- an equation to determine the liquid flow out of the reactor, as a function of the slurry volume.

3.2 The system

The system is a transient, continuous, well-mixed slurry reactor system, operating at a temperature and pressure of $240°C$ and 20 bar respectively. Two models were developed to observe the effect that VLE has on the Fischer Tropsch product disribution.

1. A model for an FT system that incorporates the Vapour Liquid Equilibrium (VLE) into the kinetics. The reaction rates are expressed in terms of species' activities, as a function of the species' fugacities.

2. A model for an FT system that does not incorporate VLE into the kinetics. This is a single-phase model whereby the reaction rates are expressed as a function of vapour-phase partial pressures.

In the system, there are $(2N + 2)$ fluid phase species (CO, H_2, H_2O, N paraffins, and $(N - 1)$ olefins), and $N + 2$ surface species ($H\theta$, $CH_2\theta$, $C_nH_{2n+1}\theta$ for n=1 to N), where N is the highest carbon-number hydrocarbon species. A schematic representation of the phase distribution of an ideal slurry system is shown in Figure 3.4.

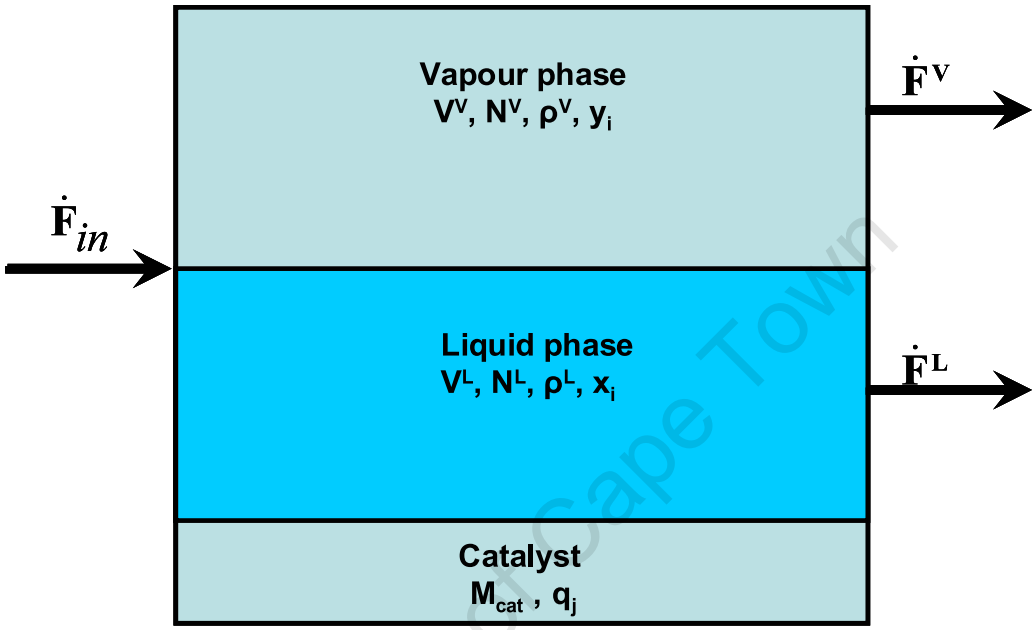

Figure 3.4: Schematic diagram of a continuous, well-mixed, transient, slurry reactor used for model development

where:

- $\dot{F}$ represents the molar flow terms. $(\dot{F}_{in})$ is the overall flow into the system, $(\dot{F}^V)$ the vapour-flow out of the system and $(\dot{F}^L)$ the liquid flow out of the system,
- N^V and N^L represent the total number of moles in the vapour and liquid phases respectively, and
- ρ^V and ρ^L represent the total densities of the vapour and liquid phases respectively.

Realistically, the catalyst is suspended in the slurry, but is envisioned as a catalyst layer in this work, to effectively model the surface reactions. q_j represents the number of moles of surface species j on the surface, and M_{cat} the total mass of active catalyst in the system.The following system assumptions were made:

- The reactor behaves as a perfectly mixed flow reactor.
- The gas-to-liquid interphase mass transfer resistance is negligible, that is, the gas and liquid phases are in thermodynamic equilibrium.

- The temperature and pressure in the reactor remain constant at 240°C and 20 bar respectively.
- The reactor liquid and vapour volumes are maintained constant at $0.5m^3$ each, and are controlled such that the dynamics of the system adapts to maintain the volumes at the specified level.
- The catalyst loading in the reactor is $400kg.m^{-3}$.

3.3 Modelling the VLE

Vapour-liquid equilibrium calculations were required to determine the vapour-to-liquid split of each component through the calculation of the *K-value* (equation 2.13), and to check whether two phases are present in the system under the FTS reaction conditions in the slurry reactor. The partial molar fugacities, $\bar{f}_i$, required for the VLE calculations were obtained according to equation B.16 for each phase, using the Peng Robinson Equation of State. The partial molar fugacities ($\bar{f}_i(T, P, z)$) and the pure component fugacities at $P = 1$ bar, (equation B.15), required for the determination of the species' activities ($\bar{a}_i$, equation 3.1), were modelled in conjunction with the *K-value* calculation, that is, in the same thermodynamic routine.

The PREOS parameters a and b for the mixture, were obtained by applying the Van der Waals mixing rules, with a modification to the κ function for longer chain hydrocarbons, as shown by Twu et al. (1995) (see Appendix B). The binary interaction parameters, k_{ij}, for water, CO and hydrogen with hydrocarbons were obtained from the experimental work of Bukur et al. (2005), which were based on the experimental data from literature on the solubility of inorganic species in various hydrocarbons. Hydrocarbon-to-hydrocarbon binary interaction parameters were assumed to be equal to zero. It is known that the Twu and Coon mixing rules may be too simple to use for such a hydrocarbon system, but the focus of the work is to observe the sole effect of VLE on the product distribution.

3.4 Transient reactor model with VLE

The system to be solved for is a Differential Algebraic Equations (DAE) system, made up of $7N + 10$ equations, where N is the highest carbon-number hydrocarbon chain. The DAE system, with reference to Figure 3.4, is made up of:

- $2N + 2$ Fluid-phase species' overall material balances,
- $2N + 2$ Vapour Liquid Equilibrium equations,
- $N + 2$ Surface species' material balances,
- $2N + 2$ Volume balances, and
- 2 Mole fraction summation equations

Fluid-phase species' overall material balances ($2N + 2$ equations)

For every fluid phase species i in the system, the overall transient material balance is given by equation 3.2,

$$\frac{dN_i}{dt} = \dot{f}_{i,in} - \dot{f}_i^L - \dot{f}_i^V - \left(\sum_{k=1}^{NR} \nu_{i,k} \cdot r_k\right) \cdot M_{cat} \tag{3.2}$$

which is further expanded to equation 3.3,

$$\frac{dN_i}{dt} = \dot{f}_{i,in} - x_i \cdot \dot{F}^L - y_i \cdot \dot{F}^V - \left(\sum_{k=1}^{NR} \nu_{i,k} \cdot r_k\right) \cdot M_{cat} \tag{3.3}$$

where:
N_i is the number of moles of each fluid-phase species i, $[mol]$,
$\dot{f}_{i,in}$ is the molar flowrate of species i flowing into the system, $[mol.s^{-1}]$,
$\dot{f}_i^L$ is the molar flowrate of species i flowing out in the liquid stream, $[mol.s^{-1}]$,
$\dot{f}_i^V$ is the molar flowrate of species i flowing out in the vapour stream, $[mol.s^{-1}]$,
r_k is the elementraty reaction rate of mechanistic step k, given by Table 3.7,
$\nu_{i,k}$ is the stoichiometric coefficient of species i in reaction mechanistic step k, which is positive or negative for the formation or consumption of species i in reaction k respectively,
NR is the total number of reactions in the mechanism.

Vapour Liquid Equilibrium ($2N + 2$ equations)

There are 2N+2 phase-equilibrium equations, given by equation 2.13. The partial molar fugacity coefficients, $\bar{\phi}_i(T, P, z)$, are determined in the VLE model as explained in section 3.3. A detailed algorithm is given in chapter 4.

Surface species' material balances ($N + 2$ equations)

There are $(N + 2)$ surface species (j). The material balance for each of these surface species is given by equation 3.4, where $\nu_{j,k}$ is the stoichiometric coffecient of species j, in reaction mechanistic step k.

$$\frac{dq_j}{dt} = \left(\sum_{k=1}^{NR} \nu_{j,k} \cdot r_k\right) \cdot M_{cat} \tag{3.4}$$

This equation is the same as that for a batch reactor, as the surface species do not flow through the reactor. The concentration on the catalyst site is expressed as the fraction of sites occupied by an intermediate j, θ_{j*}, and the fraction of sites that are vacant, θ_v, for the adsorption and catalyst surface reactions. A balance for the moles of vacant and occupied sites is given by:

$$q_{cat} = q_{vacant} + \sum q_j \tag{3.5}$$

where q_{cat} is the total no. of moles of active catalyst $[mol]$, q_{vacant} is the number of moles of vacant catalyt sites $[mol]$, and q_j is the number of moles of catalyst site occupied by species j

$[mol]$. Dividing through by q_{cat}, the catalyst site balance equation 3.6 is obtained.

$$1 = \theta_v + \sum \theta_{j*} \tag{3.6}$$

Volume Balances ($2N + 2$ equations)

The total number of moles in the liquid phase, N^L, and in the vapour phase, N^V, have to satisfy the volume constraints: $N_L = \rho^L \cdot V^L$ and $N^V = \rho_V \cdot V^V$.
ρ^L and ρ^V are the molar densities of the liquid and vapour phases respectively, which change with changing composition. The densities for each phase are obtained from the VLE model, as it is given by equation 3.7. The applicable compressibility factor, Z, is considered for each phase,

$$\rho = \frac{P}{Z \cdot R \cdot T} \tag{3.7}$$

V^L and V^V are the volumes of the liquid and vapour phases respectively. This leads to the algebraic volume balance for each fluid species i in the system (equation 3.8).

$$N_i = x_i \cdot V^L \cdot \rho^L + y_i \cdot V^V \cdot \rho^V \tag{3.8}$$

Mole fraction summation equations (2 equations)

The sum of the liquid and the vapour mole fractions has to add up to 1, as shown in equations 3.9 and 3.10.

$$\sum x_i = 1 \tag{3.9}$$

$$\sum y_i = 1 \tag{3.10}$$

Therefore, there are $7N + 10$ unknowns (N_i, x_i, y_i, q_j, $\dot{F}^V$ and $\dot{F}^L$) and $7N + 10$ equations to be simultaneously solved for.

3.5 Transient reactor model without VLE

For this model, DAE system comprises of $(5N + 7)$ equations, namely:

- $2N + 2$ fluid phase species' overall material balances,
- $2N + 2$ Volume balances,
- $N + 2$ surface species' material balances (given by equation 3.4), and
- 1 mole fraction summation equation.

Fluid phase species' overall material balances ($2N + 2$ equations)

The overall material balance for every generic species i is given by equation 3.11

$$\frac{dN_i}{dt} = \dot{f}_{i,in} - z_i \cdot \dot{F_{out}} - \left(\sum_{k=1}^{NR} \nu_{i,k} \cdot r_k \right) \cdot M_{cat} \tag{3.11}$$

where z_i is the overall mole fraction of species i.

Volume balances ($2N + 2$ equations)

The volume balance is given by equation 3.12, where V_T is the total volume of the reactor.

$$N_i = z_i \cdot V_T \cdot \rho \tag{3.12}$$

Summation equation (1 equation)

The sum of the mole fractions of all the species has to add up to 1, as given by equation 3.13

$$\sum z_i = 1 \tag{3.13}$$

Therefore, there are $(5N + 7)$ unknowns (N_i, z_i, q_j and $\dot{F_{out}}$) and $5N + 7$ equations to be simultaneously solved for.

3.6 Obtaining consistent initial conditions

The DAE solver, DASPK 3.1, requires consistent initial conditions. Initially, the reactor is filled with an equi-molar mixture of syngas (CO and H_2), H_2O, C_1 to C_N paraffins and C_2 to C_N olefins, which was equilibrated at the operating conditions using an isothermal flash calculation. It is assumed that there are no surface reactions and no flow during the initial equilibrium stage. The temperature (T), pressure (P), Feed (N_0^F) and feed composition ($z_{i,0}$) in the reactor are known, from which the initial liquid and vapour compositions in the system $x_{i,0}$ and $y_{i,0}$, and the total number of moles in the vapour (N_0^V) and liquid (N_0^L) phases after the split can be calculated. Based on the assumption that mass is conserved during the phase split, the sum of the moles of component i in the vapour phase $N_{i,0}^V$ and the moles of component i in the liquid phase, $N_{i,0}^L$, is equal to the moles of component i in the feed, $N_{i,0}^F$ (equation 3.14).

$$N_{i,0}^F = N_{i,0}^V + N_{i,0}^L \tag{3.14}$$

This can be further expanded to equation 3.15.

$$N_0^F \cdot z_{i,0} = N_0^V \cdot y_{i,0} + N_0^L \cdot x_{i,0} \tag{3.15}$$

By combining the component mass balance (equation 3.15), with the phase distribution relation and criterion for VLE (equation 2.13) and the total mole balance ($N_0^F = N_0^L + N_0^V$), the expressions for the vapour and liquid mole fractions are given by equations 3.16 and 3.17,

$$x_{i,0} = \frac{z_{i,0}}{\psi + K_i(1-\psi)} \tag{3.16}$$

$$y_{i,0} = \frac{z_{i,0} \cdot K_i}{\psi + K_i(1-\psi)} \tag{3.17}$$

where ψ is defined as the liquid:feed ratio $\frac{N_0^L}{N_0^F}$. This results in the bootstrap function 3.18.

$$g(\psi) = \sum_i \frac{z_{i,0}(1-K_i)}{\psi + K_i(1-\psi)} = 0 \tag{3.18}$$

The phase distribution constant (*K value*) K_i is calculated from the ratio of the partial molar fugacity coeffients of species i, as shown in section 2.2.1. Equation 3.18 is solved iteratively for ψ, $x_{i,0}$ and $y_{i,0}$, with a numerical root-finding technique. The algorithm for this calculation is given in chapter 4. The volume ratio at this stage is incorrect, therefore the next steps are to use the calculated initial compositions and initial liquid and vapour densities, ($x_{i,0}$ and $y_{i,0}$, ρ_0^L and ρ_0^V respectively) to estimate the initial molar species in the reactor, given the $0.5m^3$ liquid volume and vapour volume constraint respectively. This gives the initial number of moles in both phases, $N_{i,0}^V$ and $N_{i,0}^L$, according to equations 3.19 and 3.20 respectively.

$$N_{i,0}^V = x_{i,0} \cdot \rho_0^V \cdot V^V \tag{3.19}$$

$$N_{i,0}^L = x_{i,0} \cdot \rho_0^L \cdot V^L \tag{3.20}$$

Once this is established, syngas is allowed into the reactor for the commencement of the Fischer Tropsch reactions. The flowrate of syngas into the system starts at zero and is ramped exponentially to its final steady state values.

3.7 Reaction scheme

The proposed reaction mechanism is similar to that proposed by Visconti et al. (2007) and to van der Laan and Beenackers (1999b). The mechanism, and the related elementary reaction rate equations are given in Table 3.7, where the following assumptions were made:

- There is only one type of active catalyst site on which the adsorption reaction takes place.
- The reactants are adsorbed and in thermal equilibrium before they react.
- The chain-growth reaction is initiated by the formation of the methyl species $CH_3\theta$) and the chain growth takes place by the successive insertion of methylene ($CH_2\theta$) into the active site alkyl bond (as reported by Visconti et al. (2007) and Schulz and Claeys (1999)).

- The kinetic rate constants, describing the growth of surface species and the hydrocarbon formation, are independent of the carbon number of the intermediates involved in their reactions.

- Reaction steps **1.1 to 1.6** occur very quickly, with the net reaction **1** and corresponding reaction rate equation, r_1.

Table 3.1: Proposed Fischer Tropsch Reaction Mechanism and corresponding rate equations

Reaction type	**Rxn No.**	**Chemical Reaction**	**Rate Equation**
CO Adsorption	1.1	$CO + \theta \rightarrow CO\theta$	
	1.2	$CO\theta + \theta \rightarrow C\theta + O\theta$	
Surface Reactions	1.3	$C\theta + H\theta \rightarrow CH\theta + \theta$	
	1.4	$CH\theta + H\theta \rightarrow CH_2\theta + \theta$	
	1.5	$O\theta + H\theta \rightarrow OH\theta + \theta$	
	1.6	$OH\theta + H\theta \rightarrow H_2O + 2\theta$	
	1	$CO + 4H\theta \rightarrow H_2O + CH_2\theta + 3\theta$	$r_1 = k_1 \bar{a}_{CO} \theta_{H*}$
H_2 adsorption	2	$H_2 + 2\theta \rightarrow 2H\theta$	$r_2 = k_2 \bar{a}_{H2} \theta^2$
Chain initiation	3	$CH_2\theta + H\theta \rightarrow CH_3\theta + \theta$	$r_3 = k_3 \theta_{CH2*} \theta_{H*}$
Methanation	4	$CH_3\theta + H\theta \rightarrow CH_4 + 2\theta$	$r_4 = k_4 \theta_{CH3*} \theta_{H*}$
Chain Growth (n=1,59)	5	$CH_2\theta + C_nH_{2n+1}\theta \rightarrow C_{n+1}H_{2n+3}\theta + \theta$	$r_5 = k_5 \theta_{CH_2*} \theta_{C_nH_{2n+1}*}$
β-dehydrogenation to olefins (n=2,60)	6	$C_nH_{2n+1}\theta \leftrightarrow C_nH_{2n} + H\theta$	$r_6 = k_{6f} \theta_{Cn+2n+1*} - k_{6r} \bar{a}_{CnH2n} \theta_{H*}$
Hydrogenation to paraffins (n=2,60)	7	$C_nH_{2n+1}\theta + H\theta \rightarrow C_nH_{2n+2} + 2\theta$	$r_7 = k_7 \theta_{CnH2n+1*} \theta_{H*}$

The method by which the specific reaction rate constants (k_j) were estimated for each reaction is given in section 3.8. For the transient model with VLE, $\bar{a}_i$, the activity of fluid phase species i, is defined by equation 3.1. For the model without VLE, the activity is defined by equation 3.21, Smith et al. (2001), essentially a normalised partial pressure measure.

$$\bar{a}_i = \frac{z_i \cdot P}{P = 1bar} \tag{3.21}$$

3.8 Model parameters

As shown in Table 3.7, there are eight specific reaction rate constants (k_j). As an initial starting point, reaction rate constant k_1 was set to 0.1 $mol \cdot (s \cdot g_{cat})^{-1}$, and the rest of the constants were set as ratios to k_1, on the basis of work carried out by Visconti et al. (2007). To adapt the constants to this particular system (which differs from that of Visconti et al. (2007)) the effect of each of the constants on the product distribution was studied. This was done by varying each of the constants, within the same order of magnitude as according to the experimental observations, and observing the individual and combined effects on:

- the intermediate species' formation, particularly the formation of chain growth initiation species, $CH_2\theta$ and $CH_3\theta$,
- the paraffin product formation and distribution,
- the olefin product formation and distribution, and
- the hydrocarbon product distributions.

Section 5.5 shows the sensitivity of the profiles to parameter changes. Parameter estimation requires the fitting of experimental data (C_n vs. time) over a range of T and P conditions. What this work does is guess reasonable model parameters based on other research, as a starting point to optimisation.

Chapter 4

Numerical Simulation

The two models were solved using FORTRAN routine DASPK 3.1, and the steady state results were obtained after ten residence times. With reference to Figure 4.1, the methodology that was followed in developing the model is summarised as follows:

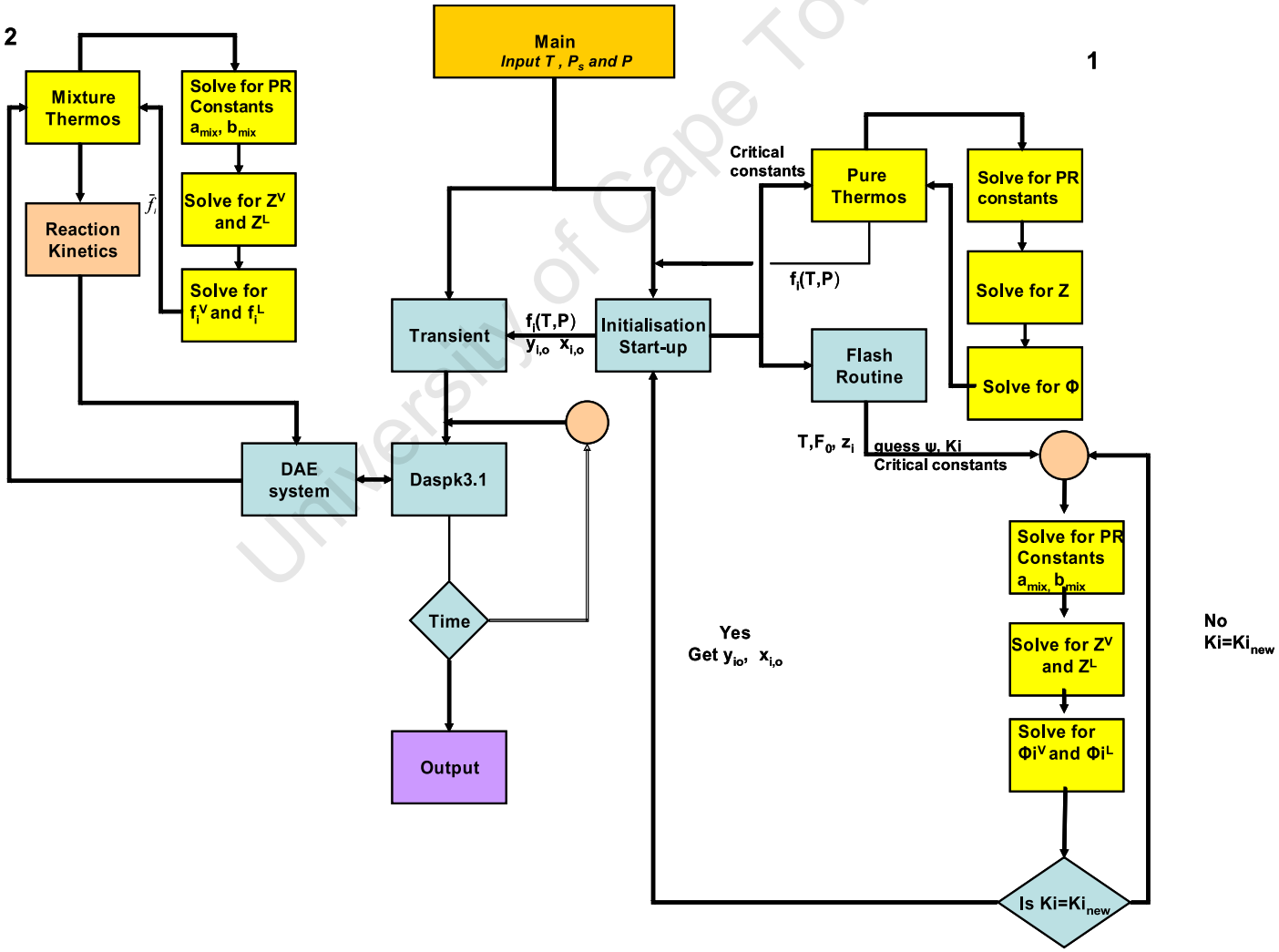

Figure 4.1: FTS block flow diagram of model development procedure

The computer simulation starts off in the routine labelled ***Main***, whereby the operating conditions (T and P) and the standard pressure $P_s = 1$bar, are entered. The vectors are sized

according to the number of components in the system. The model has been set in two sections with different routine 'blocks' and will be explained accordingly.

1. **Initialisation and Start-up routine**

   Initialisation block: This is the routine whereby the pure component fugacities are calculated at the standard pressure and temperature ($f_i(T, P = 1bar)$). The critical constants (T_c, P_c, ω) for each component are used to calculate the Peng Robinson Equation of State constants a_i and b_i (equations B.3 and B.4 respectively). Thereafter, the compressibility factor (Z_i) and the fugacity coefficients (ϕ_i) for each component are calculated, so as to obtain the pure component fugacities (equations B.12 and B.15 respectively). The pure component fugacity is required for the calculating the species' activities in the kinetics routine, thus these values are sent to the ***Transient*** block. The critical values for all the species up to C_{20} were obtained from Daubert et al. (1999), and correlations for obtaining critical constants at higher carbon numbers are given in Apepndix A.

   Start-up block: The aim of the start-up routine is to obtain initial compositions $x_{i,0}$, $y_{i,0}$ and consequently the initial number of moles ($N^V_{i,0}$, $N^L_{i,0}$) for the integration of the system of DAE's in the *Transient* block. An isothermal flash calculation is conducted as explained in section 3.6, and it involves an iterative process whereby ψ and the K_i values are guessed. x_i and y_i are then calculated according to equations 3.16 and 2.13 respectively. The compositions and the critical constants are sent to a mixture thermodynamics block that calculates the PR constants (a_{mix} and b_{mix}) and consequently the compressibility factors (Z^V and Z^L) for the mixture in both phases. Thereafter, the partial molar fugacity coefficients ($\bar{\phi}_i$) can be determined and new K_i values are calculated as functions of the ($\bar{\phi}_i$) values, equation 2.13. A numerical method is used to iterate to convergence, until such time the $K_{i_{old}} = K_{i_{new}}$. The solution yields the initial compositions, and the densities of the liquid and vapour phases.

2. **Transient routine** The input into the transient block is therefore the pure component fugacities at P=1 bar, and the initial compositions and densities. The volume of the liquid and vapour phases are set constant at 0.5m^3 each, and therefore the initial number of moles are calculated according to equations 3.19 and 3.20 respectively. The important parameters for DASPK 3.1 are set in this routine, including the relative and absolute tolerance. The first time step is set at 0, with a logarithmic time change. A call is then made to DASPK 3.1 to solve the system of equations set up in ***DAE system*** routine.

   DAE System The system of equations is entered into the DAE solver as indicated in chapter 3. The syngas flowrate is set at a H_2:CO ratio of 2:1 and the catalyst loading is set to 400000 $g.m^{-3}$. The catalytic site balance is included in this routine, as it is a constraint that has to be met at all times. With every time step, the

reaction rates are developed in the ***Reaction Kinetics*** block, where a call is made to the ***Mixture thermodynamics*** block to obtain the partial molar fugacities at each updated composition (as the species form or are consumed, and with the simultaneous solving of the DAE system). This occurs in a loop until a converged solution is obtained for that time step. Once the solution is obtained at the given time step, it is sent back to the ***Transient*** block to move onto the next time step and write the data in an external file.

Output The results are then written out for each time step, and sorted according x, y, F^V, F^L, N_i^V and N_i^L values with time respectively.

By setting up the complete FTS model in this way, it is easy to investigate each of the blocks independently, to see if they are working optimally. The code has been written such that it is easy to modify the system to any size, by simply indicating a different number of components. It also makes it easy to vary the operating conditions and observe how the system behaves. This code has been written in a general way in order to make it user-friendly and adaptable to any FT DAE system.

Part III

Results and Discussion

Chapter 5

Results and Discussion

5.1 Start-up

CO, H_2, H_2O in equal molar proportions, and an ASF distributed hydrocarbon system (paraffins and olefins up to C_{60}) with a chain growth probability constant, $\alpha = 0.7$, were isothermally flashed at 240°C and 20bar. The hydrocarbon feed to the flash was distributed as shown in Figure 5.1, and the values obtained from the flash given in Table 5.1.

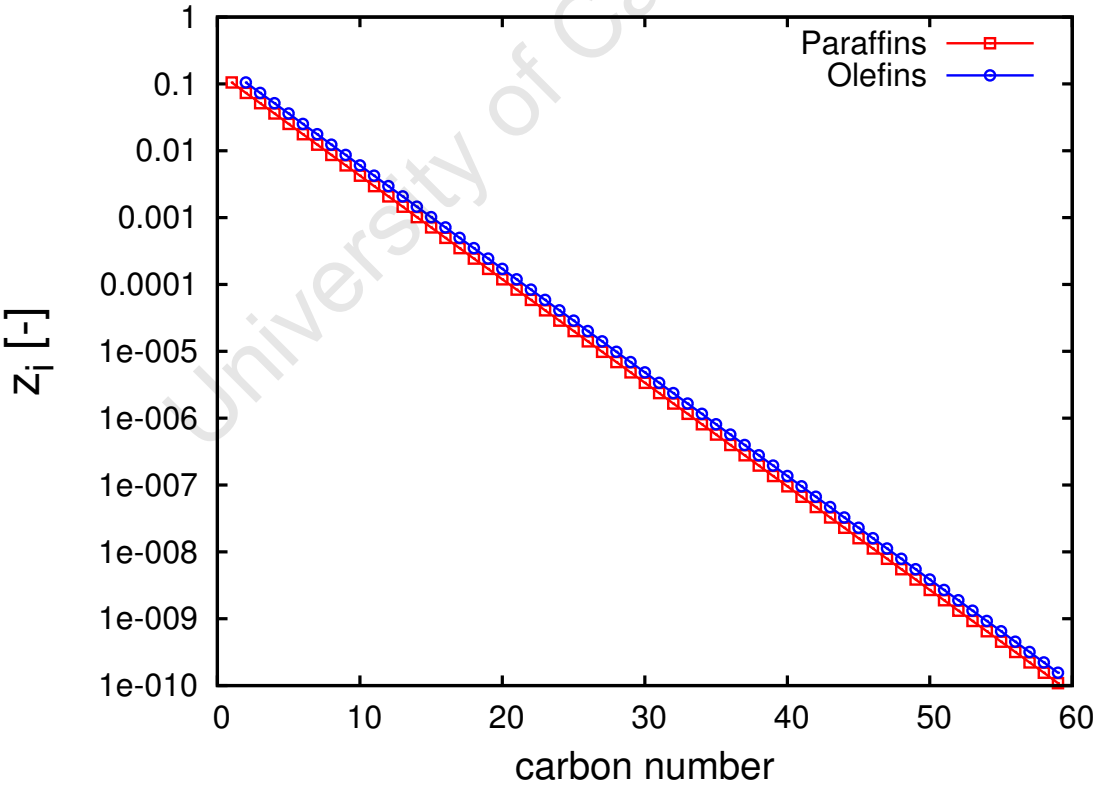

Figure 5.1: Initial hydrocarbon distribution fed into isothermal flash, at $\alpha = 0.7$

Initial conditions of the slurry reactor model had to adhere to the liquid and vapour volume constraints of $V^V = V^L = 0.5$ m^3. The number of moles in the system were adjusted according to equations 3.19 and 3.20. This, therefore, distorted the initial hydrocarbon distribution,

Table 5.1: Calculated values from Rachford-Rice Isothermal Flash calculation

Variable	Value	Units
V^L	$3.88E-05$	m^3
V^V	1.99	m^3
$L/F(\psi)$	1.00E − 04	-
V/F	0.99	-

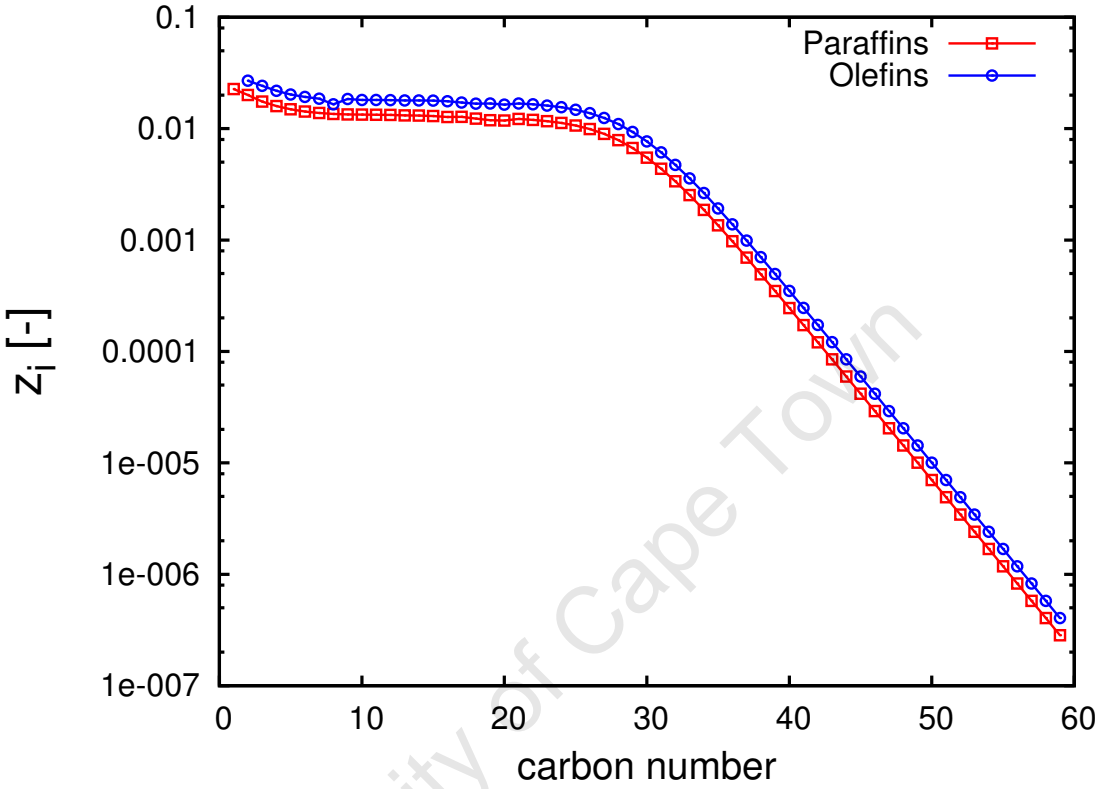

Figure 5.2: Modified hydrocarbon distribution after satisfying the volume constraints.

yielding curvature as exhibited in Figure 5.2. The initial feed composition to the integrator does not have an effect on the final outcome, as long as there is consistency in the initial conditions, and as long as steady state is reached. An ASF distributed hydrocarbon feed was chosen as the initial feed to the flash, so as to approximate a realistic FT distribution. The K-values, vapour and liquid mole fraction data for all the species after flashing, are shown in Table E.1.

5.2 Model parameters

The input variables for both the single- and two-phase models, and the optimal estimated kinetic rate constants, from the proposed mechanism (Table 3.7), are given in Tables 5.2 and 5.3 respectively. Realistically, the vapour-to-liquid volume ratio is much less than 1. The ratio of vapour to liquid only affects the dynamics of the system, and has no effect on steady state operation. The constants were adapted from Visconti et al. (2007)'s model as a guideline. Each of the rate constants were carefully considered, and the final kinetic parameter choices were

Table 5.2: Model variables for the single- and two- phase models

Parameter	Value	Units
Flowrates		
CO Flowrate in	500	$mol.s^{-}1$
H_2 Flowrate in	$2 \times F_{CO}$	$mol.s^{-1}$
C_{60} Flowrate in	1E-04$\times F_{CO}$	$mol.s^{-1}$
Operating conditions		
Temperature	240	°C
Pressure	20	bar
Vapour Volume	0.5	m^3
Liquid Volume	0.5	m^3
Catalyst loading	4.0E05	$g.m^{-3}$

Table 5.3: Kinetic rate constants corresponding to proposed mechanism

Parameter	Value	Units
k_1	0.1	$mol.s^{-1}.(g_{cat})^{-1}$
k_2	$k_1/70$	$mol.s^{-1}.(g_{cat})^{-1}$
k_3	$k_1 \times$ 2.42E02	$mol.s^{-1}.(g_{cat})^{-1}$
k_4	$k_1 \times$ 2.18E03	$mol.s^{-1}.(g_{cat})^{-1}$
k_5	$k_1 \times$ 1.56E03	$mol.s^{-1}.(g_{cat})^{-1}$
k_{6f}	$k_1 \times 4$	$mol.s^{-1}.(g_{cat})^{-1}$
k_{6r}	$k_1 \times 6.7\text{E}-07$	$mol.s^{-1}.(g_{cat})^{-1}$
k_7	$k_1 \times$ 9.71E01	$mol.s^{-1}.(g_{cat})^{-1}$

made on the basis of an ideal ASF product distribution in the single phase model. Because both models use the same constants, the sole effect of VLE on the product distribution can be observed.

5.3 Comparative model results

5.3.1 Product distribution

For the conditions given in section 5.2 the hydrocarbon distributions for both models are shown in Figure 5.3. As observed, the profiles for both the single- and the two-phase models indicate a decrease in the hydrocarbon product selectivity with increasing carbon number, for both olefins and paraffins, as expected. The chain growth probability constants from the two models are given in Table 5.4.

Table 5.4: Comparison of α values and CO conversion (X_{CO}) from the two models

Parameter	Single-phase model	Two-phase model
α_1	0.62	0.82
α_2	0.62	0.63

*α_1 was calculated from the ASF plot using the slope between C_2 and C_{15}

** α_2 was calculated from the ASF plot using the slope between C_{35} and C_{55}

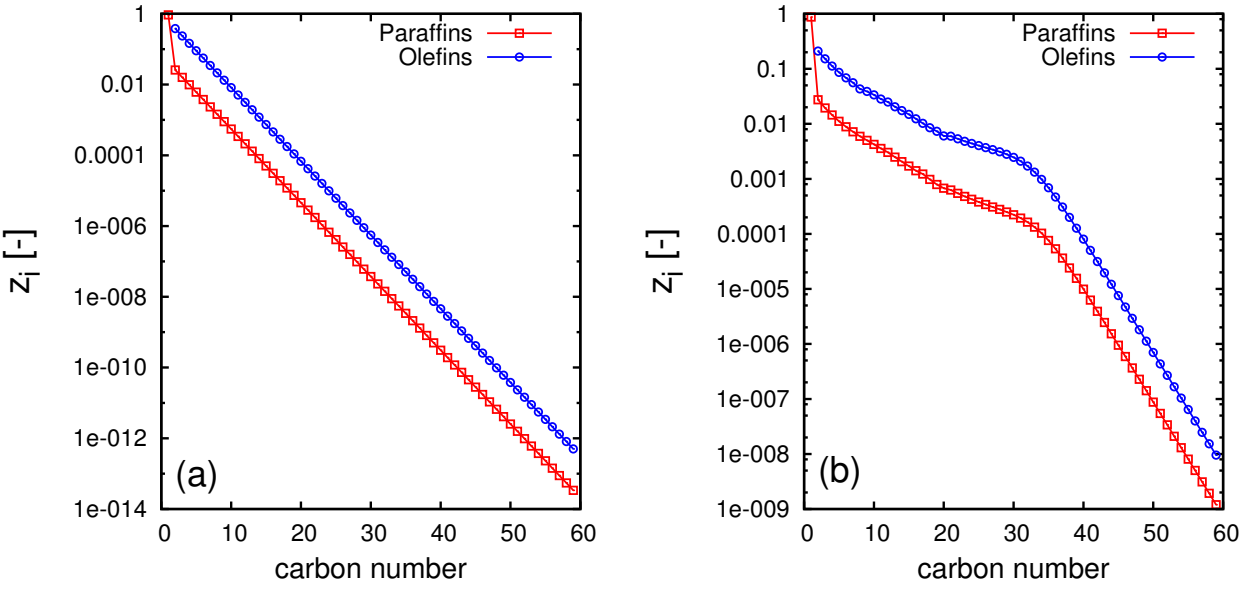

Figure 5.3: a. Hydrocarbon product distribution for single phase model, b. Hydrocarbon product distribution for two-phase model

Single-phase model A linear distribution, typical of an 'ideal' ASF product distribution is observed in the single-phase model, with one chain growth probability constant ($\alpha_1 = \alpha_2 = 0.62$).

Two-phase model There are two product distributions observed in the two-phase model, where the change in distribution happens at C_{32} for the olefin curve, and C_{33} for the paraffin curve. α_1 is determined from the ASF plot by using the slope between C_2-C_{15}, and α_2 by using the slope between C_{35}-C_{55}.

The alpha values $\alpha_2 < \alpha_1$ which indicates a negative deviation of the 'second' distribution from the 'first' distribution. This means that the probability of forming longer chains decreases beyond C_{32}. This is observed for hydrocarbons $> C_{25}$, according to the work by Raje and Davis (1996), as shown in FIgure 2.4. Even though a linear approximation is made to determine α_1, there is slight upward curvature in the distribution curves corresponding to α_1. This agrees with experimental observations, which indicate a positive deviation in the ASF plot with increasing carbon numbers, up to $\approx C_{30}$.

α_2 in the two-phase model is approximately equal to α_1 in the single-phase model, suggesting that after C_{32}, the species are concentrated in one phase. This is confirmed by considering a plot of the hydrocarbon liquid fraction distribution, $(Ni^L/Ni^{Total}) = \psi$ vs. carbon number, in Figure 5.4. The species' distribution between vapour and liquid changes with carbon number, as shown in Figure 5.4. The system remains in 2-phase operation for all conditions. At small carbon numbers, the vapour phase dominates, and at high carbon numbers liquid phase dominates. Observing the data, see (Table G.1), the paraffins are essentially in the liquid phase from carbon number C_{33}, and the olefins from

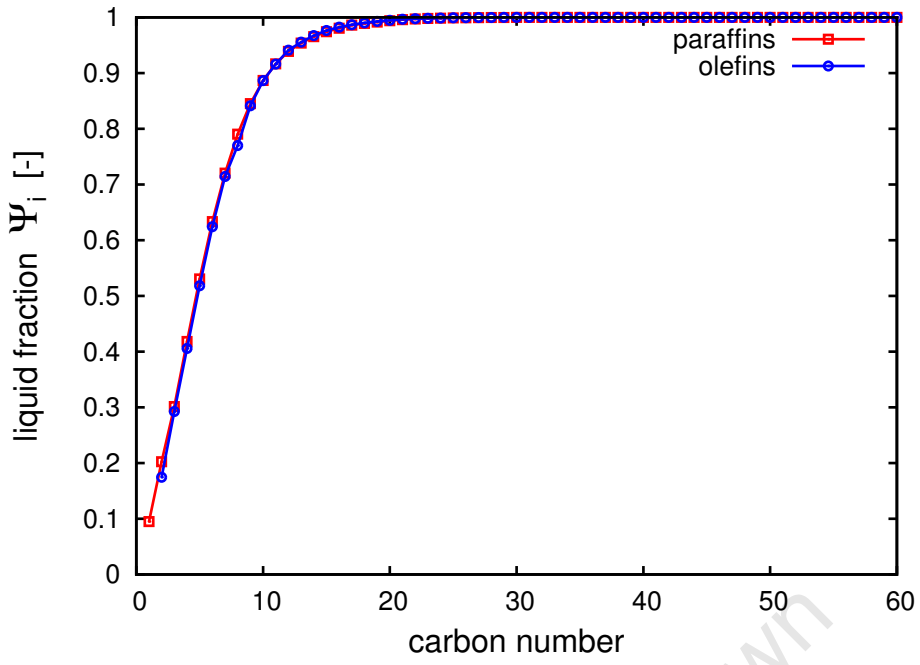

Figure 5.4: Fraction of component i in the liquid phase as a function of carbon number

carbon number C_{32}. The reason that $\alpha_1 > \alpha_2$ in the two phase model, is due to the combined equilibrium and kinetic effects. Before the point of inflection, there's a distribution of hydrocarbon species across the two phases, with a movement from a vapour-rich equilibrium state to a liquid-rich equilibrium state with increasing carbon number(see Figure 5.4). The reaction takes place in the liquid phase, and with the increase in liquid species due to the interaction of kinetics and equilibrium, the formation of longer hydrocarbon chains is favoured (up to C_{32} and C_{33} for olefins and paraffins respectively).

5.3.2 Selectivity

Anomalies of C_1 and C_2 hydrocarbons Both models show the C_1 anomaly that is reported in literature, with methane having a higher selectivity than the rest of the hydrocarbons. The C_1:C_2 molar ratio $\left(\frac{z_{C_1}}{z_{C_2}}\right)$ is higher in the single-phase model, at 36.3 compared to 31.9 in the two-phase model. This shows a larger drop from C_1 to C_2 in the single-phase model. The difference between these values is due to a thermodynamic factor (γ) present in the two-phase system, discussed under 'Olefin:Paraffin selectivity ratio'. This anomaly is accounted for in the model by distinguishing the methanation reaction r_4 from the polymerisation reactions (r_5, r_6 and r_7).

Overall hydrocarbon selectivity The overall hydrocarbon selectivity is higher in the two-phase model, with $z_{C_{59}}$ of the order 1E-08, compared to 1E-015 in the single-phase model. Considering Figure 5.5, a single-phase distribution with chain growth probability factor $\alpha = 0.62$ (as observed for the single-phase model) would be represented by linear curves "Paraffins" and "Olefins". The 'shift' is due to the effect of equilibrium, which causes a

higher overall hydrocarbon selectivity.

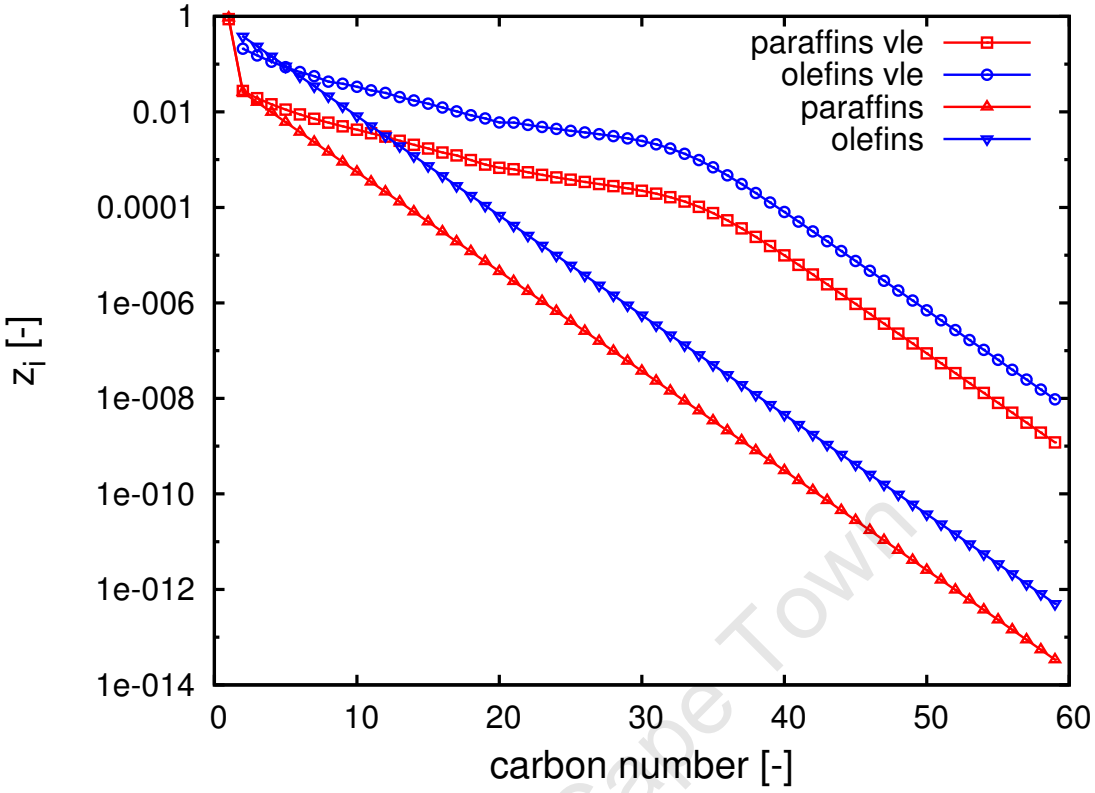

Figure 5.5: Product distribution curve illustrating the equilibrium effect on hydrocarbon selectivity, single-phase ('Paraffins', 'Olefins'), two-phase ('Paraffins VLE', 'Olefins VLE')

Olefin:Paraffin selectivity ratio As observed in Figure 5.3, the position of olefin distribution curve is above the paraffin distribution curve for both models. The difference between the two curves (the 'gap' between them) is defined as the selectivity ratio, S_R, and given by equation 5.1, where i is the respective carbon number, for $i \geq 2$.

$$S_R = \frac{z_{Ol_i}}{z_{Pn_i}} \tag{5.1}$$

- For the single-phase model, a constant selectivity ratio of 9.6 was obtained.
- For the two-phase model, the selectivity ratio was not constant due to the slight curvature observed with increasing carbon number and the variation in VLE between paraffins and olefins. As mentioned earlier, there are two identifiable distributions in the two-phase model, as shown in Figure 5.6. Due to the changing S_R, an average selectivity ratio was calculated for both regions (S_{R1} and S_{R2}). The selectivity ratios corresponding to the two regions are given by $S_{R1} = 9.1$ and $S_{R2} = 8.2$. The decrease in the selectivity ratio from region 1 to 2 is as a result of the species distribution moving from a vapour-dominant region to a liquid-dominant region.

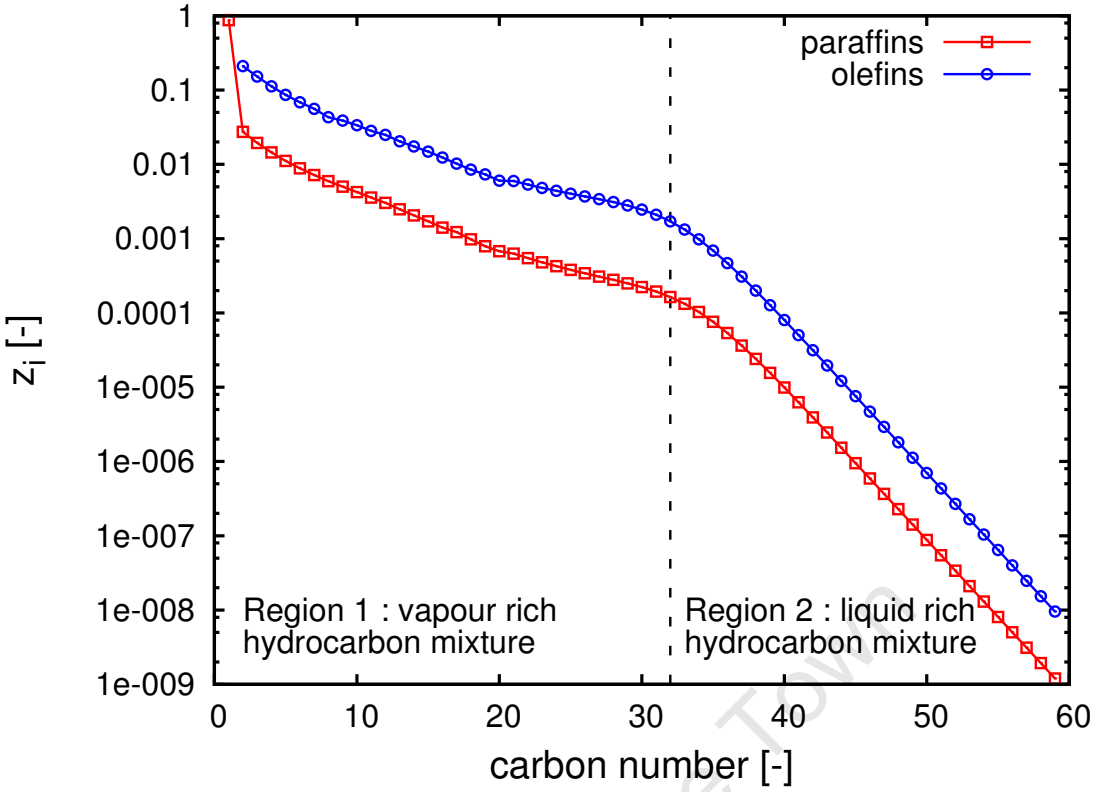

Figure 5.6: Identifying 2 regions in the hydrocarbon product distribution: two-phase model

The selectivity ratio in the single-phase model exceeds the selectivity ratios in the two-phase model. Considering that the differences in the two models is the description of the species' activities, consider the following:

For the **single-phase model**, the definition for activity is given by equation 3.21. Therefore the ratio of the olefin:paraffin activities is

$$\frac{\bar{a}_{Ol_i}}{\bar{a}_{Pn_i}} = \frac{z_{Ol_i} \cdot P \cdot (P = 1bar)}{(P = 1bar) \cdot z_{Pn_i} \cdot P} \tag{5.2}$$

where Ol_i is an olefin with carbon number i and Pn_i is paraffin of carbon number i, for $i \geq 2$. Simplifying,

$$\frac{z_{Ol_i}}{z_{Pn_i}} = \frac{\bar{a}_{Ol_i}}{\bar{a}_{Pn_i}} \tag{5.3}$$

According to the single phase model, the olefin:paraffin molar ratio is equal to the olefin:paraffin activity ratio, and for ideal gases this is the ratio of the partial pressures.

For the **two-phase model**, the ratio of the olefin:paraffin activities is given by:

$$\frac{\bar{a}_{Ol_i}}{\bar{a}_{Pn_i}} = \frac{\bar{f}_{Ol_i} \cdot f_{Pn_i}(T, P = 1bar)}{f_{Ol_i}(T, P = 1bar) \cdot \bar{f}_{Pn_i}} \tag{5.4}$$

Equation 5.4 expands to

$$\frac{\bar{a}_{Ol_i}}{a_{Pn_i}} = \frac{\bar{\phi_{Ol_i}} \cdot z_{Ol_i} \cdot f_{Pn_i}(T, P = 1bar)}{\bar{\phi_{Pn_i}} \cdot z_{Pn_i} \cdot f_{Ol_i}(T, P = 1bar)} \tag{5.5}$$

$$\frac{\bar{a}_{Ol_i}}{a_{Pn_i}} = \left(\frac{z_{Ol_i}}{z_{Pn_i}}\right) \cdot \left(\frac{f_{Pn_i}(T, P = 1bar)}{f_{Ol_i}(T, P = 1bar)}\right) \cdot \left(\frac{\bar{\phi_{Ol_i}}}{\bar{\phi_{Pn_i}}}\right) = \left(\frac{z_{Ol_i}}{z_{Pn_i}}\right) \cdot \gamma_{\left(\frac{Ol_i}{Pn_i}\right)} \tag{5.6}$$

and therefore

$$\frac{z_{Ol_i}}{z_{Pn_i}} = \left(\frac{\bar{a}_{Ol_i}}{\bar{a}_{Pn_i}}\right) \cdot \frac{1}{\gamma_{\left(\frac{Ol_i}{Pn_i}\right)}} \tag{5.7}$$

Equation 5.7 explains why The selectivity ratio in the single phase model exceeds that in the two phase model, $S_{R_{\text{single-phase}}} > S_{R_{\text{two-phase}}}$, due to the olefin:paraffin activity ratio being divided by the thermodynamic factor $\gamma_{\left(\frac{Ol_i}{Pn_i}\right)}$.

5.3.3 Ratio of olefin reaction rate to paraffin reaction rate

The value of the olefin production rate: paraffin production rate ratio is determined by the kinetics. For the two models, the ratios that were obtained are:

$$\left(\frac{r_6}{r_7}\right)_{\text{single-phase}} = 9.60$$
$$\left(\frac{r_6}{r_7}\right)_{\text{two-phase}} = 9.65$$

The ratios are approximately equal. Considering the formulation $\left(\frac{r_6}{r_7}\right)$,

$$\frac{r_6}{r_7} = \frac{k_{6f}\theta_{Cn+2n+1*} - k_{6r}\bar{a}_{C_nH_{2n}}\theta_{H*}}{k_7\theta_{C_nH_{2n+1*}}\theta_{H*}} \tag{5.8}$$

$$\frac{r_6}{r_7} = \frac{k_{6f}}{k_7\theta_{H*}} - \frac{k_{6r}a_{C_nH_{2n}}}{k_7\theta_{C_nH_{2n+1*}}} \tag{5.9}$$

$$\frac{r_6}{r_7} \approx \frac{k_{6f}}{k_7\theta_{H*}} \tag{5.10}$$

The concentration of the hydrogen intermediate has an effect on which reaction rate is favoured. Seeing that the reverse reaction rate constant is so small in the base case, $k_{6r} = k_1 \times 6.7E-07$, the second term has very little effect, considering the ratio by equation 5.10. The constants k_{6f} and k_7 are identical for both models, therefore the slight difference lies in the concentration of the hydrogen intermediate, θ_{H*}.

Table 5.5: Variables to explain $\left(\frac{r_6}{r_7}\right)$ for the two models

Variable	**Single-phase**	**Two-phase**
$\left(\frac{r_6}{r_7}\right)$	9.60	9.65
θ_{H*}	4.31E-03	4.27E-03
$\bar{a}_{H_2}$	2.38	2.41
$\bar{a}_{CO}$	1.67	1.68

The kinetics are driven primarily by the activities of syngas, and the consequent formation and consumption of hydrogen intermediate θ_{H*} for the initiation stages (See the mechanism in Table 3.7). The values of the syngas activities, and concentration of the hydrogen intermediate are given in Table 5.5. As observed, this explains the closeness of the olefin:paraffin rate ratio values. The distribution of hydrocarbon surface species ($\theta_{C_nH_{2n+1}}$) with carbon number is illustrated in Figure 5.7. and as observed, for the two models, the surface species' distribution

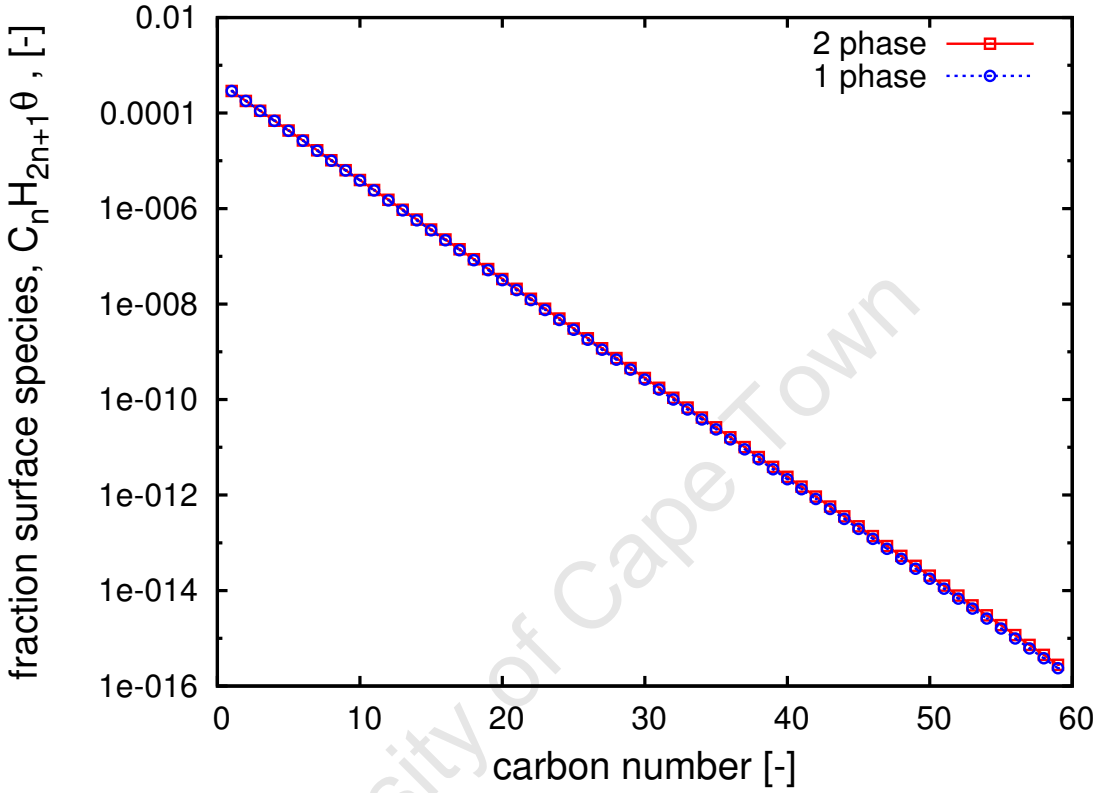

Figure 5.7: Hydrocarbon surface species ($C_nH_{2n+1}\theta$) distribution for both models

is similar.

5.3.4 The difference in product distributions

As observed in section 5.3.3, the ratio of the olefin:paraffin formation rates are almost identical in both models. The syngas activities and concentration of the hydrogen surface species (the drivers of the kinetics) are similar (as shown in Table 5.5). The following questions are posed:

1. Why are the product distribution curves different for both models if their kinetic models are similar?
2. What is the relationship between the mole fractions of species i (z_i) in both models?
3. What is the factor that distorts the classical ASF distribution, resulting in two distributions, as observed in the 2-phase model?

The difference between the product distributions in both models is accounted to the following:

Olefin activities Referring to the reaction scheme in Table 3.7, the reversible olefin formation reaction (reaction 6, with corresponding reaction rate r_6) has a significant contribution to the differences in product distribution, particularly with respect to the olefin readsorption reaction rate (reverse reaction 6), a function of the olefin activities $\bar{a}_{CnH2n}$ and the hydrogen surface species θ_{H*}. The olefin activities as a function of carbon number, for both models are shown in Figure 5.8.

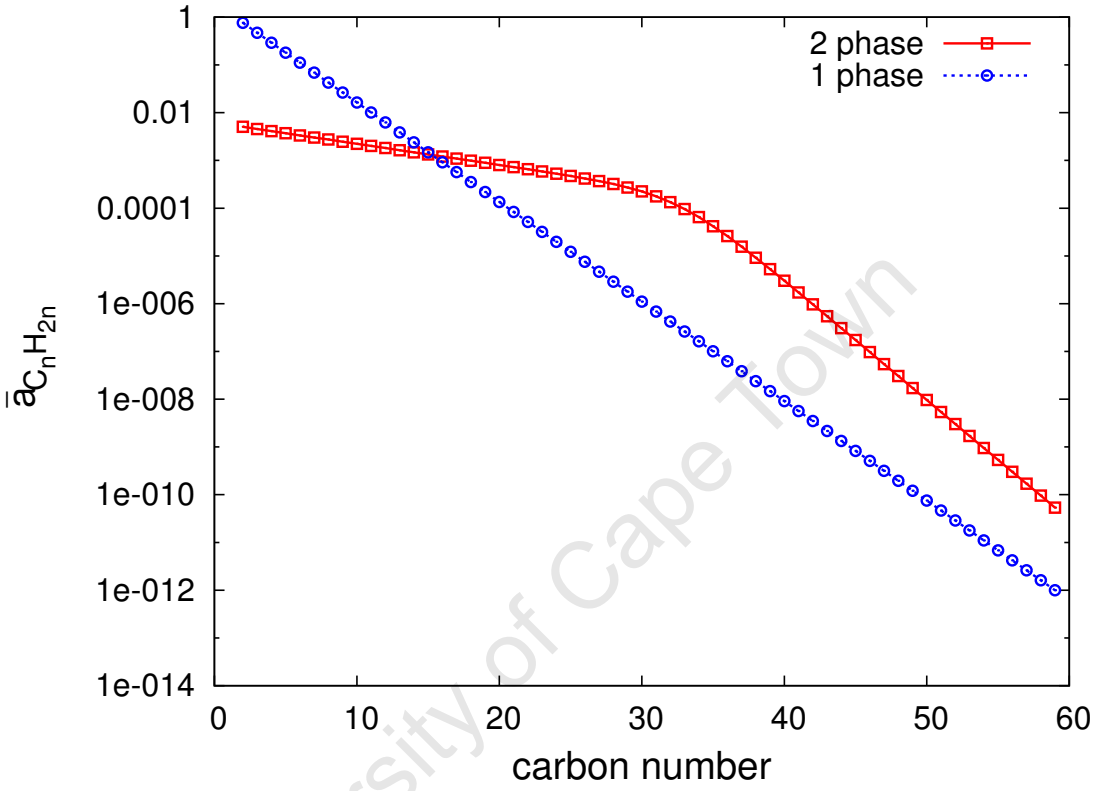

Figure 5.8: Olefin activities, $\bar{a}_{CnH2n}$, as a function of carbon number

For the single-phase model, the activity is the ratio of the partial pressure to the total pressure (as shown in equation 3.21). The activities are directly dependent on the molar composition of the species, z_i. For the two-phase model, the activity is defined according to equation 3.1, a function of the partial molar fugacities of the olefins. The activity is a function dependent on species interactions across the two phases. Before the intersection point of the two activity distribution curves (at $\approx C_{18}$ in figure 5.8) the olefin activities in the single-phase model exceed the olefin activities in the two-phase model. The molar fractions of light hydrocarbons are higher in the single-phase model, yielding an ASF-like distribution typical of the polymerisation reaction. There are lower olefin activities at low carbon numbers in the two-phase model, as a result of interaction with liquid in the reactor, with species being distributed across both phases. The point of intersection of the two curves corresponds to the point at which there is primarily liquid in the two-phase model, as shown in Figure 5.4). This further explains the higher olefin activity in the two-phase model after this point at higher carbon numbers.

Relationship between molar compositions in both models Considering the material balances of species i in both models at steady state.

Single-phase model:

$$\dot{f}_{i,in_1} - z_{i_1} \cdot \dot{F}_{out_1} - r_{i_{net1}}(\mathrm{z_{i_1}}, \mathrm{P}, \mathrm{P} = 1\mathrm{bar}) \cdot M_{cat} = 0 \tag{5.11}$$

where $r_{i_{net1}}(\mathrm{z_{i_1}}, \mathrm{P}, \mathrm{P} = 1\mathrm{bar})$ is the net rate of consumption of species i in the single phase model, a function of the partial pressure of species i, and the standard pressure (P=1bar). Therefore the expression for z_{i_1} is:

$$z_{i_1} = \frac{r_{i_{net1}} \cdot M_{cat} - \dot{f}_{i,in_1}}{\dot{F}_{out_1}} \tag{5.12}$$

Two-phase model:

$$\dot{f}_{i,in_2} - z_{i_2} \cdot \dot{F}_{out_2} - r_{i_{net2}}(\mathrm{z_{i_2}}, \mathrm{P}, \bar{\phi}_{\mathrm{i}}, f_i(\mathrm{T}, \mathrm{P}=1\mathrm{bar})) \cdot M_{cat} = 0 \tag{5.13}$$

where $r_{i_{net2}}(\mathrm{z_{i_2}}, \mathrm{P}, \bar{\phi}_{\mathrm{i}}, f(\mathrm{T}, \mathrm{P}=1\mathrm{bar}))$ is the net rate of consumption of species i in the two-phase model, a function of z_{i_2}, the partial molar fugacity coefficient ($\bar{\phi}_i$), pure component fugacity at standard pressure (f_i(T,P=1bar)) and the pressure. Therefore the expression for z_{i_2} is:

$$z_{i_2} = \frac{r_{i_{net2}} \cdot M_{cat} - \dot{f}_{i,in_2}}{\dot{F}_{out_2}} \tag{5.14}$$

$\dot{F}_{out_2} \approx \dot{F}_{out_1} \approx F_{out}$ (which is later confirmed in section 5.3.5) then z_{i_2} can be expressed as a function z_{i_1} as follows:

$$\frac{z_{i_2}}{z_{i_1}} = \frac{\left(r_{i_{net2}} \cdot M_{cat} - \dot{f}_{i,in_2}\right)}{\left(r_{i_{net1}} \cdot M_{cat} - \dot{f}_{i,in_1}\right)} \tag{5.15}$$

which can be simplified to

$$\frac{z_{i_2}}{z_{i_1}} = \left(\frac{r_{i_{net2}} \cdot \dfrac{M_{cat}}{f_{i,in}} - 1}{r_{i_{net1}} \cdot \dfrac{M_{cat}}{f_{i,in}} - 1} \right) \tag{5.16}$$

since $f_{i,in_2} = f_{i,in_1} = f_{i,in}$ (=0 for products). Let

$$\frac{M_{cat}}{f_{i,in}} = \tau_i$$

then

$$z_{i_2} = \left(\frac{r_{i_{net2}} \cdot \tau_i - 1}{r_{i_{net1}} \cdot \tau_i - 1} \right) \cdot z_{i_1} \tag{5.17}$$

This equation can be written as

$$z_{i_2} = D \cdot z_{i_1} \tag{5.18}$$

where

$$D = \left(\frac{r_{i_{net2}} \cdot \tau_i - 1}{r_{i_{net1}} \cdot \tau_i - 1} \right) \tag{5.19}$$

D is a factor that distorts the single-phase distribution, resulting in a two-phase product distribution that deviates from the classical linear distribution. The reaction rates in the two-phase system deviate from the single-phase system due to the VLE.

5.3.5 Steady state results

The steady state results for both models are given in Table 5.6. The CO conversion, X_{CO}, is defined by equation 5.20.

$$X_{CO} = \frac{F_{CO,in} - F^V_{CO}}{F_{CO,in}} \tag{5.20}$$

The CO conversion values for both models are not identical, but very close to each other. This is due to the kinetics being driven by the activities of the CO and H_2, which are almost identical. The thermodynamic factor, $\gamma_{\left(\frac{H_2}{CO}\right)}$, is ≈ 1. It takes 873 times longer to reach steady state in the two-phase model than the single phase model. This is due to the slow dynamics of the liquid-phase. The liquid flowrate is low and the liquid molar density is of the order of 100 times greater than the vapour density. Thus, the liquid phase takes a long time to reach steady state.

Table 5.6: Steady state results for both models

Variable	Single-phase model	Two-phase model	Units
Flowrates			
CO			
FCO_{in}	500	500	$(mol.s^{-1})$
FCO_{out}	89.9		$(mol.s^{-1})$
FCO^{V}_{out}		87.7	$(mol.s^{-1})$
FCO^{L}_{out}		1.46E-04	$(mol.s^{-1})$
Hydrogen			
$FH_{2_{in}}$	$2 \times FCO_{in}$	$2 \times FCO_{in}$	$(mol.s^{-1})$
$FH_{2_{out}}$	63.1		$(mol.s^{-1})$
$FH^{V}_{2_{out}}$		59.6	$(mol.s^{-1})$
$FH^{L}_{2_{out}}$		5.98 E-05	$(mol.s^{-1})$
$\mathbf{C_{60}H_{122}}$			
$FC_{60_{in}}$	$10^{-4} \times FCO_{in}$	$10^{-04} \times FCO_{in}$	$(mol.s^{-1})$
$FC_{60_{out}}$	6.12E-11		$(mol.s^{-1})$
$FC^{V}_{60_{out}}$		7.3E-11	$(mol.s^{-1})$
$FC^{L}_{60_{out}}$		1.3E-16	$(mol.s^{-1})$
Total flows			
F_{out}	755		$(mol.s^{-1})$
F^{V}_{out}		751	$(mol.s^{-1})$
F^{L}_{out}		6.68E-02	$(mol.s^{-1})$
Elemental flows			
C			
FC_{in}	503	503	$(mol.s^{-1})$
FC_{out}	503	503	$(mol.s^{-1})$
H			
FH_{in}	2006	2006	$(mol.s^{-1})$
FH_{out}	2006	2006	$(mol.s^{-1})$
O			
FO_{in}	500	500	$(mol.s^{-1})$
FO_{out}	500	500	$(mol.s^{-1})$
X_{CO}	0.82	0.82	-
$H_2 : CO$ ratio	0.70	0.68	-
Time to reach steady state	500	4.37E05	seconds

5.3.6 Overall VLE effect: base case

When comparing the two models, it can be summarised that VLE has the following effect on FTS.

- The hydrocarbon chain growth probability, for carbon numbers $< C_{32}$ for olefins, and $< C_{33}$ for paraffins, is higher than for higher carbon numbers due to VLE causing the movement of species from a predominantly vapour-rich phase to a predominantly liquid-rich phase.
- VLE increases the carbon chain length.
- VLE increases the paraffin:olefin selectivity ratio for carbon numbers $< C_{32}$ for olefins, and $< C_{33}$ for paraffins, after which point all the hydrocarbons are effectively in the liquid phase.
- VLE has a very small (almost no) effect on the kinetics in the two phase model. This is because the kinetics are driven by the activities of CO and H_2 (as shown in the proposed mechanism, Table 3.7) which are very similar. The reason there's a deviation from the classical ASF distribution, is due to a distortion factor D, which is a function of the relative reaction rates in the reactor, which differ as a result of VLE.

Even though the kinetics are the same in both models, the product distributions are different as a result of the large role the VLE plays in the species' transient material balances. The resulting DAE systems for both models are significantly different, thus the product distributions are different.

5.4 Profile sensitivity to process parameters

5.4.1 Variation in catalyst loading

The catalyst loading was varied in both models, *ceteris parabus*, to observe the effect on chain growth probability and conversion. The CO conversion and chain-growth probability as a function of catalyst loading are given in Table 5.7.

Table 5.7: Conversion and alpha as a function of catalyst loading

	Single-phase model		**Two-phase model**		
Catalyst loading	X_{CO}	α_1	X_{CO}	α_1	α_2
4E04	0.44	0.73	0.44	0.98	0.74
4E05 (base case)	0.82	0.62	0.82	0.82	0.63
4E06	0.91	0.46	0.92	0.61	0.66

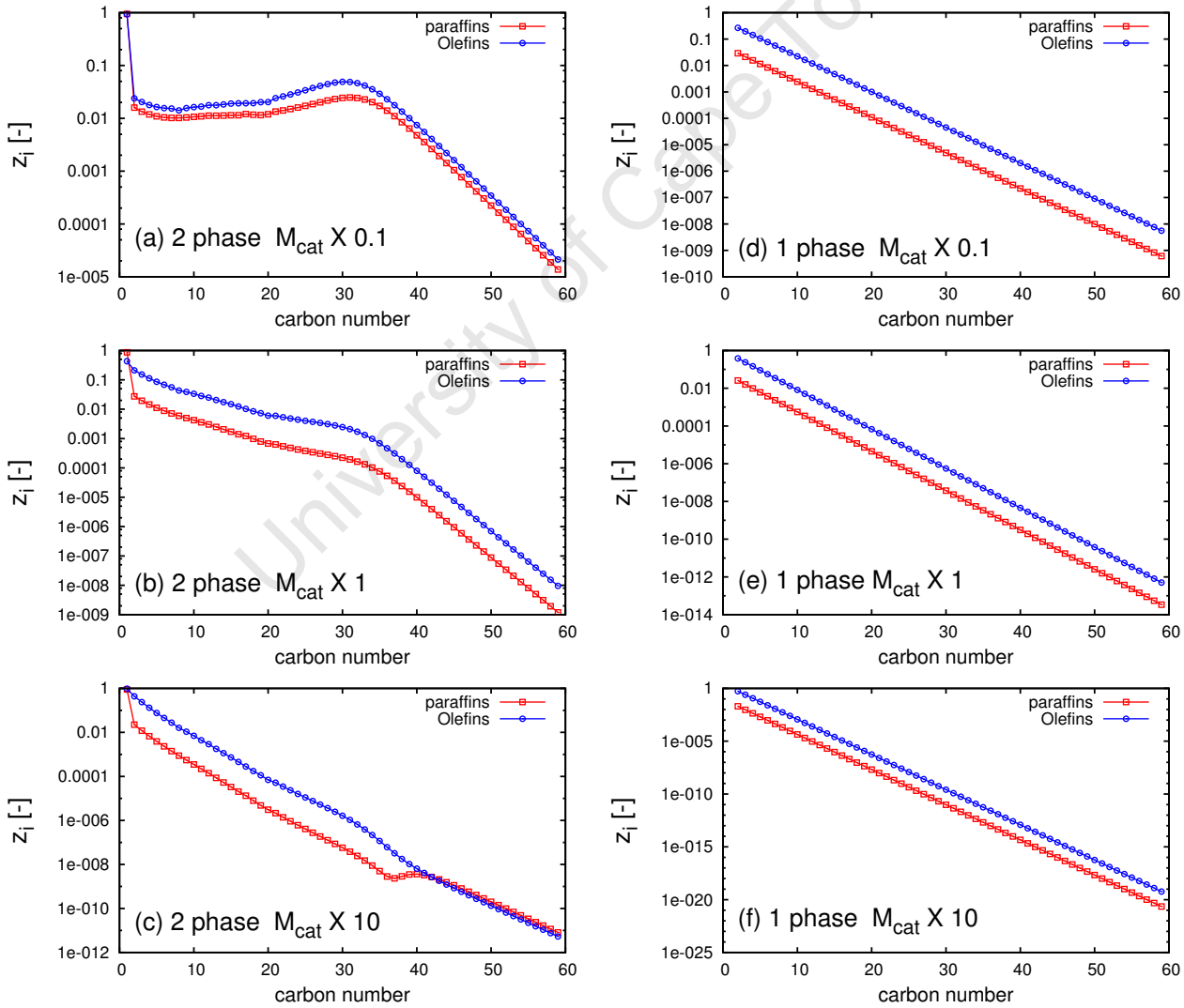

Figure 5.9: Hydrocarbon product distribution plots for single-phase and two-phase models for variations in catalyst mass

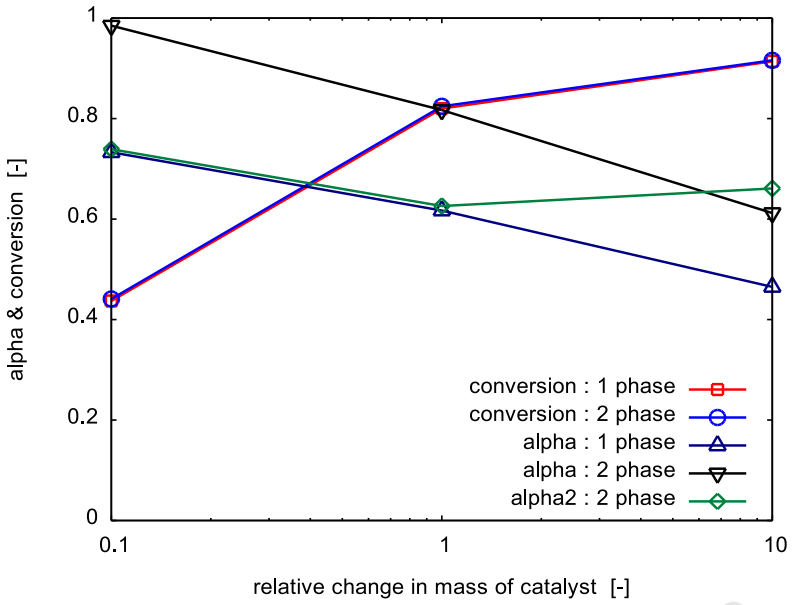

Figure 5.10: α and X_{CO} as a function of the relative change in catalyst mass

Conversion

As observed, an increase in the catalyst loading increases the CO conversions of both the single-phase, and the two-phase model. A change in the catalyst loading affects the surface reaction balances directly (as observed in the surface species material balance equation 3.4) more so, than the fluid-phase species balances, equations 3.3 and 3.11 for the two-phase model and the single-phase model respectively. An increase in the catalyst loading, increases the H_2 adsorption rate r_2, and consequently the concentration of hydrogen surface species θ_{H*}. An increase in this concentration results in an increased rate of CO consumption (rate r_1), and consequently, an increase in the CO conversion. This is further explained by considering the mathematical relationship between CO conversion, X_{CO}, and the catalyst loading, M_{cat}. From the steady state material balance for CO, equation 5.21.

$$F_{CO,in} - F_{CO}^{V} - r_1 \cdot M_{cat} = 0 \tag{5.21}$$

Substituting the definition for conversion (equation 5.20)

$$X_{CO} \cdot F_{CO,in} - r_1 \cdot M_{cat} = 0 \tag{5.22}$$

therefore

$$X_{CO} \cdot F_{CO,in} = r_1 \cdot M_{cat} \tag{5.23}$$

$$X_{CO} = r_1 \cdot \frac{M_{cat}}{F_{CO,in}} \tag{5.24}$$

The term that causes an increase in the conversion is $\left(\frac{M_{cat}}{F_{CO,in}}\right)$, equivalent to the residence time. CO conversion is proportional to the catalyst loading ($X_{CO} \propto M_{cat}$) and rate r_1. An

increase in either one of these terms increases the CO conversion.

Product distribution

The behaviour of the product distribution profiles, with an increase in catalyst loading are discussed, and the product distribution curves for each catalyst variation, for both models, is given in Figure 5.9.

Single-phase model α_1 decreases with increasing catalyst loading. A decrease in the chain growth probability (corresponding to a steeper slope) is indicative of a negative deviation, meaning that the probability of forming of long chain hydrocarbons is reduced. At a catalyst loading of 4E06, the accuracy of the results at higher caarbon numbers cannot be guaranteed, as the z_i values are lower than the machine precision of the order of 10^{-16}. However, a deviation in the linear distribution is not observed.

Two-phase model In this model α_1 and α_2 also decrease with increasing catalyst loading, as observed for the single phase model. The product distribution profiles shown distinct differences. Observing the two distributions separately:

- *α_1 :region with combined equilibrium effect and kinetic effect (region $< C_{32}$)* The 'equilibrium effect' is defined here as the increase in hydrocarbon selectivity due to an increase in the hydrocarbon liquid fraction with increasing carbon number(recall Figure 5.4). The 'kinetic effect' is defined here as the observation of a decrease in the hydrocarbon selectivity with increasing carbon numbers, due to the polymerisation nature of the FTS reactions. At the lowest catalyst loading, there is a distinct convex curvature upwards exhibiting an increase in the product selectivity with increasing carbon numbers. This can be explained by a dominating phase-equilibrium effect, more so than the kinetic effect (confirmed by the lowest X_{CO} at this loading). As the catalyst loading increases, the kinetic effect increasingly dominates (and X_{CO} increases), and the overall hydrocarbon selectivity decreases. This is caused by decreasing α_1, which reduces the liquid fraction, and thus closely approximates a single-phase. This is observed for both the paraffin- and olefin- distribution curves.
- *α_2 :region with dominant kinetic effect (region $> C_{32}$)* With increasing catalyst loading, α_2 decreases up to a relative change in catalyst mass of 1, like the single-phase model, but increases slightly thereafter. What is interesting is the olefin and paraffin distribution curves having the same selectivity at higher carbon numbers, for a catalyst loading of 4E06. In this region, all the species essentially reside in the liquid phase. These species approximate single-phase behaviour and thus it is expected to have similar α to the single-phase model, as observed at low conversions. At a conversion of 0.9, this is not observed. The response curve shows numerical instability around C_{40}, and appears to have reached integrator resolution. The two-phase model contains many additional routines other than the kinetics, each with their

own tolerances, and each of which provides additional constraints on the DASPK 3.1 integrator.

5.4.2 Variation in pressure

The pressure was varied in the both models in order to determine the relationship between CO conversion (X_{CO}) and chain-growth probability constant(α). Alpha as a function of pressure for both models is shown in Figure 5.11.

Single-phase model A single, linear distribution was observed and the results shown in Table 5.8. Both the conversion and the chain growth probability increase with increasing

Table 5.8: Conversion and α as a function of pressure for the single-phase model

Pressure (bar)	X_{CO}	α_1
2	0.72	0.36
4	0.80	0.46
8	0.87	0.53
15	0.91	0.58
20 (base case)	0.93	0.60
40	0.96	0.63

pressure. With an increase in the pressure, the activities of CO and H_2 increase (see equation 3.21). This in turn increases the conversion of CO.

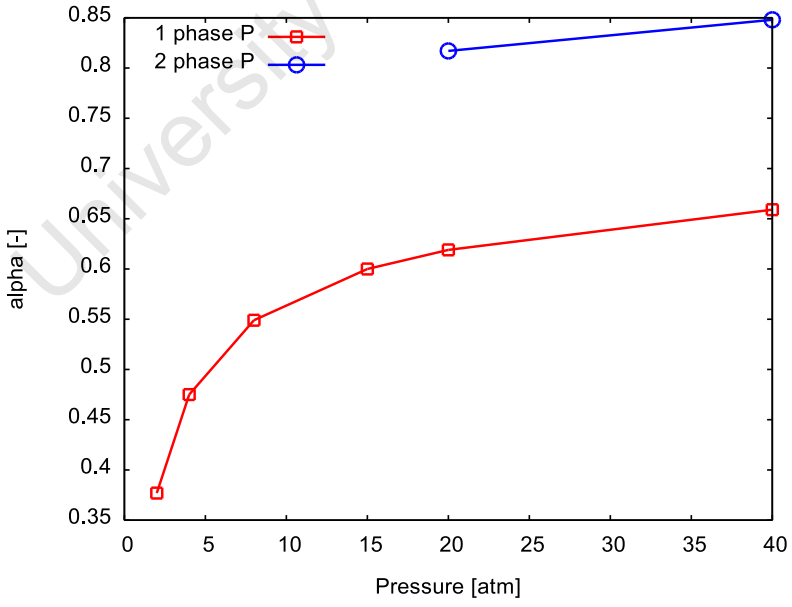

Figure 5.11: α as a function of pressure for both models

Two-phase model At pressures lower than 20bar, there was only one phase in the system, and therefore no solution to the model. The CO conversion and α values for higher pressures are given in Table 5.9, where two alpha distributions were observed as expected.

Table 5.9: Conversion and α as a fuction of pressure for the two-phase model

Pressure (bar)	X_{CO}	α_1	α_2
20	0.82	0.81	0.63
40	0.89	0.85	0.67

An increase in the pressure corresponded to an increase in the conversion. This is expected as the syngas activities are proportional to the pressure, as per equation 5.25.

$$\bar{a_i} = \frac{\bar{f_i}(T, P, z)}{f_i(T, P = 1bar)} = \frac{z_i \cdot \bar{\phi_i} \cdot P}{f_i(T, P = 1bar)} \tag{5.25}$$

There was an increase in the two chain growth probabilities with an increase in the pressure, as observed for the single-phase. An increase in pressure, increases the concentration of the liquid species. A high conversion corresponds to a lower CO and H_2 concentration.

However, the increase in conversion is not as large as expected for both models when doubling the pressure (from 20bar to 40 bar). Doubling the pressure should effectively double the reaction rate r_1 and r_2, which should in turn increase the other reaction rates. The complexity of the kinetic model prevents simplified interpretation of the pressure effect on all reaction steps.

5.4.3 Relationship between α and conversion

On the basis of the results from varying the catalyst loading and the pressure, the relationship betwen α and CO conversion was determined. With reference to Figure 5.12, α decreases with increasing conversion for the catalyst loading curves for both models, and $\alpha_{\text{two-phase}} > \alpha_{\text{one-phase}}$ For the pressure variation curves, α increases with an increase in conversion. It can be concluded that α is not solely dependent on conversion, but dependent on the operating conditions and catalyst loading. The model response is non-linear with varying M_{cat} and P. This means that the CO is consumed and there's a higher probability to form short-chain hydrocarbons chains. With an increase in the pressure, both the CO conversion and the α value increase (Table 5.8).

5.5 Profiles sensitivity to kinetic constants in the VLE model

In this section the response of the VLE product distribution is observed for changes in the kinetic parameters, *ceteris parabus*. The base case rate constants those given in Table 5.3.

5.5.1 Effect of reaction rate constant k_1 on FTS product distribution

The sole effect of varying kinetic constant k_1, corresponding to reaction 1 (and rate r_1) is discussed.

$$CO + 4H\theta \longrightarrow H_2O + CH_2\theta + 3\theta$$

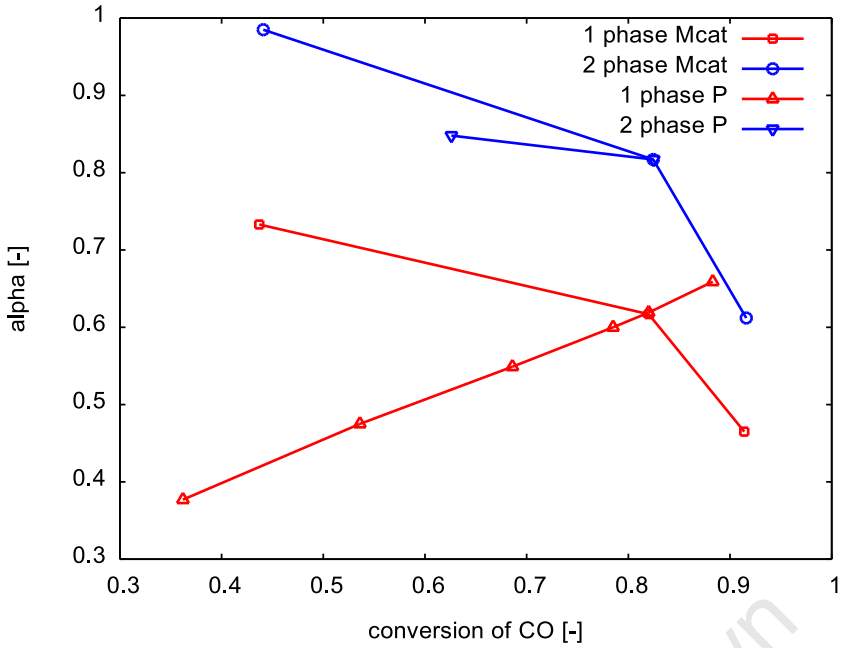

Figure 5.12: α as a function of CO conversion with a variation in M_{cat} and pressure (P)

$$r_1 = k_1 \bar{a}_{CO} \theta_{H*}$$

The product distributions for both the single and the two-phase models are shown in Figure 5.13, where the parameters are expressed as multiples of the base case. The conversion and chain growth probability data as a function of k_1 are given in Table 5.10. For both models, the CO conversion increases with an increase in k_1, as reaction rate r_1 increases, and more CO is consumed. This is further shown by equation 5.24, where CO conversion is directly proportional to r_1. The product distribution and selectivity for each model is discussed.

Table 5.10: Conversion and α as a function of k_1

	Single-phase model		**Two-phase model**		
$\mathbf{k_1}$	X_{CO}	α_1	X_{CO}	α_1	α_2
$k_1 \times 0.1$	0.64	0.30	0.64	0.39	0.76
$k_1 \times 1$ (base case)	0.82	0.62	0.82	0.82	0.63
$k_1 \times 3$	0.88	0.70	0.89	0.92	0.70
$k_1 \times 10$	0.93	0.78	0.93	1.07	0.78

Single-phase model The overall hydrocarbon selectivity increases with an increase in k_1. At $k_1 \times 0.1$, the model is not accurate at higher carbon numbers, since the values are below the machine precision of 10^{-16}. The paraffin selectivity decreases with an increase in k_1, observed by the increasing olefin:paraffin selectivity ratio. This occurs due to reactions r_1 and the paraffin formation rate, r_7, competing for the hydrogen surface species $H\theta$. There is one α distribution (ignoring the second distribution for parameter $k_1 \times 0.1$) which increases with increasing k_1, therefore the probability of forming longer chains increases.

Two-phase model The overall hydrocarbon selectivity increases, due to an increase in X_{CO}.

The opposite effect is observed for the olefin:paraffin selectivity ratio, whereby the paraffin and olefin curves approach each other with increasing k_1.

Two chain growth probabilities are observed. At the lowest k_1, the selectivity of higher carbon numbers is very low, (observed by z_i to the order 10^{-16}). Just as observed for the single-phase model, the chain growth probability constants increase. Notably, with an increase in k_1, α_1 increases due to the dominating equilibrium effect, where there's a higher liquid fraction.

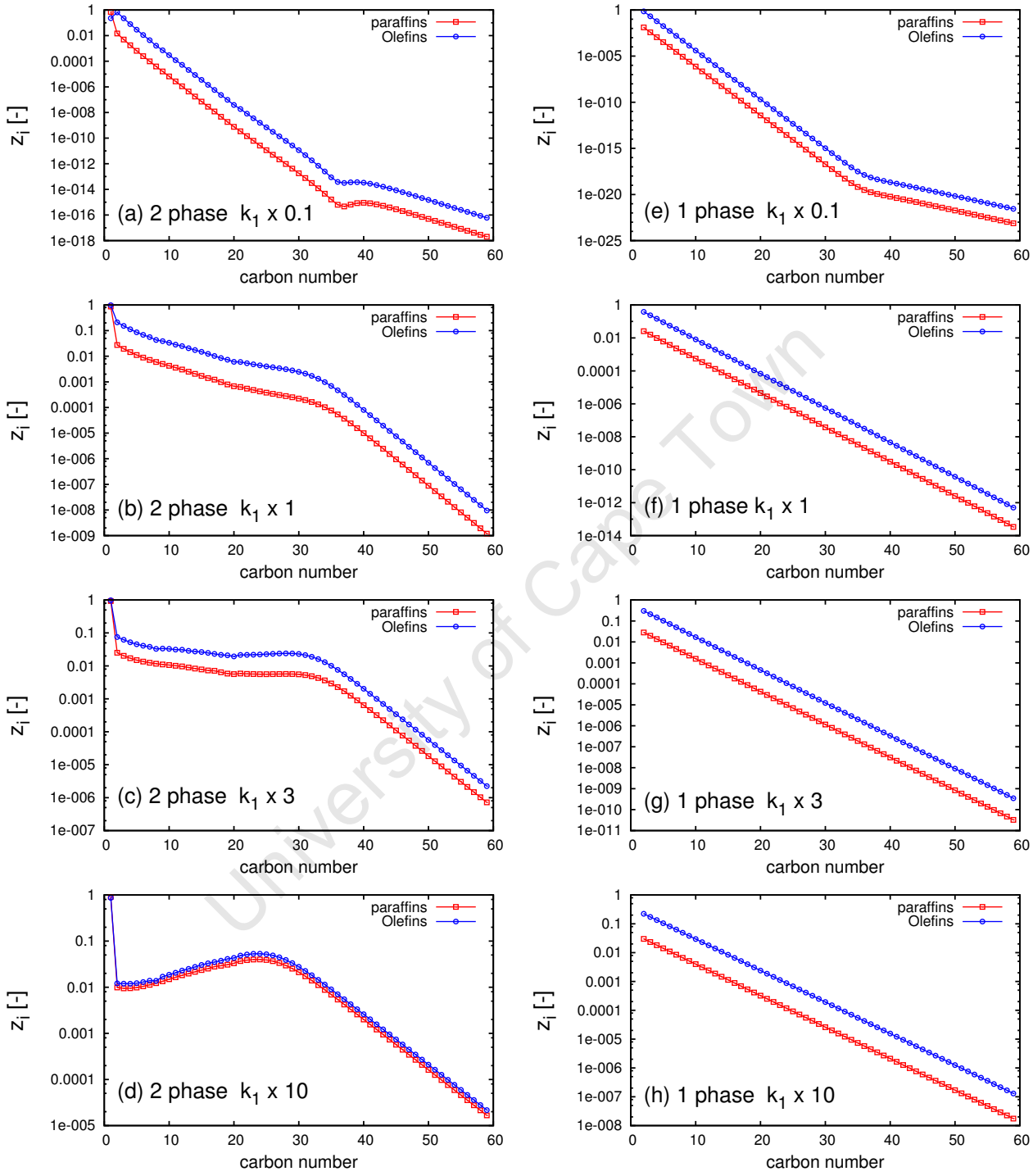

Figure 5.13: Hydrocarbon product distribution for single-phase and two-phase models, with a variation in kinetic parameter k_1

5.5.2 Effect of reaction rate constant k_2 on FTS product distribution

The effect of varying kinetic constant k_2, corresponding to reaction 2 with rate r_2, is discussed.

$$H_2 + 2\theta \longrightarrow 2H\theta$$

$$r_2 = k_2 \bar{a}_{H2} \theta^2$$

The product distribution curves in response to changes in k_2 are shown in Figure 5.14. Conversion and α values as a function of k_2 are displayed in Table 5.11.

Table 5.11: Conversion and α as a function of k_2

	Single-phase model		**Two-phase model**		
$\mathbf{k_2}$	X_{CO}	α_1	X_{CO}	α_1	α_2
$k_2 \times 0.03$	0.20	0.70	0.20	0.94	0.71
$k_2 \times 0.1$	0.50	0.69	0.50	0.92	0.69
$k_2 \times 1$ (base case)	0.82	0.62	0.82	0.82	0.63
$k_2 \times 3$	0.84	0.61	0.85	0.80	0.62

As observed for both models, the CO conversion increases with an increase in k_2. This is due to an increased production of $H\theta$ and consequently an increase in the consumption rate of CO (reaction r_1).

Single-phase model The methane selectivity increases with increasing k_2. This is noticed from the first paraffin point in the distribution curve, which moves up as k_2 increases. With the increase in the formation of $H\theta$ there's an increased methane formation rate, r_4. The olefin:paraffin selectivity ratio decreases with increasing k_2, due to an increase in the paraffin selectivity (reaction r_7 increases with a higher concentration of $H\theta$). The probability of forming long hydrocarbon chains (α) decreases with an increase in k_2, as the probability of forming methane, and short-chain hydrocarbons increases.

Two-phase model Both α values decrease with increasing k_2 as observed for the single-phase model. For the first distribution, corresponding to α_1, the equilibrium effect decreases with increasing k_2 as the formation of shorter hydrocarbons (predominantly in the vapour phase) is encouraged.

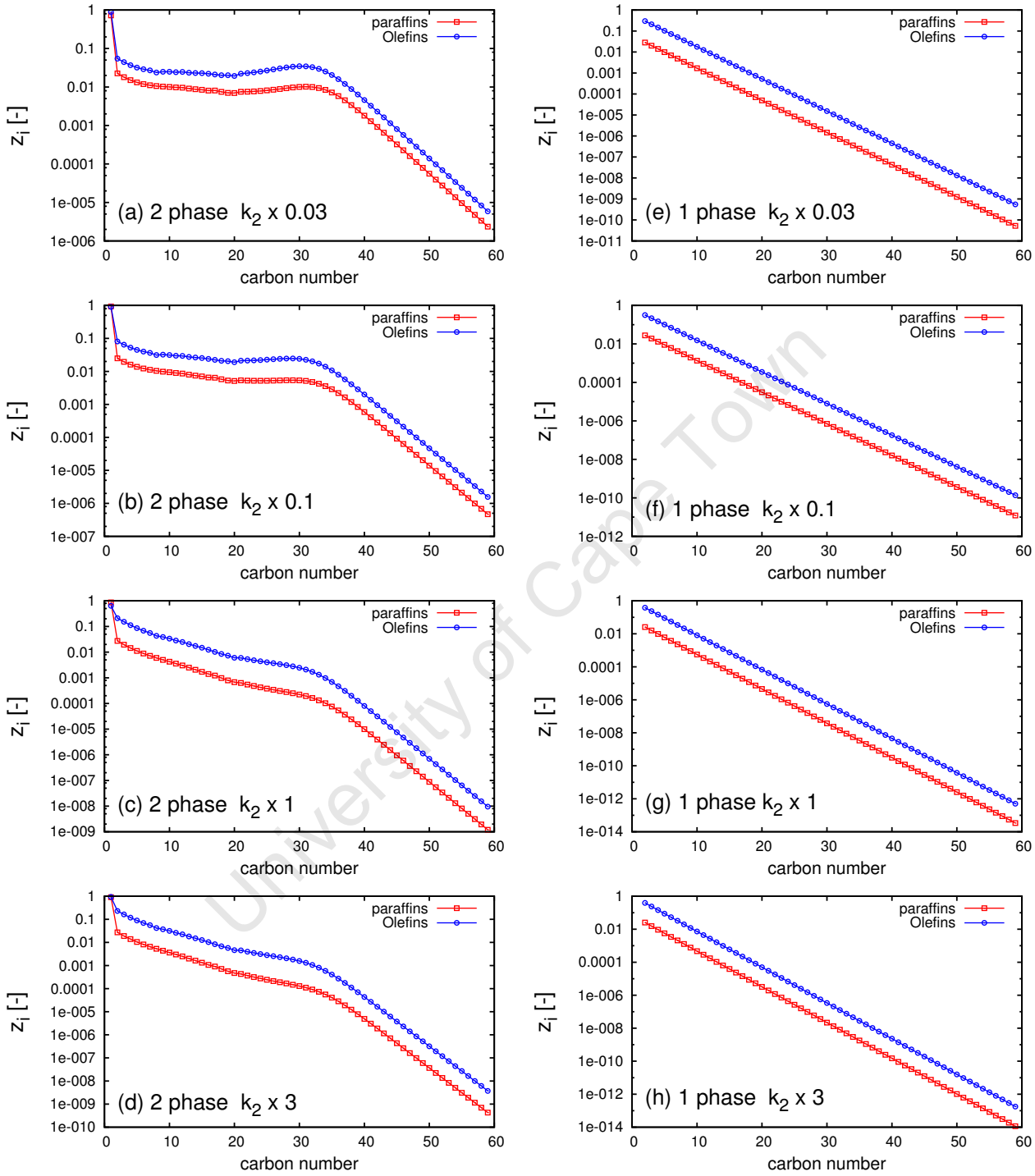

Figure 5.14: Hydrocarbon product distribution for single-phase and two-phase models, with a variation in kinetic parameter k_2

5.5.3 Effect of reaction rate constant k_3 on FTS product distribution

The effect of varying kinetic constant k_3, corresponding to chain initiation reaction 3 with rate r_3, is discussed.

$$CH_2\theta + H\theta \rightarrow CH_3\theta + \theta$$

$$r_3 = k_3\theta_{CH2*}\theta_{H*}$$

The product distribution curves for both models, in response to variation in k_3 are shown in Figure 5.15. With an increase in k_3, there's an increase in the production of $CH_3\theta$ and the

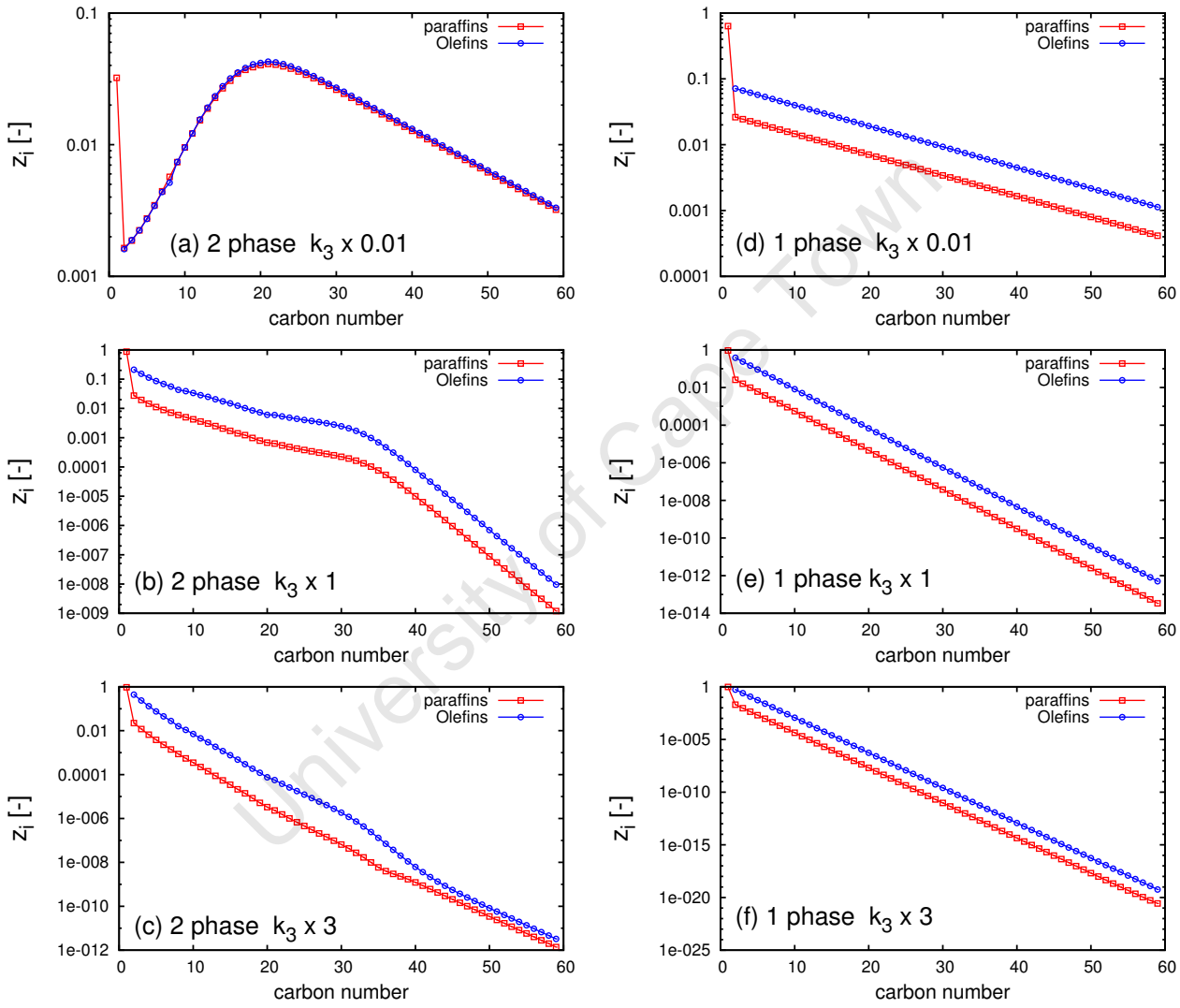

Figure 5.15: Hydrocarbon product distribution for single-phase and two-phase models, with a variation in kinetic parameter k_3

consumption of $H\theta$. It is expected, therefore that the selectivity of methane would increase with incresing k_3. This is indeed observed for both models. Due to the increased consumption of $H\theta$, it is expected that reaction 3 would compete with CO and the hydrocarbon surface species (C_nH_{2n+1}) (in reactions 1 and 7 respectively) for the hydrogen surface species. The hydrocarbon selectivity is expected to decrease with increasing k_3, as the formation of methane is encouraged. As reaction rate r_1 decreases (competing with reaction 3 for $H\theta$), the CO

conversion is therefore expected to decreasese in both models. As observed in Table 5.12, this is indeed so for both models. The product distribution for the separate models is discussed.

Table 5.12: Conversion and alpha as a function of k_3

	Single-phase model		**Two-phase model**		
k_3	X_{CO}	α_1	X_{CO}	α_1	α_2
$k_3 \times 0.01$	0.93	0.93	0.94	1.24	0.93
$k_3 \times 1$ (base case)	0.82	0.62	0.82	0.82	0.63
$k_3 \times 3$	0.77	0.47	0.77	0.61	0.64

Single-phase model With an increase in k_3, the chain growth probability factor decreases. This is expected as the formation of methane and lighter hydrocarbons is favoured.

Two-phase model With an increase in k_3, α_1 decreases, where the distribution curve goes from a positive slope (showing an increase in selectivity with increasing carbon number until a peak), to a negative slope exhibiting classical polymerisation nature. The probability of forming shorter chains is very high, for low k_3 values. For the second distribution, α_2 decreases as the formation of methane and shorter chains is favoured.

5.5.4 Effect of reaction rate constant k_4 on FTS product distribution

Reaction 4 is the methanation reaction:

$$CH_3\theta + H\theta \rightarrow CH_4 + 2\theta$$

and the corresponding reaction rate equation (r_4) is given by:

$$r_4 = k_4\theta_{CH3*}\theta_{H*}$$

The anomaly that is observed for C_1 is a common occurence in FTS product distribution, where a higher selectivity for methane is observed relative to the rest of the hydrocarbons. It is expected that with increasing k_4, an increase in the methane selectivity would be evident for both models. This is evident in both models, as shown in Figure 5.16. It is also expected that the hydrogen adsorption reaction rate (r_2) would increase, due to the availability of vacant sites. The conversion and alpha values for the two models are displayed in Table 5.13. With an

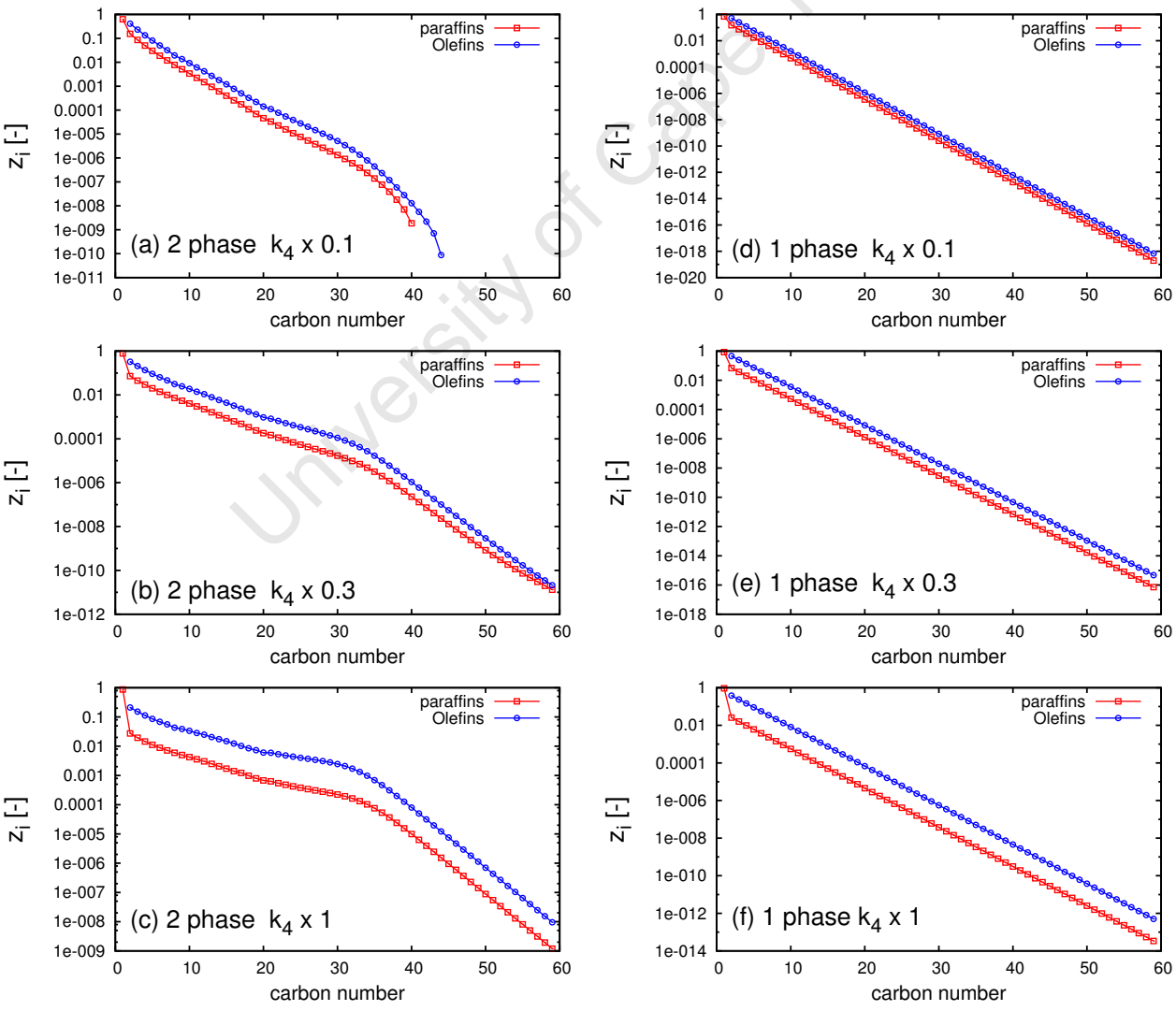

Figure 5.16: Hydrocarbon product distribution for single-phase and two-phase models, with a variation in kinetic parameter k_4

increase in k_4 the CO conversion decreases. This is due to the increased consumption of surface species $CH_3\theta$, which plays a significant role in starting the chain growth. This causes the CO conversion to decrease, as the hydrocarbon throughput is reduced. The product distribution curves for both models are discussed separately as follows.

Table 5.13: Conversion and alpha as a function of k_4

	Single-phase model		**Two-phase model**		
k_4	X_{CO}	α_1	X_{CO}	α_1	α_2
$k_4 \times 0.1$	0.90	0.41	0.88	0.64	-
$k_4 \times 0.3$	0.85	0.55	0.86	0.72	0.56
$k_4 \times 1$ (base case)	0.82	0.62	0.82	0.82	0.63
$k_4 \times 3$	0.79	0.68	0.79	0.91	0.69
$k_4 \times 10$	0.74	0.75	0.75	1.00	0.75

Single-phase model With increasing k_4 α increases, favouring the formation of longer chains. However, the selectivity of these hydrocarbons is low, a result of the increasing methane selectivity and the first chain-growth reaction (involving $CH_3\theta$) being a limiting step.

Two-phase model At the lowest k_4, there is no solution for the model beyond C_{40}, thus illustrating that there is possibly a single-phase. As k_4 increases, there are distinctly two distributions. Seeing the values in Table 5.13, for even higher k_4 values, α_1 increases, causing an upward distribution curve which reaches a maximum before the second distribution. Ignoring α_2 at $k_4 \times 0.1$, α_2 also increases with an increase in k_4. This is caused by the increasing equilibrium effect, which causes the peak to shift towards shorter hydrocarbon chains.

5.5.5 Effect of reaction rate constant k_5 on FTS product distribution

The associated reaction is the chain growth reaction 5 with reaction rate r_5.

$$CH_2\theta + C_nH_{2n+1}\theta \rightarrow C_{n+1}H_{2n+3}\theta + \theta$$

$$r_5 = k_5\theta_{CH_2*}\theta_{C_nH_{2n+1}*}$$

Table 5.14 displays the conversion and α values for both models.

Table 5.14: Conversion and alpha as a function of k_5

	Single-phase model		**Two-phase model**		
$\mathbf{k_5}$	X_{CO}	α_1	X_{CO}	α_1	α_2
$k_5 \times 0.3$	0.77	0.45	0.77	0.59	-
$k_5 \times 1$ (base case)	0.82	0.62	0.82	0.82	0.63
$k_5 \times 3$	0.86	0.74	0.87	0.99	0.74
$k_5 \times 10$	0.90	0.83	0.90	1.15	0.83

With an increase in k_5, longer-chain formation is expected as a result of the chain-growth reaction increasing. As displayed in Table 5.14, CO conversion increases with an increase in k_5 for both models due to the higher hydrocarbon throughput. The olefin:paraffin selectivity ratios (S_R) decrease in the both the single-phase and the two-phase model. An increase in k_5 increases the formation of θ, thereby increasing the hydrogen rate r_2. This, in turn, increases the CO consumption rate and increases the conversion. The paraffin formation rate is favoured (as the concentration of $H\theta$ increases), and therefore the paraffin curve approaches the olefin curve. (In the single-phase ASF plots, the scaling makes it difficult to see this). The overall hydrocarbon selectivities increase in both models, due to a consequent increase in the olefin and paraffin formation rates (r_6 and r_7). In all cases, the methane selectivity decreases, and the C_1:C_2 ratio decreases. The product distribution for both models with a variation in k_5 is illustrated in Figure 5.17.

Single-phase model With an increase in the chain growth rate, the probability of forming long chains increases (shown by the increase in α).

Two-phase model There are two chain growth probabilities. With increasing k_5, α_1 and α_2 increase, in response to the dominating equilibrium effect. The olefin:paraffin selectivity ratio is higher for distribution 1, than distribution 2 ($S_{R1} > S_{R2}$) .

With an increase in r_5, the chain initiation reaction r_3 becomes rate limiting. So an increase in k_5 has an opposite effect to an increase in k_3 (Confirmed by the ASF plots from varying k_3 in Figure 5.15). With a decrease in rate r_3, the methane selectivity therefore decreases (methanation rate r_4 limited by r_3), and the paraffin rate increases due to higher concentrations of $CH_2\theta$ and $H\theta$.

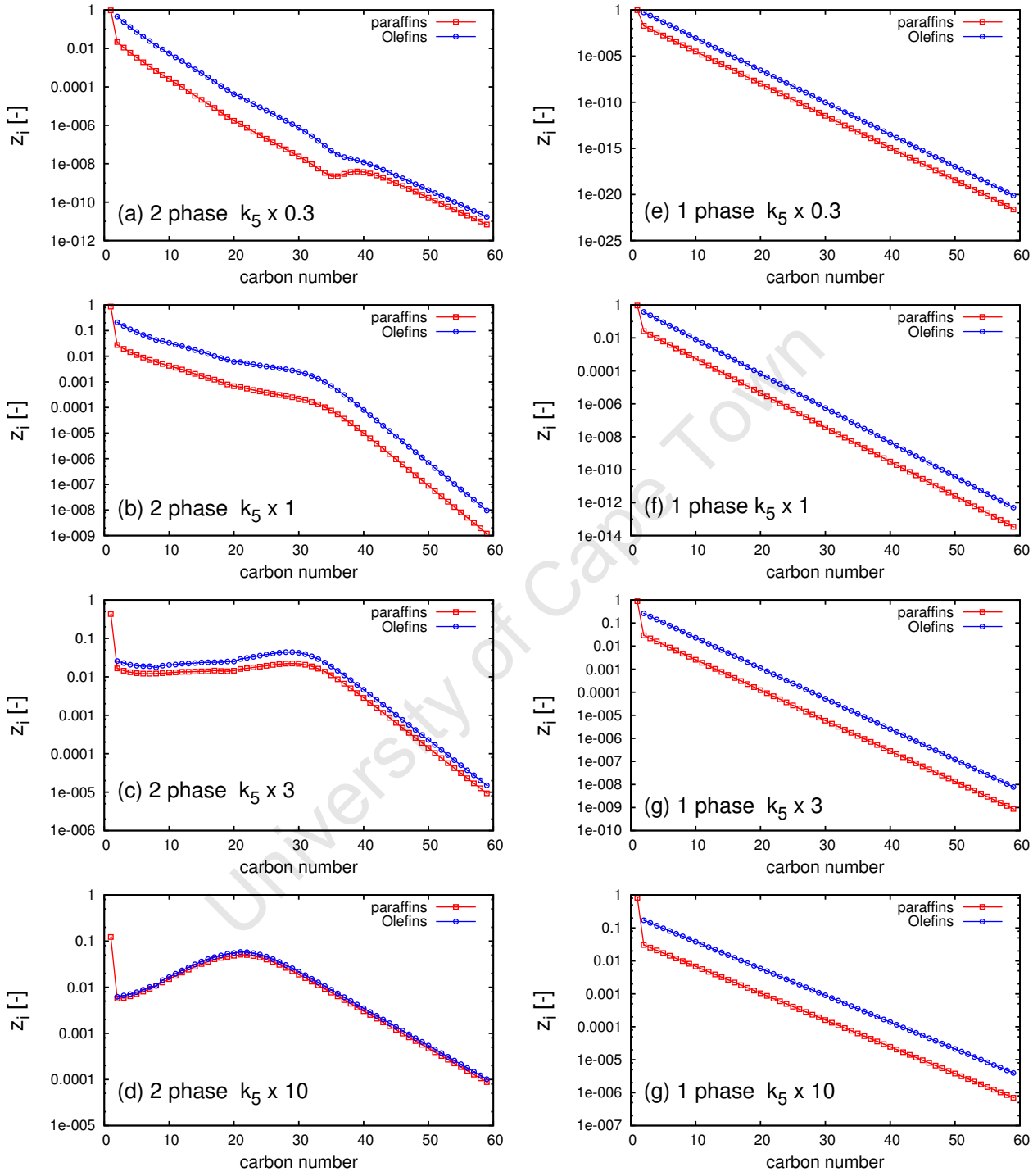

Figure 5.17: Hydrocarbon product distribution for single-phase and two-phase models, with a variation in kinetic parameter k_5

5.5.6 Effect of reaction rate constant k_{6f} on FTS product distribution

The olefin forward reaction discussed in this section is

$$C_nH_{2n+1}\theta \longrightarrow C_nH_{2n} + H\theta$$

with reaction rate r_6.

$$r_6 = k_{6f}\theta_{Cn+2n+1*}$$

With an increase in the olefin formation rate, the selectivity of olefins is expected to increase for both models. Conversion and alpha as a function of k_{6f} are displayed in Table 5.15.

Table 5.15: Conversion and alpha as a function of k_{6f}

	Single-phase model		**Two-phase model**		
$\mathbf{k_{6f}}$	X_{CO}	α_1	X_{CO}	α_1	α_2
$k_{6f} \times 0.1$	0.84	0.85	0.84	1.18	0.85
$k_{6f} \times 0.3$	0.83	0.78	0.83	1.10	0.78
$k_{6f} \times 1$ (base case)	0.82	0.62	0.82	0.82	0.63

An increase in k_{6f} results in a slight decrease in CO conversion and a large decrease in α. The small change is due to the increase in the hydrogen adsorption rate r_2 (as more vacant sites are available (θ) and the consequent increase in $H\theta$). This shows that by increasing k_{6f}, α can be varied with no (or very little) change in the CO conversion. The product distribution curves are displayed in Figure 5.18, and discussed separately for the two models.

Single-phase model With an increase in k_{6f}, the olefin:paraffin selectivity ratio (S_R) increases as a result of the higher olefin formation rate, and the chain growth probability factor, α decreases.

Two-phase model The olefin:paraffin selectivity ratio also increases with increasing k_{6f}, as observed in the single phase model. With an increase in k_{6f} the alpha values for both distributions decrease (α_1 and α_2). As alpha decreases, the liquid fraction is reduced, and single-phase behaviour is approached.

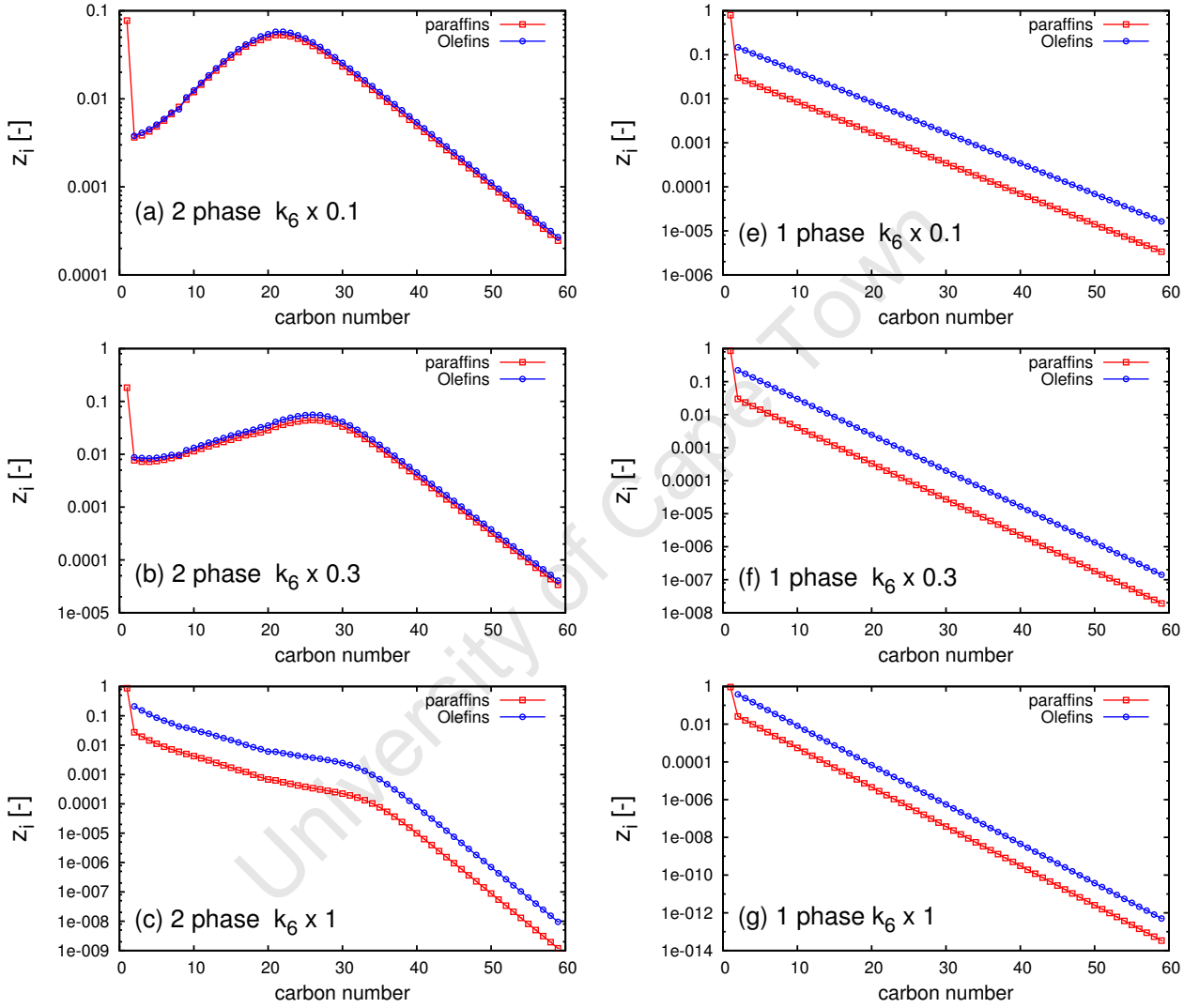

Figure 5.18: Hydrocarbon product distribution for single-phase and two-phase models, with a variation in kinetic parameter k_{6f}

5.5.7 Effect of olefin reverse reaction rate constant k_{6r} on FTS product distribution

One of the important discussion points in FTS is the effect of olefin readsorption on the FTS product distribution, as deviations from ASF distribution have often been attributed to this. The reaction is given by:

$$C_nH_{2n+1}\theta \leftrightarrow C_nH_{2n} + H\theta$$

with reaction rate r_6

$$r_6 = k_{6f}\theta_{Cn+2n+1*} - k_{6r}\bar{a}_{CnH2n}\theta_{H*}$$

The base case is a reverse rate constant, $k_{6r} = k_1 \times 6.7E-07$, meaning that the reverse reaction rate is a lot slower than the forward reaction rate, encouraging the formation rate of olefins. The results to varying this rate constant for the two-phase system are shown in Figure 5.19.

Table 5.16: Conversion and alpha as a function of k_{6r}

	Single-phase model		**Two-phase model**		
$\mathbf{k_{6r}}$	X_{CO}	α_1	X_{CO}	α_1	α_2
$k_{6r} \times 10^2$	0.82	0.62	0.82	0.82	0.64
$k_{6r} \times 10^4$	0.82	0.62	0.82	0.82	0.93
$k_{6r} \times 10^6$	0.82	0.80	0.82	0.85	1.00

An increase in k_{6r} has no effect on the conversion of CO. As the olefin readsorption reaction increases, the formation of hydrocarbon surface species $\theta_{C_nH_{2n+1}}$ increases. This results in an increase in the chain-growth reaction rate r_5 and the paraffin formation rate r_7. The paraffin selectivity therefore increases, and is observed for both models. The conversion does not change, as reaction rates r_1 and r_2 do not change. $H\theta$ being consumed in reverse reaction r_6 is made up by $H\theta$ being produced in reaction r_2 (increased θ from reaction r_7 and r_5), causing a zero net effect on conversion.

Single-phase model There is no effect on α at smaller k_6r values because reversibility is not yet significant. With an increase in k_{6r} there is an increase in α (from 0.62 to 0.8) due to an increase in the chain growth reaction rate r_5. This encourages the formation of longer chains, thus the chain growth probability increases. The olefin:paraffin selectivity ratio increases with increasing k_{6r} as a result of the reduced olefin formation. There is an upward movement in the product distribution curve with increasing k_{6r} signifying an increase in the hydrocarbon selectivity ($z_{C_{59}}$) increases by orders of magnitude $\approx$ 1E-14 to 1E-08).

Two-phase model There's interesting behaviour observed in the two-phase model curves. With an increase in k_{6r}, there's an increase in the overall hydrocarbon selectivity, shown by the upward shifting of the distribution curves ($z_{C_{59}}$ increases by orders of magnitude $\approx$ 1E-08 to 0.01). There is a significant increase in the paraffin selectivity, where it exceeds the olefin selectivity at the highest k_{6r}. This is explained by a decrease in the olefin

formation rate r_6 and the consequent increase in the paraffin formation rate r_7. The olefin curve decreases by following a double exponetial decrease. The paraffin product distribution curve rises, displaying an increase in the paraffin formation rate, until the kinetic effect overcomes the equilibrium effect, at carbon numbers $C_n > C_{33}$.

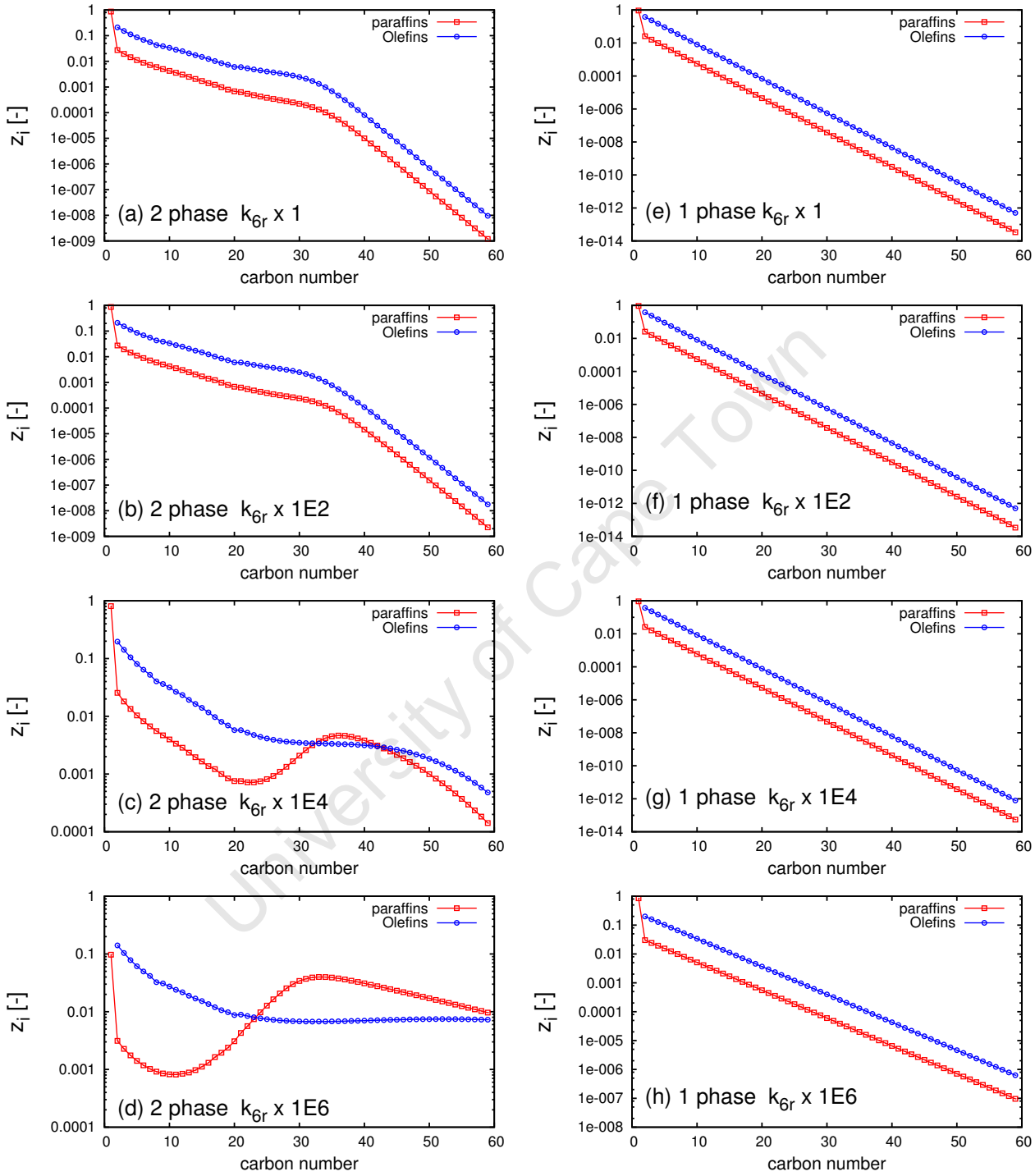

Figure 5.19: Hydrocarbon product distribution for single-phase and two-phase models, with a variation in kinetic parameter k_{6r}

5.5.8 Effect of paraffin reaction rate constant k_7 on FTS product distribution

The paraffin formation reaction is given by reaction 7 in the proposed mechanism:

$$C_nH_{2n+1}\theta + H\theta \rightarrow C_nH_{2n+2} + 2\theta$$

with reaction rate r_7

$$r_7 = k_7\theta_{CnH2n+1*}\theta_{H*}$$

The effect of varying the paraffin formation rate constant k_7 on FTS product distributions is given in Figure 5.20 for both models.

Table 5.17: Conversion and alpha as a function of k_7

	Single-phase model		**Two-phase model**		
$\mathbf{k_7}$	X_{CO}	α_1	X_{CO}	α_1	α_2
$k_7 \times 0.1$	0.82	0.63	0.83	0.84	0.64
$k_7 \times 0.3$	0.82	0.63	0.83	0.83	0.64
$k_7 \times 1$ (base case)	0.82	0.62	0.82	0.82	0.63
$k_7 \times 3$	0.81	0.59	0.82	0.78	0.60
$k_7 \times 10$	0.79	0.52	0.80	0.69	0.58

As observed, at lower k_7 values, there is a gap between the paraffin and the olefin curves, with the olefin distribution above the paraffin distribution (exhibiting a higher olefin:paraffin selectivity ratio S_R). As the value of k_7 increases, S_R decreases. This is expected as the magnitude of paraffins produced increases as a result of the rate increase, approaching a distribution identical to the olefin distribution. This is shown in the equation for $\left(\frac{r_6}{r_7}\right)$:

$$\frac{r_6}{r_7} = \frac{k_{6f}}{k_7\theta_{H*}} - \frac{k_{6r}a_{C_nH_{2n}}}{k_7\theta_{C_nH_{2n+1*}}}$$

$$\frac{r_6}{r_7} = \left(\frac{1}{k_7}\right) \cdot \left(\frac{k_{6f}}{\theta_{H*}} - \frac{k_{6r}a_{C_nH_{2n}}}{\theta_{C_nH_{2n+1*}}}\right)$$

An increase in k_7 decreases the olefin production rate relative to the paraffin production rate, thus the paraffin curve moves up. Observing these trends, the paraffin rate constant does not affect the olefin distribution curve until such time that the distribution curves are equal ($k_7 = k_1 \times 9.71E01$). The olefin curve sets the upper limit to the paraffin distribution curve. Instead of exceeding the olefin curve, and having a larger distribution than the olefin curve, the 'peak' in the curve shifts to higher carbon numbers, and exhibits a much flatter slope. This can be explained by the paraffin formation rate equation r_7 being dependent on the production of $H\theta$ from the olefin reaction r_6. The only way that the paraffin curve can exceed the olefin curve is through a larger olefin reverse rate constant k_{6r}.

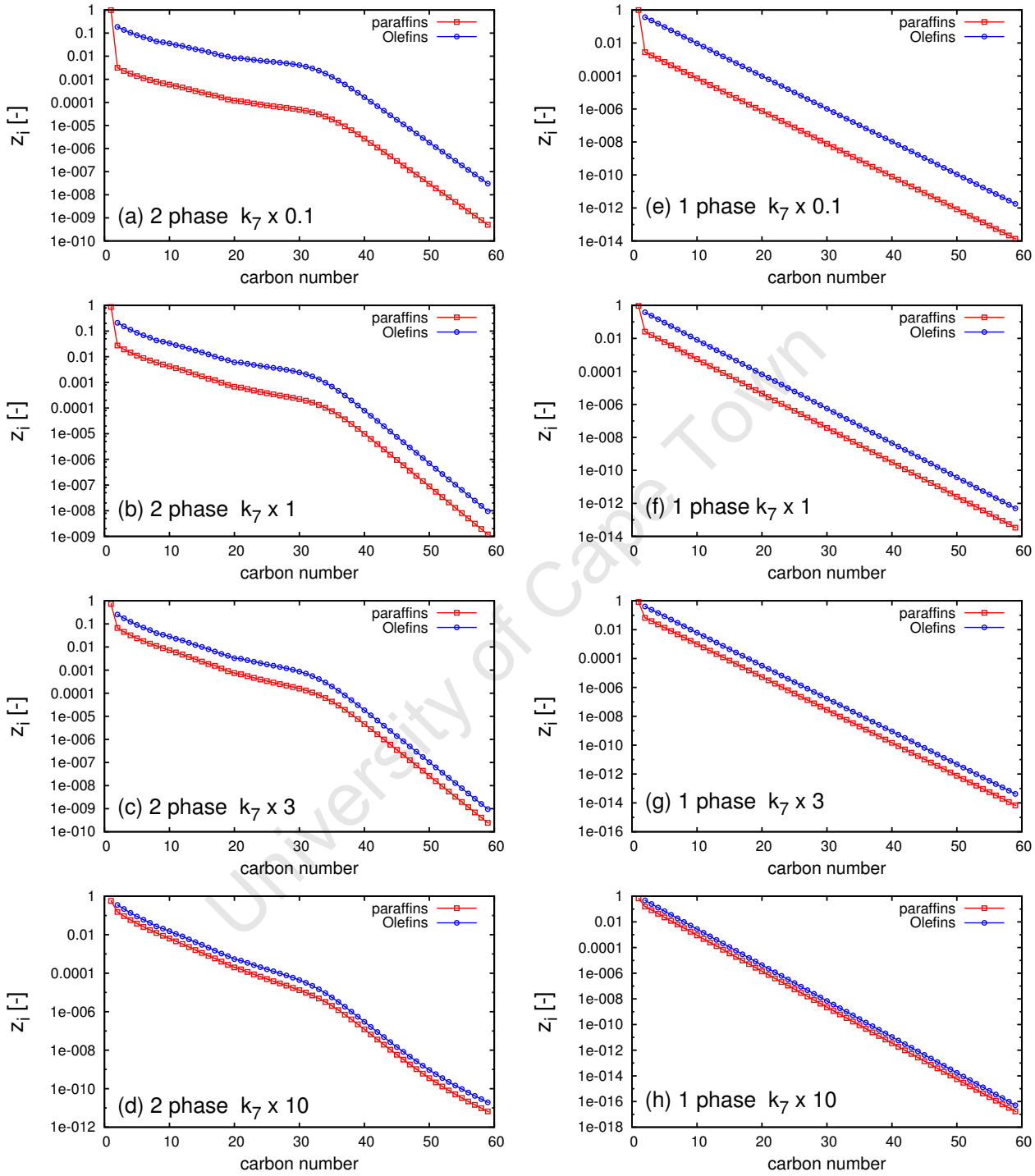

Figure 5.20: Hydrocarbon product distribution for single-phase and two-phase models, with a variation in kinetic parameter k_7

5.6 Overall analysis of the kinetic parameters on the FTS product distribution

The effects of all the kinetic parameters on the FTS product distribution is summarised below, and the optimal combination of constants determined. Table 5.18 shows the effect that increasing the kinetic parameters has on selectivity, conversion and chain growth probability constant α. The overall selectivity is influenced by the methane selectivity, which controls the starting points of the distribution curves. It is defined as an increase in the entire hydrocarbon selectivity, and shown by the upward or downward shift of the distribution curve.

Table 5.18: Summary of the effects of increasing kinetic parameters

		Effect on both models		**Effect on single-phase model**		**Effect on two-phase model**		
k_i	**Reaction rate**	**X_{CO}**	**Overall selectivity**	**Olefin:paraffin selectivity ratio**	**α_1**	**Olefin:paraffin selectivity ratio**	**α_1**	**α_2**
$k_1 \uparrow$	$r_1 \uparrow$	$\uparrow$	$\uparrow$	$\uparrow$	$\uparrow$	$\downarrow$	$\uparrow$	$\downarrow\uparrow$
$k_2 \uparrow$	$r_2 \uparrow$	$\uparrow$	$\downarrow$	$\downarrow$	$\downarrow$	$\downarrow$	$\downarrow$	$\downarrow$
$k_3 \uparrow$	$r_3 \uparrow$	$\downarrow$	$\downarrow$	$\downarrow$	$\downarrow$	$\uparrow$	$\downarrow$	$\downarrow$
$k_4 \uparrow$	$r_4 \uparrow$	$\downarrow$	$\downarrow$	$\uparrow$	$\uparrow$	$\uparrow$	$\uparrow$	$\uparrow$
$k_5 \uparrow$	$r_5 \uparrow$	$\uparrow$	$\uparrow$	$\downarrow$	$\uparrow$	$\downarrow$	$\uparrow$	$\uparrow$
$k_{6f} \uparrow$	$r_{6f} \uparrow$	$\downarrow$	$\downarrow$	$\uparrow$	$\downarrow$	$\uparrow$	$\downarrow$	$\downarrow$
$k_{6r} \uparrow$	$r_{6r} \uparrow$	-	$\uparrow$	$\downarrow$	$\uparrow$	$\uparrow$	$\uparrow$	$\uparrow$
$k_7 \uparrow$	$r_7 \uparrow$	$\downarrow$	$\downarrow$	$\downarrow$	$\downarrow$	$\uparrow$	$\downarrow$	$\downarrow$

Looking at the relationship between α and conversion, an increase in reaction rates (r_1,r_3, r_5 and r_7) either increases or decreases both the conversion and α. The parameters corresponding to these reactions (k_1, k_3, k_5 and k_7) are classified under group 1. An increase in reaction rates (r_2 and r_4) causes α and conversion to have opposite effects, that is α decreases with increasing X_{CO} and vice versa respectively. The parameters for these reactions (k_2 and k_4) are classified under group 2. Reaction r_6 doesn't affect the conversion as much as the other reactions,

whereby there's an increase in α with very little (or no change) in conversion. The parameters for reaction r_6 (k_{6f} and k_{6r}) are classified under group 3. Alpha vs. Conversion is plotted for both the single-phase and the two-phase models for the 3 parameter groups, to demonstrate this.

Single-phase model As shown in Figure 5.21, α increases linearly with conversion for group 1 constants, decreases logarithmically with conversion for group 2 constants, and increases at a constant conversion for group 3 parameters.

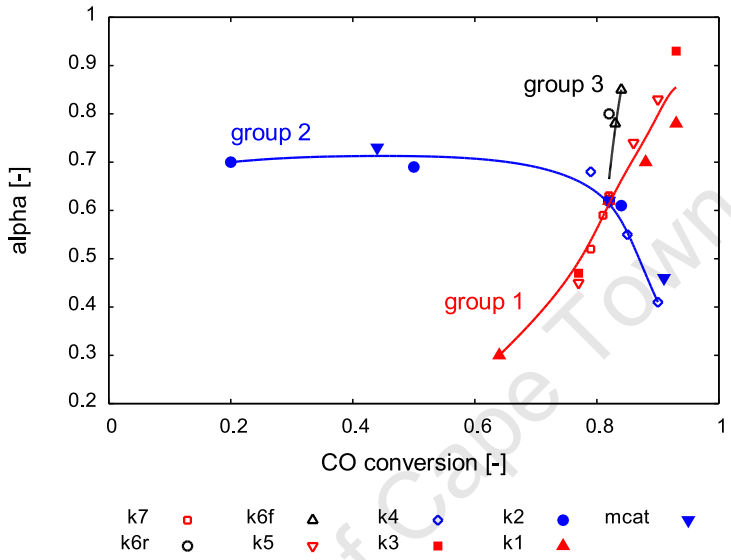

Figure 5.21: α as a function of conversion for the 3 parameter groups for the single-phase model

Two-phase model There are two chain-growth probabilities, α_1 and α_2. α_1 follows similar behaviour as for the single-phase model, as shown in Figure 5.22, The main difference

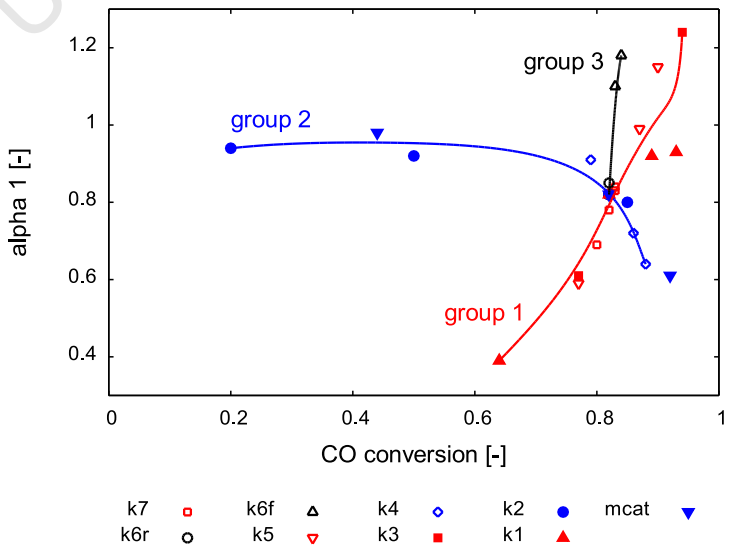

Figure 5.22: α_1 as a function of conversion for the 3 parameter groups in the two-phase model

between these trends and those observed in the single-phase model, is a wider range of α due to the effect of VLE.

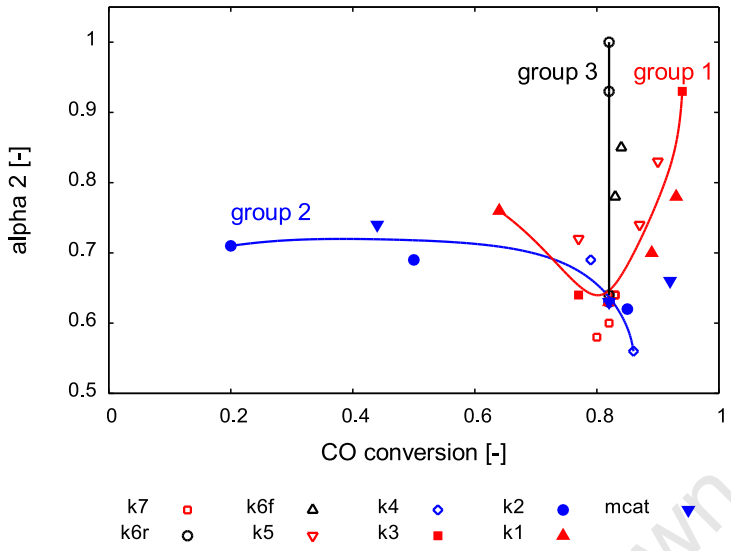

Figure 5.23: α_2 as a function of conversion for the 3 parameter groups in the two-phase model

The second chain growth probability factor α_2 exhibits different behaviour to the single-phase model for the group 1 constants. The α curve is parabolic with a minimum at $X_{CO} = 0.8$. This is due to the effect of constant k_1. The combination of the catalyst loading and the k_1 value is important. As shown in equation 5.24, CO conversion is directly proportional to both the catalyst loading and reaction rate r_1. Recalling Figure 5.12, α decreased with increasing conversion. Therefore, for a constant catalyst loading, at low k_1, the α decreases (following a trend as observed in Figure 5.12), until k_1 is high enough to increase α vs. conversion trend. Similar trends, as observed in Figures 5.21 and 5.22, are observed for group 2 and group 3 constants, with the increase in α_2 being greater for the group 3 parameters.

This information makes it possible to determine which kinetic constants to vary so as to maximise FTS yield. For example, in order to maximise wax production in realistic two-phase operation, constants which result in an increase in both conversion and chain growth probability would be increased, as in parameters k_1 and k_5. The olefin:paraffin selectivity ratio would decrease with an increase in these kinetic constants for both cases, so this is something that would have to be considered. Similarly, to favour the formation of shorter hydrocarbon chains, the constant(s) which result in a high conversion and lower α would be increased, such as parameter k_2. The practical way in which the kinetic constants can be modified is by observing nd altering the cobalt catalyst properties.

Chapter 6

Conclusions and Recommendations

6.1 Conclusions

The objectives in this work were to:

- develop a complete two-phase Fischer Tropsch model,
- predict the hydrocarbon product distribution,
- determine the effect that VLE has on the product distribution, selectivity and the kinetics, and
- determine whether the deviations from "ideal" ASF distribution can be described to VLE

The objectives of this work were realised and a complete FTS model was developed both for a system that doesn't take equilibrium into account, and one that does. The hydrocarbon product distribution was predicted, and compared to standard product distribution models for this sort of system. The effect of VLE on the distribution was determined, and it was confirmed that VLE plays a significant role in the selectivity and distribution of hydrocarbons for this continuous system. The system's sensitivity to a variation in process conditions and kinetic parameters was studied, so as to determine which conditions result in optimal FTS yield.

6.1.1 Developing the complete Fischer Tropsch models

Two models were developed for modelling FTS in a slurry phase reactor: a-single phase model and a two-phase model. For the two-phase model, the effect of VLE on the FTS product distribution and selectivity was studied, by modelling the kinetics as a function of the thermodynamic variable activity. In the two-phase model, activity was defined as the ratio of the partial molar fugacity of the species to the fugacity of the pure component at a pressure $P = 1$bar. In the single phase model, the activity was considered as the ratio of the species partial pressure to the standard pressure. To conduct an effective comparison, the operating conditions and kinetic parameters for both models were the same, the only difference being the activity. This was done to observe the sole effect of VLE on FTS product distribution and selectivity.

6.1.2 The effect of VLE on product distribution, selectivity and kinetics

Effect on product distribution VLE causes a movement of hydrocarbon species from a prodominantly vapour-rich phase to a predominantly liquid rich phase, and thus increases the chain-growth probability. Therefore, the probability of forming longer hydrocarbon chains is increased.

Effect on product selectivity A higher methane selectivity than the rest of the hydrocarbons was observed for both models as expected, where the C_1:C_2 molar ratio $\left(\frac{z_{C_1}}{z_{C_2}}\right)$ was higher in the single-phase model at 36.3, than the two-phase model, at 31.9. Therefore, VLE decreases the $C_1 : C_2$ ratio.

VLE increases the overall hydrocarbon selectivity, and increases the paraffin:olefin selectivity ratio for carbon numbers $< C_{32}$ for olefins, and $< C_{33}$ for paraffins, after which point all the hydrocarbons are effectively in the liquid phase, and the selectivity ratio drops. The selectivity ratio in the two-phase model is lower in the single-phase model, due to the effect of the thermodynamic factor γ.

Effect on kinetics VLE has a very small (almost no) effect on the kinetics in the two phase model. This is because the kinetics are driven by the activities of CO and H_2 (as shown in the proposed mechanism, Table 3.7) which are very similar. The reason there's a deviation from the classical ASF distribution in the two-phase model, is due to a distortion factor D, a function of the relative rates in the reactor, which differ as a result of VLE. The resulting Differential Algebraic Equations (DAE) systems for both models are significantly different, thus the product distributions are different.

6.1.3 Effect of process parameters on FTS chain growth probability and conversion

A variation in catalyst loading and pressure was conducted in order to observe the effect on the FTS product distribution, and to determine the relationship between α and conversion.

- Increasing catalyst loading, increases the CO conversion, as it is directly proportional to the residence time, and decreases α. This applies to both the single-phase and two-phase model.

- Increasing the pressure increases both the CO conversion and the probability of forming longer chains (α).

6.1.4 Effect of kinetic parameters on FTS chain growth probability and conversion

The effects of the kinetic parameters, as per the proposed reaction mechanism, on the FTS product distribution and selectivity, for the two-phase model were studied. An increase in the rates of the CO adsorption reaction r_1 and the chain growth reaction r_5, result in both the CO conversion and α increasing. An increase in the chain initiation reaction r_3 and the paraffin formation reaction r_7, result in both the CO conversion and α decreasing. The constants associated with both X_{CO} and α increasing or decreasing were placed in group 1. An increase in the hydrogen adsorption rate r_2 decreases α with increasing conversion, and increasing the methanation rate r_4 has the opposite effect. Increasing reaction rate r_6 has very little (or no) effect on the conversion, and shows a slight increase in α.

6.1.5 Relationship between α and conversion

The relationship between CO conversion (X_{CO}) and chain-growth probability factor is determined by a combination of operating parameters (pressure and catalyst loading) and the kinetic parameters. From sudying the effect of both the process parameters and the kinetic parameters on the FTS product distribution, the following conclusions are drawn to determine the relationship α and conversion.

High conversion, large alpha

In order to have a high CO conversion, with a large chain-growth probability factor, as in the event of maximising wax yield:

1. operate at higher pressures ($P \geq 20$bar) and
2. increase the net CO adsorption and chain-growth reaction rate constants (k_1 and k_5 respectively) to increase the CO consumption and increase the rate of forming longer hydrocarbon intermediates respectively.

High conversion, small alpha

In order to have a high conversion with a small chain-growth probability factor, as in the event of maximising on shorter-chain hydrocarbon yield:

- increase the catalyst loading and
- increase the hydrogen adsorption reaction constant k_2.

α is not solely dependent on conversion, but dependent on a combination of process parameters (catalyst loading and pressure) and the kinetic parameters.

6.2 Recommendations

In such a system, there are numerous studies that can be performed. The two-phase model is setup such that it is easy to observe the behaviour of the FTS product distribution with modifications on the parameters. The following recommendations are made for the improvement of the model:

- Data for a two-phase slurry reactor could be fitted to the model in order to determine the kinetic constants, by following a regression technique. The findings from this work could then be applied to the constants to optimise on FT processes.
- Even though a variation in each of these individual constants exhibited an effect on the distribution, the combined effect of these constants could be investigated by conducting a thorough statistical analysis and sensitivity analysis.

Bibliography

Ahon, V. R., Costa, Jr., E. F., Monteagudo, J. E., Fontes, C. E., Biscaia, Jr., E. C., Lage, P. L., Feb. 2005. A comprehensive mathematical model for the Fischer-Tropsch synthesis in well-mixed slurry reactors. Chemical Engineering Science 60 (3), 677–694.

Anfray, J., Bremaud, M., Fongarland, P., Khodakov, A., Jallais, S., Schweich, D., 2007. Kinetic study and modeling of Fischer-Tropsch reaction over a Co/Al_2O_3 catalyst in a slurry reactor. Chemical Engineering Science 62 (18-20), 5353–5356.

Berger, R. J., Stitt, H. E., Marin, B. B., Freek, K., A, M. J., 2001. Chemical reaction kinetics in practice. Cattech 5, 30 – 60.

Bukur, D., Froment, G., Olewski, T., 2005. Kinetics of Slurry Phase Fischer Tropsch Synthesis. Tech. rep., Texas A & M University.

Chang, J., Bai, L., Teng, B., Zhang, R., Yang, J., Xu, Y., Xiang, H., Li, Y., 2007. Kinetic modeling of Fischer-Tropsch synthesis over Fe-Cu-K-SiO2 catalyst in slurry phase reactor. Chemical Engineering Science 62 (18-20), 4983–4991.

Daubert, T., Danner, R., Sibul, H., Stebbins, C., Rowley, R., Wilding, W., Oscarson, J., Adams, M., T.L., M., 1999. Physical and thermodynamic properties of pure chemicals. Taylor & Francis, Philadelphia, USA.

Dictor, R. A., Bell, A. T., 1983. An explanation for deviations of Fischer-Tropsch products from a Schulz-Flory distribution. Ind. Eng. Chem. Process Des. Dev. 22 (4), 678681.

Donnelly, T. J., Yates, I. C., Satterfield, C. N., Nov. 1988. Analysis and prediction of product distributions of the Fischer-Tropsch Synthesis. Energy & Fuels 2 (6), 734–739.

Dry, M. E., 1982. Catalytic aspects of industrial Fischer Tropsch Synthesis. J. Molecular Catalysis 17, 133–144.

Dry, M. E., May 1996. Practical and theoretical aspects of the catalytic Fischer-Tropsch process. Applied Catalysis A: General 138 (2), 319–344.

Dry, M. E., Jan. 2002. The Fischer-Tropsch process: 1950-2000. Catalysis Today 71 (3-4), 227–241.

Elliot, J. R., Lira, C. T., 1999. Introductory Chemical Engineering Thermodynamics. Prentice Hall International Series.

Fogler, H. S., 1999. Elements of Chemical Reaction Engineering, 3rd Edition. Prentice Hall.

Hall, C. C., 1949. Recent Research on the Fischer -Tropsch Synthesis. In: The Industrial Chemist.

Heese, F. P., 1998. The thermodynamics, mechanism and kinetics of the catalytic conversion of propylene and water to diisopropyl ether over amethyst 15. Ph.D. thesis, University of Cape Town.

Krishna, R., Sie, S. T., May 2000. Design and scale-up of the Fischer-Tropsch bubble column slurry reactor. Fuel Processing Technology 64 (1-3), 73–105.

Krishnamoorthy, S., Tu, M., Ojeda, M. P., Pinna, D., Iglesia, E., Oct. 2002. An investigation of the effects of water on rate and selectivity for the fischer-tropsch synthesis on cobalt-based catalysts. Journal of Catalysis 211 (2), 422–433.

Kuipers, E., Scheper, C., Wison, J., Vinkenburg, I., Oostarbeek, H., 1996. Non-ASF product distributions due to secondary reactions during Fischer-Tropsch synthesis. Journal of Catalysis 158, 288 – 300.

Ledakowicz, S., Nettelhoff, H., Kokuun, R., Deckwer, W. D., Oct. 1985. Kinetics of the Fischer-Tropsch synthesis in the slurry phase on a potassium promoted iron catalyst. Industrial & Engineering Chemistry Process Design and Development 24 (4), 1043–1049.

Lox, E., Froment, G., 1993. Kinetics of the Fischer-Tropsch reaction on a precipitated promoted iron catalyst. Ind Eng. Chem Res 32, 71–82.

Lozano-Blanco, G., Thybaut, J. W., Surla, K., Galtier, P., Marin, G. B., Aug. 2008. Single-Event Microkinetic Model for Fischer Tropsch Synthesis on Iron-Based Catalysts. Industrial & Engineering Chemistry Research 47 (16), 5879–5891.

Mushrif, S. H., 2004. Determining Equation Of State Binary Interaction Parameters Using K and L Points. Master's thesis, University of Saskatchewan.

Nishiumi, H., Gotoh, H., 1990. Generalization of binary interaction parameters of Peng-Robinson equation of state for systems containing hydrogen. Fluid Phase Equilibria 56, 81–88.

Orbey, H., Sandler, S., 1997. Cubic Equations of State for Modeling the Vapour-Liquid Equilibrium of NonIdeal Mixtures. University of Delaware, Newark.

Patzlaff, J., Liu, Y., Graffman, C., Gaube, J., 1999. Studies on product distributions of iron and cobalt catalyzed Fischer-Tropsch synthesis. Applied Catalysis 186, 109 – 119.

Petersen, C. S., 1989. A Systematic and Consistent Approach to Determine Binary Interaction Coefficients for the Peng-Robinson Equation of State. SPE ReserVoir Eng. 1, 488494.

Puskas, I., Hurlbut, R. S., Aug. 2003. Comments about the causes of deviations from the Anderson-Schulz-Flory distribution of the Fischer-Tropsch reaction products. Catalysis Today 84 (1-2), 99–109.

Raje, A. P., Davis, B. H., Jan. 1996. Effect of VaporLiquid Equilibrium on FischerTropsch Hydrocarbon Selectivity for a Deactivating Catalyst in a Slurry Reactor. Energy & Fuels 10 (3), 552–560.

Sandler, S. I., 1999. Chemical and Engineering Thermodynamics, 3rd Edition. John Wiley & Sons, Inc.

Schulz, H., Claeys, M., Oct. 1999. Kinetic modelling of Fischer-Tropsch product distributions. Applied Catalysis A: General 186 (1-2), 91–107.

Smith, M., Van Ness, H, C., Abbott, M, M., 2001. Introduction to Chemical Engineering Thermodynamics. McGraw Hill.

Teng, B., Chang, J., Wan, H., Lu, J., Zheng, S., Liu, Y., Guo, X., 2007. A Corrected Comprehensive Kinetic Model of Fischer-Tropsch Synthesis. Chinese Journal of Catalysis 28, 687 – 695.

Twu, C. H., Coon, J. E., 2000a. Convenient methods for the derivation of binary interaction parameters for cubic equations. Tech. rep., Simulation Sciences Inc.

Twu, C. H., Coon, J. E., 2000b. Shortcut method for estimating binary interaction parameters between pseudo-components for use in cubic equation of state. Tech. rep., Simulation Sciences Inc.

Twu, C. H., Coon, J. E., Cunningham, J. R., Mar. 1995. A new generalized alpha function for a cubic equation of state part 2. redlich-kwong equation. Fluid Phase Equilibria 105 (1), 61–69.

van der Laan, G., Beenackers, A., 1999a. Hydrocarbon Selectivity Model for the Gas-Solid Fischer Tropsch Synthesis on Precipitated Iron Catalysts. Industrial and Engineering Chemistry Research 38 (4), 1277 – 1290.

van der Laan, G., Beenackers, A., 1999b. Kinetics and Selectivity of Fischer-Tropch Synthesis: a literature review. Catalysis Reviews. Science and Engineering 41, 255 – 318.

van der Laan, G., Beenackers, A. A., Rajamani, K., 1999. Multicomponent reaction engineering model for Fe-catalyzed Fischer-Tropsch synthesis in commercial scale slurry bubble column reactors. Chemical Engineering Science 54, 5013 – 5019.

van Steen, E., Schulz, H., Oct. 1999. Polymerisation kinetics of the Fischer-Tropsch CO hydrogenation using iron and cobalt based catalysts. Applied Catalysis A: General 186 (1-2), 309–320.

Vessia, O., February 2002. Fischer- tropsch reactor fed by syngas. `http://www.zero.no/transport/bio/fischer-tropsch-reactor-fed-by-syngas`.

Visconti, C. G., Tronconi, E., Lietti, L., Zennaro, R., Forzatti, P., 2007. Development of a complete kinetic model for the Fischer-Tropsch synthesis over Co/Al2O3 catalysts. Chemical Engineering Science 62 (18-20), 5338–5343.

Wang, G., Wang, Y.-N., Yang, J., Xu, Y.-Y., Bai, L., Xiang, H.-W., Li, Y.-W., May 2004. Modeling Analysis of the FischerTropsch Synthesis in a Stirred-Tank Slurry Reactor. Industrial & Engineering Chemistry Research 43 (10), 2330–2336.

Withers, H. P., Eliezer, K. F., Mitchell, J. W., Sep. 1990. Slurry-phase Fischer-Tropsch synthesis and kinetic studies over supported cobalt carbonyl derived catalysts. Industrial & Engineering Chemistry Research 29 (9), 1807–1814.

Yang, J., Liu, Y., Chang, J., Wang, Y.-N., Bai, L., Xu, Y.-Y., Xiang, H.-W., Li, Y.-W., Zhong, B., Oct. 2003. Detailed Kinetics of FischerTropsch Synthesis on an Industrial FeMn Catalyst. Industrial & Engineering Chemistry Research 42 (21), 5066–5090.

Yates, I. C., Satterfield, C. N., 1991. Intrinsic kinetics of the Fischer Tropsch synthesis on a cobalt catalyst. Energy Fuels 5, 168–173.

Zhan, X., Davis, B. H., 2000. Two alpha Fischer Tropsch Product Distribution. A role for Vapour-Liquid Equilibrium? Petroleum Science and Technology 18, 1037 – 1053.

Zimmerman, W. H., Bukur, D., Ledakowicz, S., 1992. Kinetic model of Fischer-Tropsch selectivity in the slurry phase. Chemical Engineering Science 47, 2707 – 2712.

Appendix A

Correlation of critical values to higher carbon numbers

The critical values of higher carbon number paraffins and olefins were obtained by extrapolating existing data to higher carbon numbers, on the basis of proposed correlations. A least squares approach was taken, where the parameters that minimize the sum of the squared differences between the actual data and the fitted values were calculated for.

The critical pressure (P_c) values were observed to follow a decreasing exponential function with slight deviation at lower carbon numbers, whereas the accentric factor values increased with increasing carbon number; Correlation A.1 was proposed to fit the critical pressure and accentric factor data.

$$y = A \cdot \exp\left(-B \cdot C_n\right) + \frac{C}{C_n} + D \tag{A.1}$$

A, B, C and D were the constants to be solved for and C_n denotes the carbon number. The critical temperature exhibited an increasing logarithmic rise with increasing carbon number. A least squares fit could not be obtained from correlation A.1, therefore correlation A.2 was proposed.

$$y = A \cdot \ln C_n + \frac{C}{C_n} + D \tag{A.2}$$

The obtained parameter values are given in Table A, and the graphical results exhibited in Figures A.1 for the paraffins, and Figure A.2 for the olefins.

Table A.1: Correlated constants for critical pressure and accentric factor

y	**A**	**B**	**C**	**D**
P_c **paraffins**	4.65E+06	1.37E-01	1.06E+06	8.13E+05
P_c **olefins**	5.7E+06	1.51E-01	-2.57E+05	9.78E+05
ω **paraffins**	-4.1E+02	1.03E-03	-1.45E-01	4.06E+01
ω **olefins**	1.18E+04	-3.57E-05	-1.08E-01	3.39E+04
T_c **paraffins**	2.35E+02	9.0E-03	1.6E+02	6.06E+01
T_c **olefins**	2.33E+02	2.0E-03	1.05E+02	7.01E+01

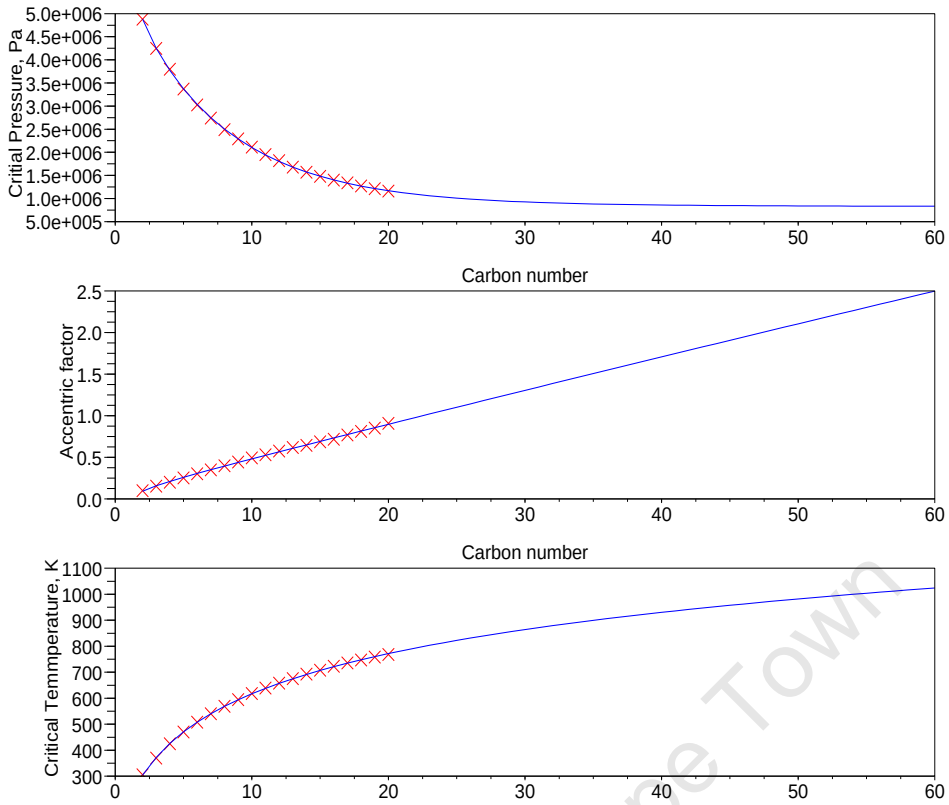

Figure A.1: Actual (×) and Correlated(–) corresponding states' values for paraffins

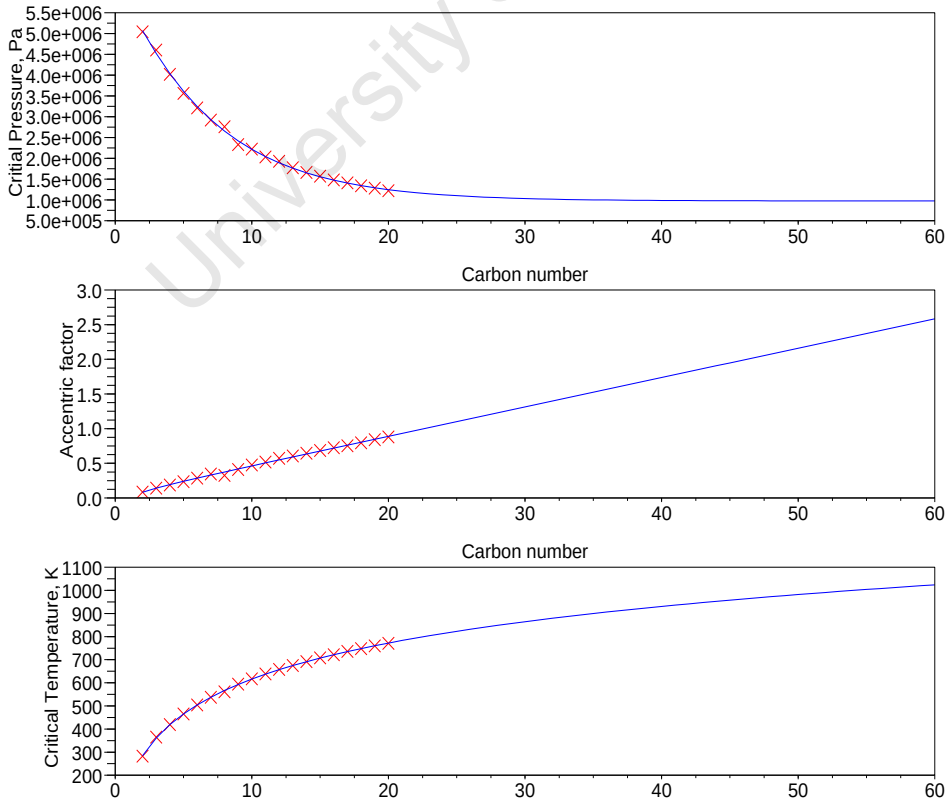

Figure A.2: Actual (×) and Correlated (–) corresponding states' values for olefins

Appendix B

Thermodynamic calculations

The measurement of multi-component VLE over a wide range of compositions, pressures and temperature is a tedious task. Compositions in each phase are predicted through the use of Thermodynamic models. The thermodynamic understanding of this multi-component FT system relies on the extension from binary mixing data to multicomponent mixing data through the application of mixing rules. The accuracy of the results depend on the pure component properties and on the thermodynamic model that is chosen to describe the behaviour of each phase. This section will explain, in detail, how the equations that determine the thermodynamic calculations are reached and the principles with which they are associated.

B.0.1 Pure component thermodynamics

The most accurate and practical way to determine the properties of a component and the relation between a component's pressure (P), volume (V) and temperature (T) ,is through an Equation of State. Van der Waal proposed the ideal gas equation of state in 1873, shown in equation B.1,

$$P \cdot V = N \cdot R \cdot T \tag{B.1}$$

where R is the ideal gas constant and N the number of moles present in the system. Seeing that not all gases behave ideally, there have been many proposed complex equations of state to describe the relation between P, V and T. Cubic equations of state (CEOS) are more widely recognized and are used because of the accuracy and algebraic simplicity they employ (Heese, 1998). They have been the most widely used methods for the calculation of vapour-liquid equilibrium (VLE) in petroleum processes, as they allow the accurate prediction of the phase equilibrium for mixtures containing non-polar components (Twu and Coon, 2000a). One of the most popular and more widely used equation of state is the Peng Robinson Equation of State (PREOS) which was intended mainly for hydrocarbons and other non-polar species.

A general two-parameter CEOS can be represented by the equation B.2,

$$P = \frac{R \cdot T}{\bar{V} - b} - \frac{a}{(\bar{V} + u \cdot b)(\bar{V} + w \cdot b)} \tag{B.2}$$

where: $\bar{V}$ is the molar volume, a is the temperature dependent attractive term which, for a pure component i, is given by equation B.3 and b is the covolume term, independent of temperature and given by equation B.4 for component i.

$$a_i = 0.45724 \cdot (\frac{R^2 T_{c,i}^2}{P_{c,i}}) \cdot \kappa(T) \tag{B.3}$$

$$b_i = 0.07780 \cdot \frac{R \cdot T_{c,i}}{P_{c,i}} \tag{B.4}$$

$\kappa(T_{r,i})$ is a function of the reduced temperature (T_r) and accentric factor ω and is given by equation B.5

$$\kappa(T) = \left(1 + (0.37464 + 1.54226 \cdot \omega - 0.2699 \cdot \omega^2) \cdot \left[1 - \sqrt{Tr, i}\right]\right)^2 \tag{B.5}$$

The constants u and w in equation B.2 are EOS-dependent. For the Soave-Redlich-Kwong (SRK) EOS, $w = 1$ and $u = 0$. The CEOS which will be used in this work is the PREOS, for which $w = \sqrt{2} + 1$ and $u = -\frac{1}{w}$. The form of this EOS was originally chosen to give a reasonable representation of the volumetric behaviour of hydrocarbons in the gasoline product range (Orbey and Sandler, 1997). Twu et al. (1995) gave a more accurate account of the κ function, through an extension of the EOS to heavier hydrocarbons. Equation B.6 is the κ function used in this work,

$$\kappa(T_r) = \kappa_1 + \omega \cdot (\kappa_2 - \kappa_1) \tag{B.6}$$

where κ_1 and κ_1 are given by equations B.7 and B.8 respectively.

$$\kappa_1 = T_r^{-0.171813} \cdot \exp 0.125282 \cdot (1.d0 - T_r^{1.77634}) \tag{B.7}$$

$$\kappa_2 = T_r^{-0.607352} \cdot \exp 0.511614 \cdot (1.d0 - T_r^{2.20517}) \tag{B.8}$$

Fugacity is one of the most important thermodynamic functions and is used because phase and chemical equilibrium calculations are simplified by its relation to the Gibbs free energy. It can be explained as the tendency of a species to prefer one phase over another. The tendency is for the phase with the lowest fugacity, as this corresponds to the minimisation of the the Gibbs' free energy. The fugacity of a pure component i, $f_i(T, P)$ is mathematically expressed as shown in equation B.9.

$$f_i(T, P) = P \cdot \exp\left[\frac{1}{R \cdot T} \cdot \int_0^P \left(\bar{V_i} - \frac{R \cdot T}{P}\right) dP\right] \tag{B.9}$$

To account for deviations from ideal gas behaviour, the compressibility factor, Z_i, is introduced and given by:

$$Z_i = \frac{P \cdot \bar{V_i}}{R \cdot T} \tag{B.10}$$

The introduction of equation B.10, allows for the modification of equation B.9 to a molar

volume basis:

$$\ln\left[\frac{f_i(T,P)}{P}\right] = \frac{1}{R\cdot T}\cdot\int_{\bar{V}=\infty}^{\bar{V}_i}\left[\left(\frac{R\cdot T}{\bar{V}} - P\right)d\bar{V}_i\right] - \ln Z_i + (Z_i - 1) \tag{B.11}$$

By substituting the EOS equation (equation B.2) into equation B.10, one can express the EOS in a dimensionless form, in terms of equation of state variables, as follows:

$$Z^3 - (1-B)\cdot Z^2 + (A - 3B^2 - 2B)\cdot Z - (AB - B^2 - B^3) = 0 \tag{B.12}$$

where, the dimensionless parameters A and B are:

$$A = \frac{a\cdot P}{R^2\cdot T^2} \tag{B.13}$$

$$B = \frac{b\cdot P}{R\cdot T} \tag{B.14}$$

Equation B.12 yields one root for a one-phase system, or three roots for a two-phase mixture system. In the case of a two-phase region, the largest real root gives the compressibility factor of the vapour phase (Z^V) whereas the smallest positive root gives the compressibility factor of the liquid phase (Z^L) (Bukur et al., 2005). For each phase, the respective compressibility root will be used in the calculation of the fugacity as follows:

$$\ln\left[\frac{f_i(T,P)}{P}\right] = -\ln(Z-B) - \frac{A}{B\sqrt{8}}\cdot\ln\left[\frac{Z+(1+\sqrt{2})B}{Z+(1-\sqrt{2})B}\right] + Z - 1 \tag{B.15}$$

B.0.2 Mixture thermodynamics

Mixture thermodynamics deal with the non-idealities of the pure components and the non-idealities caused by the interactions between the components in a mixture (Heese, 1998). To account for the differences from ideal mixing behaviour, the partial molar fugacity of a species i in a mixture is introduced and denoted $\bar{f}_i(z_i,T,P)$. The fugacity coefficient ($\bar{\phi}_i$) is the relation of the species' fugacity to its partial pressure. According to Smith et al. (2001), $\bar{f}_i(z_i,T,P)$ can be determined by equation B.16, obtained from the PREOS.

$$\ln\left[\frac{\bar{f}_i(z_i,T,P)}{z_i\cdot P}\right] = \ln\bar{\phi}_i = \frac{b_i}{b}(Z-1) - \ln(Z-B) - \bar{q}_i\cdot I \tag{B.16}$$

$$\bar{q}_i = A\left(1 + \frac{a_i}{a} - \frac{b_i}{b}\right) \tag{B.17}$$

$$I = \frac{1}{\sigma-\eta}\ln\left[\frac{Z+\sigma\cdot B}{Z+\eta\cdot B}\right] \tag{B.18}$$

a_i and b_i for each component i are obtained as per equations B.3 and B.4 respectively, a and b for the mixture are correlated with critical properties of the components and follow mixing rules, A and B are obtained as per equations B.13 and B.14 respectively, $\sigma = 1+\sqrt{2}$, $\eta = 1-\sqrt{2}$, and z_i is a generic mole fraction term, equal to x_i in the liquid phase and y_i in the vapour phase. The compressibility factor used in equations B.16 and B.18 corresponds to the respective root in the solving of the cubic compressibility equation B.12.

Mixing Rules

The ability of a CEOS to correlate and predict the phase equilibrium of mixtures strongly depends on the mixing rule which applies. This becomes even more significant when dealing with highly non-ideal mixtures in the liquid phase. As mentioned previously, equations of state have been successfully used for the prediction of pure component properties and have been improved over the last two decades (Orbey and Sandler, 1997). These equations of state have to be extended and modified to predict the same properties for mixtures, taking the composition of the mixture into account. The PREOS is practically applicable to different mixing rules which result in different composition dependencies for the EOS parameters a and b in Equation B.2. There are many mixing rules proposed in literature. Two of them are discussed in this section, and motivation is given for the mixing rule of choice for this FT system.

Van der Waals' Mixing Rules: The mixing rules were originally proposed by Van der Waal (VdW) where a and b were obtained by averaging the pure components' a_i and b_i parameter values (obtained as shown in equations B.3 and B.4 respectively). To further account for non-ideal mixing and to obtain a better agreement in mixture equation of state calculations, the binary interaction parameter k_{ij} was introduced. The purpose of the binary interaction parameter is to enhance the capability of an equation of state to predict the desired phase behaviour (Mushrif, 2004). There have been various correlations to determine the binary interaction parameters of hydrocarbon systems, for example Nishiumi and Gotoh (1990) correlated the binary interaction parameters of the PREOS in terms of the ratio of critical molar volumes and the absolute difference in the accentric factor of each component. Petersen (1989), proposed a power function to determine the binary interaction parameters for complex hydrocarbon mixtures which related the parameters to the molecular weights of the components. Values of k_{ij} are obtained from the regression of experimental data for each binary pair in the mixture. The calculations of the equation of state parameters by using the VdW's mixing rule are given by:

$$a(T) = \sum_{i=1}^{n}\sum_{j=1}^{n} z_i z_j a_{ij} \tag{B.19}$$

$$a_{ij} = \sqrt{a_i a_j}\,(1 - k_{ij}) \tag{B.20}$$

$$b = \sum_{i=1}^{n} z_i b_i \tag{B.21}$$

When fitting VLE data with the VdW's mixing rules, it was found that the binary interaction parameter were approximately zero for simple mixtures such as alkane mixtures; but for non-ideal systems, is non-zero and has a dependence on temperature. It is frequently assumed that in a multicomponent mixture when the binary interaction parameters of some pairs are unavailable due to a lack of data, it is acceptable to set the k_{ij} values to zero (Orbey and Sandler, 1997). Even though the conventional 'single binary interaction parameter van der Waals' mixing rule' is useful for nonpolar hydrocarbon mixtures and supercritical inorganic gases such as carbon dioxide, it has not been proven suitable for even moderately non-ideal systems containing water and a polar hydrocarbons (Heese, 1998). For many industrial mixtures, such as this FT system, the van der Waals mixing rules are not adequate.

Twu and Coon mixing rules: Twu and Coon (2000b) used the VdW mixing rules as a reference for the development of the Twu and Coon Mixing Rules. These mixing rules were found to be the most suitable as they allow nonpolar binaries in a multicomponent mixture to be described by the Van der Waals mixing rule while simultaneously using a NRTL-like activity coefficient description for the others. Twu and Coon (2000a) developed these mixing rules valid at both low and high densities, without matching the excess Gibbs energy expression from a CEOS with the corresponding excess Gibbs energy expression from an activity coefficient model like NRTL or UNIFAC. In addition, the binary interaction parameters in these mixing rules are generally regressed from the experimental vapour-liquid equilibrium data for binary systems. For the Twu and Coon mixing rules, the PREOS parameters, a and b are obtained as follows:

$$a = \sum_{i=1}^{n}\sum_{j=1}^{n} \sqrt{a_i a_j}\left(1 - \frac{\tau_{ji} G_{ji}}{\sum_k^n G_{ki} x_k}\right) \tag{B.22}$$

$$b = \sum_{i=1}^{n} z_i b_i \frac{1}{RT}\left[a - \sum_{i=1}^{n}\sum_{j=1}^{n} z_i z_j \sqrt{a_i a_j}(a - k_{ij})\right] \tag{B.23}$$

where

$$\tau_{ji} = \frac{C^*}{R \cdot T}\left[\frac{2\sqrt{a_i a_j}}{b_i + b_j}(a - k_{ij}) - \frac{a_i}{b_i}\right] \tag{B.24}$$

$$G_{ji} = \exp\left(-\beta_{ji}\tau_{ji}\right) \tag{B.25}$$

β_{ji} is a constant set to 0.2 and C^* is given by equation B.26 for the PREOS, and a_i and b_i are obtained as shown by equations B.3 and B.4 respectively.

$$C^* = \ln\frac{\sqrt{2}-1}{\sqrt{2}} = -0.62323 \tag{B.26}$$

There are other mixing rules that have been proposed in literature, where most of them use the fundamentals established by Van der Waal as a starting point. Another example of these is the Wong Sandler mixing rules, that have provided a link between equations of state and excess-free-energy models, produced the desired EOS behaviour at both low and high densities without being density dependent and allowed extrapolation over wide ranges of temperatures and pressures (Orbey and Sandler, 1997). The Twu and Coon mixing rules can be incorporated with the UNIFAC group contribution method into an equation of state to yield a completely predictive thermodynamic model, for the prediction of high pressure vapor-liquid phase equilibrium.

Appendix C

Reactor Initialisation and Start-up process models

The FORTRAN coding is given below, with reference to block flow diagram C.1

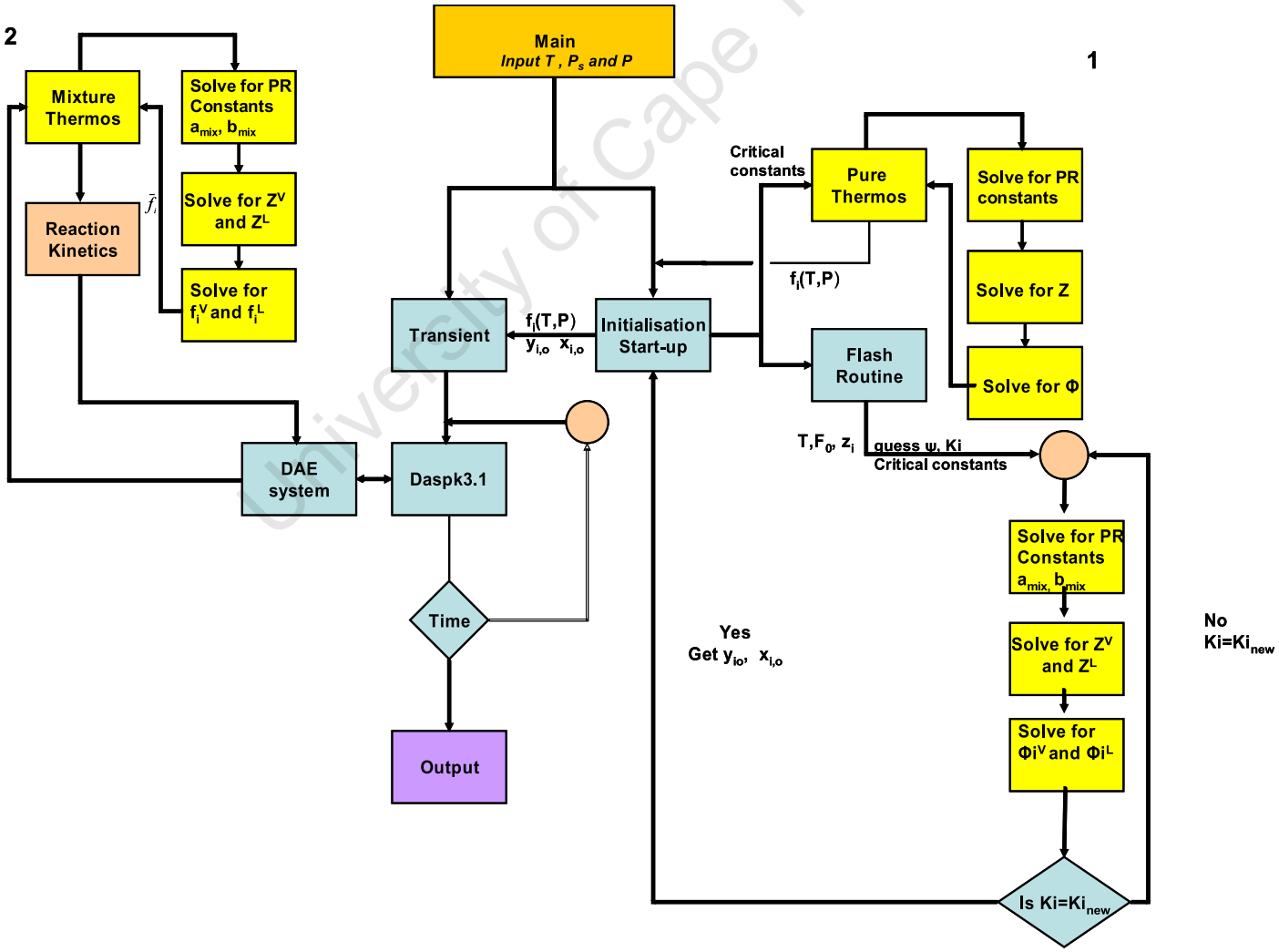

Figure C.1: FTS block flow diagram of model development procedure

C.1 Initialisation

The ***initial subroutine*** is called by the Main program. Its purpose is to calculate the pure component fugacities and prepare the input for the Isothermal flash calculation. This routine calls routines 'Initialisation and 'Flash' respctively. This is given below:

Initial subroutine

```
    subroutine intial(P,Ps, R, x, y, Ki, Zx, Zy)
implicit none
!Start up
integer:: i
integer, parameter:: m = 122, n = 60, comp = 2*n+2, neq = comp
double precision:: start(3), Vgas0, Vliq0, CC20out, R, rhol, rhov, aa, kk1, kk2
real*8:: P, Ps, PatZ, phix(comp), phiy(comp), x(comp), y(comp)
!=============================================================================
!Variables for startup
double precision:: F, input(comp), Tc1(comp), Pc1(comp), w1(comp), Zx, Zy, ki(comp)
character*12,allocatable :: dash(:),ddash(:)
character*15:: name1(comp)
!=============================================================================
!General common block
double precision:: ff(122), Temp, Tc(122), Pc(122), w(122),Z(122)
character*15:: name(122)
common ff, Temp, Tc, Pc, w, name, Z
!=============================================================================
!Flash common block
double precision:: Vtotal0, L, V
common /flash1/ Vtotal0, L, V
!=============================================================================
aa = 0.7
F = 1000.
input(1) = 0.1
input(2) = 0.1
input(3) = 0.1
do i = 4,n+3
input(i) = (1-aa)*aa**(i-4) !paraffins
enddo
input(n+4:m) = input(5:n+3) !olefins
kk1 = sum(input(4:n+3))
kk2 = sum(input(n+4:m))
input(4:n+3) = input(4:n+3)/kk1*(1-sum(input(1:3)))/2
input(n+4:m) = input(n+4:m)/kk2*(1-sum(input(1:3)))/2
write(*,*) 'suminput=', sum(input)
!To get pure component fugacities
call initialisation (P,Temp,Ps,comp, n, neq,ff,Tc, Pc, w, name, Z)
!=============================================================================
Tc1(1:comp) = Tc(1:comp)
Pc1(1:comp) = Pc(1:comp)
```

```
w1(1:comp) = w(1:comp)
name1(1:comp) = name(1:comp)
!=================================================================================
call flash(input,comp,Temp,P,F,Tc1,Pc1,w1,name1,L,V,phix,phiy,x,y, Zx, Zy, Ki)
rhol = P/(Zx*R*Temp)
rhov = P/(Zy*R*Temp)
Vgas0 = V/rhov
Vliq0 = L/rhol
Vtotal0 = Vgas0 + Vliq0
!To see what the liquid volume and gaseous volues are, after flashing.
write 'Vgas0 = ', Vgas0
write 'Vliq = ', Vliq0
end subroutine

    subroutine initialisation (P,Temp,Ps,m, n, neq,ff,Tc, Pc, w, name, Zpure)
integer:: i,m,n,neq
real*8:: input(m), fix(m)
real*8:: phi(m), ff(m), f20(m)
real*8:: y(neq)
real*8:: F, Ps, P, Temp, PZ
real*8:: Tc(122), Pc(122), Vc(122), Zc(122), w(122), Zpure(122)
character*12,allocatable :: dash(:),ddash(:)
character*20 :: bongz(neq)
character*15:: name(m)
allocate(dash(neq+1),ddash(neq+1))
OPEN (unit=13,FILE='flow.txt', FORM='FORMATTED', STATUS='OLD')
read(13,*) bongz(1:neq)
OPEN (unit=71,FILE='Tc1.txt', FORM='FORMATTED', STATUS='OLD')
OPEN (unit=72, FILE='Pc1.txt', FORM='FORMATTED', STATUS='OLD')
OPEN (unit=73, FILE='w1.txt', FORM='FORMATTED', STATUS='OLD')
OPEN (unit=74, FILE='Names1.txt', FORM='FORMATTED', STATUS='OLD')
read(71,*) Tc(1:m)
read(72,*) Pc(1:m)
read(73,*) w(1:m)
read(74,*) name(1:m)
PZ = P
call purethermo(Ps, Tc,Pc,Vc,w,name, m, Temp, phi,ff, Zpure)
end subroutine
```


Pure-thermodynamics subroutines

The following routines work together in determining the pure component fugacities.

```
subroutine purethermo(Ps, Tc,Pc,Vc,w,names, n, T, phi,f, Zpure)
implicit none
integer :: i,j,k,n,info
real*8 :: T, R
real*8 :: phi(n), f(n), a(n), b(n), Zpure(n)
real*8, allocatable :: z(:), beta(:), q(:)
```

```
real*8:: P, Ps
real*8:: Tc(n),Pc(n),Vc(n),Zc(n),w(n)
character*15:: names(n)
!data
allocate(z(n), beta(n), q(n),stat=info)
R = 8.314
P = Ps
!calc the a's and b's
call PRconstants(n,T,P,Tc,Pc,w,a,b)
q = a/(b*R*T)
beta = b*P/(R*T)
call solveZpure(n,beta,q,T,Z)
call solvePhipure(n,beta,q,Z,phi)
Zpure = Z
f = P*phi
!Determining the fugacities of every species
return
end


    Subroutine PRconstants(n,T,P,Tc,Pc,w,a,b)
!PREOS correlations for a(i),b(i) based on critical data
implicit none
integer i,j,n
real*8 :: R,sqrt2,sigma,omega,eta,psi,Zcc,T,P
real*8, dimension (n) :: Tc,Pc,Vc,Zc,w,a,b
real*8, dimension (n) :: Tr,Pr,alpha,RTc,R2Tc2, alf0, alf1
!constants
R=8.314d0
sqrt2=sqrt(2.d0)
sigma=1.d0+sqrt2
eta=1.d0-sqrt2
omega=0.0778d0
psi=0.45724d0
Zcc=0.30740d0
!vectors
Tr=T/Tc
Pr=P/Pc
!PR alpha value
!alpha=1.d0+(0.37464d0+1.54266d0*w-0.26992d0*w*w)*(1.d0-sqrt(Tr))
!alpha=alpha*alpha
!Twu, Coon, Cunningham
alf0=Tr**(-0.171813d0)*exp(0.125282d0*(1.d0-Tr**(1.77634d0)))
alf1=Tr**(-0.607352d0)*exp(0.511614d0*(1.d0-Tr**(2.20517d0)))
alpha=alf0+w*(alf1-alf0)
RTc=R*Tc
R2Tc2=RTc*RTc
!calculate a(i),b(i)
a=psi*alpha*R2Tc2/Pc
b=omega*RTc/Pc
```

```
return
end


    subroutine solveZpure(n,beta,q,T,Z)
!using a damped newton method
!the rpoly route seems to be the best
implicit none
integer :: i,j,n
character(1) :: phase
real*8, dimension (n) :: Z, beta, q
real*8 :: sqrt2,sigma,eta,T
real*8:: f, dz, temp, fd, df, znew
!Variables required for rpoly
integer, parameter:: degree = 3
real*8:: op(4)
LOGICAL FAIL
DOUBLE PRECISION ZEROR(3), ZEROI(3), Z1, z1y(n) , ee
real*8:: P
common P
!constants
sqrt2=sqrt(2.d0)
sigma=1.d0+sqrt2
eta=1.d0-sqrt2
ee = eta
do j = 1,n
op(1) = -1
op(2) = (1+beta(j)*(1-ee-sigma))
op(3) = ((ee+sigma-ee*sigma)*beta(j)**2 + (ee-q(j)+sigma)*beta(j))
op(4) = ee*sigma*beta(j)*beta(j)**2 + (ee*sigma+q(j))*beta(j)**2
call RPOLY(OP,DEGREE,ZEROR,ZEROI,FAIL)
!remove the imaginary roots
do i = 1,3
if (abs(zeroi(i)).gt.2.d-16) then
zeror(i)=0.d0
zeroi(i)=0.d0
endif
enddo
!find the max and min values
z(j)=maxVAL (zeror, MASK=zeror .gt. 0.0)
!check for bounds
if (z(j).gt.1.d0) then
z(j) = 0.99999d0
endif
if (z(j).lt.beta(j)) then
z(j) = 1.00001d0*beta(j)
endif
end do
return
end
```

```
    subroutine solvePhipure(n,beta,q,Z,phi)
!following Smith and vanNess 7th edition
implicit none
integer :: n
real*8 :: sqrt2,sigma,eta
real*8, dimension(n) ::phi, fi, Ci, z, beta, q
!constants
sqrt2=sqrt(2.d0)
sigma=1.d0+sqrt2
eta=1.d0-sqrt2
!vectors
Ci=(1.d0/(sigma-eta))*log((z+sigma*beta)/(z+eta*beta))
phi=exp((z-1.d0)-log(z-beta)-q*Ci)
return end
```

C.2 Isothermal Flash calculation

The flash routine was developed as follows:

```
subroutine flash(z,n,T,P,F,Tc,Pc,w,names,L,V,phix,phiy,x,y,zx, zy, Ki)
!Rachford rice procedure for flash using PREOS
implicit none
integer :: i,j,k,n,info
real*8 :: psinew, P, T, psi, psi1, L, F, V, ff, ff1, ffd, dpsi
real*8 :: amx, bmx, amy, bmy, zx, zy, dk
real*8 :: phix(n), phiy(n), fix(n), fiy(n), z(n), x(n), y(n)
real*8 :: Tc(n), Pc(n), Vc(n), w(n), Zc(n), a(n), b(n), Ki(n)
real*8, allocatable:: Kiold(:)
character*15 :: names(n)
allocate(Kiold(n),stat=info)
call PRconstants(n,T,P,Tc,Pc,w,a,b)
!guess psi and Ki's and get initial x,y from flash
psi=0.5d0
Ki(1) = 0.01
Ki(2) = 0.01
Ki(3) = 1
dk = (-log(0.0001)+log(100.))/60
do i = 4,63
Ki(i) = exp(log(5000.) - dk*(i-3))
enddo
do i = 64,n
Ki(i) = exp(log(5000.) - dk*(i-63))
enddo
!loop starts here, test the variation if Ki's for convergence do k=1,100
L=psi*F
V=F-L
x=z/((1.d0-psi)*Ki+psi)
y=Ki*x
```

```
call mixing(n,x,T,P,a,b,amx,bmx)
call mixing(n,y,T,P,a,b,amy,bmy)
call solveZ(n,x,P,T,amx,bmx,Zx,'L')
call solveZ(n,y,P,T,amy,bmy,Zy,'V')
call solvePhi(n,T,P,x,a,b,zx,amx,bmx,phix)
call solvePhi(n,T,P,y,a,b,zy,amy,bmy,phiy)
Kiold=Ki
Ki=Phix/Phiy
do i=1,100 !simple newton with bisection and bounds
ff=sum(z*(1.d0-Ki)/((1.d0-psi)*Ki+psi))
dpsi=max(abs(psi*0.01d0),1.d-7)
psi1=psi+dpsi
ff1=sum(z*(1.d0-Ki)/((1.d0-psi1)*Ki+psi1))
ffd=(ff1-ff)/dpsi
psinew=psi-ff/ffd
if (psinew.lt.0.d0) psinew=psi/2.d0
if (psinew.gt.1.d0) psinew=(psi+1.d0)*0.01d0
if (psi.lt.1.d-6) exit
if (abs(ff/ffd) ¡ 1.d-6) exit
psi= psinew
if (i.eq.100) write(*,*) 'flash needed 100 iterations and not converged'
enddo if (sum(abs(Kiold-Ki)/Kiold) .lt. 1.d-6) exit
if (k .eq. 100) write(*,*)'Ki loop not converged after 100 iterations'
enddo
L=psi*F
V=F-L
x=z/((1.d0-psi)*Ki+psi)
fix = phix*x*P
fiy = phiy*y*P
write(*,*) 'Zx =', Zx
write(*,*) 'Zy=', Zy
!Determining the fugacities of every species
write(87,'(a44)')'============================================'
write(87,'(a44)')'name K(i) x(i) y(i) '
write(87,'(a44)')'--------------------------------'
do i=1,n write(87,'(a8,3(1pe12.3))')names(i),Ki(i),x(i),y(i)
enddo
write(87,'(a44)')'--------------------------------' write(87,'(a8,1pe12.3)')'sumx',sum(x)
write(87,'(a8,1pe12.3)')'sumy',sum(y)
write(87,'(a8,1pe12.3)')'L/F',psi
write(87,'(a8,1pe12.3)')'V/F',1-psi
write(87,'(a8,1pe12.3)')'T(C)',T-273.15d0
write(87,'(a8,1pe12.3)')'P(atm)',P/101325d0
write(87,'(a44)')'============================================'
!Writing the fugacity coefficients
write(87,'(a44)')'============================================'
write(87,'(a44)')'name fix(i) fiy(i) '
write(87,'(a44)')'--------------------------------'
do i=1,n
```

```
write(87,'(a8,3(1pe12.3))')names(i),fix(i),fiy(i)
enddo
write(87,'(a44)')'————————————————————————————'
return
end subroutine
```

Appendix D

Transient process models

With reference to block flow diagram C.1, these are the models that were developed to solve the DAE system.

D.1 Transient two-phase model (with VLE)

```
subroutine transient(P,x0, ygas0, L, V, Ki,comp,Zx, Zy)
use dflib
implicit none
!Ddaspk variables
integer, parameter:: m =122, maxord = 5, n = 60, neq = 2*m+n+4
integer, parameter:: liw=500000, lrw= 500000
integer:: idid, iwork(liw), ipar(20), info(30), nt, i, j, comp
double precision:: dt,t0, tf, y(neq), yprime(neq), rtol, atol, rwork(lrw), rpar(20), senpar(20), tout, tend
external nless, jac, psol, Gres, ares, kres, tres
!=========================================================================
!Variables from flash start-up
double precision:: Vgas0, Vliq0, ygas0(comp), x0(comp), L, V, Ni(m), Nio(m), ygas(m), xi(m), yi(m), zi1(n),
zi2(n-1), zio(m), zio1(n), zio2(n-1)
double precision:: x(m), Nil(m), Niv(m), psii(m), psiipara(n), psiiole(n-1)
double precision:: P,R , rho(122), Vgas, Vliq, conversion
logical(4) :: hello
character*12,allocatable :: dash(:),ddash(:)
!=========================================================================
!Thermodynamic block
double precision:: Ki(m), Zx, Zy
!=========================================================================
!General Common block
double precision:: ff(122), Temp, Tc(122), Pc(122), w(122), Z(122)
character*15:: name(122)
common ff, Temp, Tc, Pc, w, name, Z
!=========================================================================
```

```
!Thermodynamic variables
double precision:: fix(122), fiy(122), phix(122), phiy(122), theta, rhol, rhov, rate(181), a(122)
common /fugacities/ fix, fiy, phix, phiy, theta,rhol, rhov, rate, a
!=====================================================================
allocate(dash(neq+1),ddash(neq+1))
!=====================================================================
!Ddaspk variables
rtol = 0.5d-6
atol = 0.5d-6
info =0
!info(10) = 2
info(16) = 1
do i = 1,m
iwork(40+i) = 1 !differential !First m equations are differential
iwork(40+i+m) =-1 !This is the equilibrium equation
iwork(40+i+m+n+2) = 1 !This is the dqi/dt equation
end do
iwork(40+2*m+n+3) = -1
iwork(40+2*m+n+4) = -1
!=====================================================================
!integration range
t0=0.d0
tend = 1.d6
nt=100!No of points
dt=log(tend)/nt
!=====================================================================
dash(:)='----------'
ddash(:)='=========='
write(31,'(a1,200(a12))')",(ddash(i),i=1,m+1)
write(31,'(a1,200(a12))')", 'time', (name(i),i=1,m)
write(35,'(a1,200(a12))')",(ddash(i),i=1,m+1)
write(35,'(a1,200(a12))')", 'time', (name(i),i=1,m)
write(36,'(a1,200(a12))')",(ddash(i),i=1,m+1)
write(37,'(a1,200(a12))')",(ddash(i),i=1,m+1)
write(37,'(a1,200(a12))')", 'time', (name(i),i=1,m)
write(32,'(a1,200(a12))')",(ddash(i),i=1,m+1)
write(33,'(a1,200(a12))')",(ddash(i),i=1,m+1)
write(34,'(a1,200(a12))')",(ddash(i),i=1,2+1)
!=====================================================================
R = 8.314
```

```
rho = P/(Z*R*Temp) !Molar density in mol/m3
Vliq = 0.5
Vgas = 0.5
!=====================================================================
!Initially
x=0.
ygas = 0.
x(1:comp) = x0
ygas(1:comp) = ygas0
y = 0.d0
yprime = 0.d0
y(1:m) = x
y(m+1:2*m) = ygas
rhol = P/(Zx*R*Temp)
rhov = P/(Zy*R*Temp)
write(*,*) 'initial rhol=', rhol
write(*,*) 'initial rhov=', rhov
Nio = ygas*rhov*Vgas + x*rhol*Vliq
zio = Nio/sum(Nio)
zio1 = zio(4:n+3)
zio2 = zio(n+4:m)
write(39,'(i3,1pe12.3e3)')1,zio1(1)
do j=2,n-1
write(39,'(i3,1pe12.3e3)')j,zio1(j)
end do
do j = 1,n-2
write(40,'(i3,1pe12.3e3)')j+1,zio2(j)
end do
!write(*,*) 'sum(x)=', sum(x)
!=====================================================================
!Calculating the no. of moles of H2 originally in the reactor
do i = 1,nt+1
!Tout= dble(i-1)*dt+1.d-3
Tout= 1.d-3+exp(dt*(i-1))-1.d0
call DDASPK (nless, NEQ, t0, Y, YPRIME, TOUT, INFO, RTOL,ATOL,IDID, RWORK, LRW, IWORK,
LIW, RPAR, IPAR, JAC, PSOL,SENPAR, GRES, KRES, TRES, ARES)
!pause
write(31,'(300(1pe12.3e3))')tout,(y(j), j = 1,m) !Displaying the liquid mol fractions
write(35,'(300(1pe12.3e3))')tout,(y(j), j = m+1,2*m) !Displaying the vapour mol fractions
write(36,'(300(1pe12.3e3))')tout,(y(j), j = 2*m+1,2*m+n+2) !displaying the intermediate theta
```

```
write(37,'(300(1pe12.3e3))')tout,(y(j), j = neq-1,neq)
write(55,'(300(1pe12.3e3))')tout,(a(j), j = 1,m) !Displaying the activities
!Writing the flowrate of each component i out of the reactor
write(32,'(200(1pe12.3e3))')tout,(y(j)*y(neq), j = 1,m) !Liquid flow out ofthe reactor
write(33,'(200(1pe12.3e3))')tout,(y(j)*y(neq-1), j = m+1,2*m) !Vapour Flow out of the reactor
write(34,'(200(1pe12.3e3))')tout,fix(32),fiy(32)
write(*,*) 'theta=', theta
!=====================================================================
xi = y(1:m)
yi = y(m+1:2*m)
Ni = xi*rhoL*Vliq + yi*rhov*Vgas
Nil = xi*rhoL*Vliq
Niv = yi*rhov*Vgas
psii = Nil/Ni
psiipara = psii(4:n+3)
psiiole = psii(n+4:m)
zi1 = Ni(4:n+3)/sum(Ni(4:n+3)) !Mol fraction paraffins in both streams
zi2 = Ni(n+4:m)/sum(Ni(n+4:m)) !mol fraction olefins
write(88,'(1pe12.3e3,1pe12.3e3,1pe12.3e3,1pe12.3e3,1pe12.3e3,1pe12.3e3 )')tout,Ni(m),xi(m), yi(m),rhol, rhov
!Writing for the surface plot; liquid mol fraction plot for paraffins
write(11,'(1pe12.3e3,i3,1pe12.3e3)')tout,1,y(4)
do j=2,n-1
write(11,'(1pe12.3e3,i3,1pe12.3e3)')tout,j,j*y(3+j)
end do
write(11,'(a20)')' '
write(11,'(a20)')' '
=====================================================================
!Writing for the surface plot; liquid mol fraction plot for olefins
write(12,'(1pe12.3e3,i3,1pe12.3e3)')tout,1,y(4)
do j=2,n-1
write(12,'(1pe12.3e3,i3,1pe12.3e3)')tout,j,j*y(n+2+j)
end do
write(12,'(a20)')' '
write(12,'(a20)')' '
!Plotting thethe C60 formation rate and the c60 intermediate formation rate
write(52,'(1pe12.3e3,1pe12.3e3)') tout, rate(n+13)/rate(m+9)
write(54,'(1pe12.3e3,1pe12.3e3,1pe12.3e3)') tout, fix(9), fiy(9)
write(53,'(1pe12.3e3,1pe12.3e3,1pe12.3e3)') tout, a(1), a(2)
enddo
!=====================================================================
```

```
write(*,*) 'rhol=', rhol
write(*,*) 'rhov=', rhov
!ASF plot for paraffins
write(15,'(i3,1pe12.3e3)')1,zi1(1)
do j=2,n-1
write(15,'(i3,1pe12.3e3)')j,zi1(j)
end do
do j = 1,n-2
write(16,'(i3,1pe12.3e3)')j+1,zi2(j)
end do
write(44,'(i3,1pe12.3e3)')1,psiipara(1)
do j=2,n
write(44,'(i3,1pe12.3e3)')j,psiipara(j)
end do
do j = 1,n-1
write(45,'(i3,1pe12.3e3)')j+1,psiiole(j)
end do write(46,'(i3,1pe12.3e3)')1,a(4)
do j=2,n
write(46,'(i3,1pe12.3e3)')j,a(j+3)
end do
do j = 1,n-1
write(47,'(i3,1pe12.3e3)')j+1,a(n+j+3)
end do
!=====================================================================
write(31,'(a1,200(a12))')",(dash(i),i=1,neq+1)
write(32,'(a1,200(a12))')",(dash(i),i=1,m+1)
write(33,'(a1,200(a12))')",(dash(i),i=1,m+1)
write(34,'(a1,200(a12))')",(dash(i),i=1,2+1)
!=====================================================================
conversion = (500 - y(m+1)*y(neq-1))/500!On the basis of vapour flow out of the reactor
write(*,*) 'CO Conversion=', conversion
hello = SYSTEMQQ('MSc2009.bat')
end subroutine
```

DAE system routine - nless

```
subroutine nless(t, y, yprime, cj, delta, ires, ipar) !, senpar)
implicit none
integer, parameter:: m =122,n=60, neq = 2*m+n+4
integer:: i
!Ddaspk variables
```

```
integer ires, ipar(20)
double precision:: senpar(20), rpar(20)
double precision:: cj, t, y(neq), delta(neq), yprime(neq)
!=======================================================================
double precision:: FV, FL, qi(m), Ni(m), yy(m), x(m), Ki(m), Fin(m), Fin0(m), zi(m), psi(m)
double precision:: Vgas, Vliq, kr(7), Ke(7), r5(n-1), r6(n-1), r7(n-1)
double precision:: FCOin, alpha, R, P, Zx, Zy
!=======================================================================
!catalyst properties
double precision:: mcat, ncat, catloading ,theta0, thetai(n+2)
!=======================================================================
!Common Variables
double precision:: ff(122), Temp, Tc(122), Pc(122), w(122), Z(122)
character*15:: name(122)
common ff, Temp, Tc, Pc, w, name, Z
!=======================================================================
!Thermodynamic variables
double precision:: fix(122), fiy(122), phix(122), phiy(122), theta, rhol, rhov, rate(181), a(122)
common /fugacities/ fix, fiy, phix, phiy, theta,rhol, rhov, rate,a
!=======================================================
!Start-up common block
double precision:: ki0(m)
common /startup/ ki0
!=======================================================
!Input variables
R = 8.314d0
P = 101325*20.d0
alpha = 2
ires = 0
Fin = 0
Fin0 = 0.
!Inlet flows
Fin0(1) = 500.d0 !mol/s
Fin0(2) = 2*Fin0(1) !mol/s
Fin0(n+3) = Fin0(1) /10000
Fin = Fin0*(1-exp(-alpha*t))*(1+0.25*sin(0*t))
!Fixed liquid and vapour volumes
Vliq = 0.5 !m3
Vgas = 0.5 !m3
!Catalyst properties
catloading = 4.d5
mcat = catloading*(Vliq+Vgas)
Ncat = mcat/58.93
!Reaction rate constants
kr = 0.1
Ke = 0.8
!Defining the variables
x = y(1:m)
yy = y(m+1:2*m)
```

```
thetai = y(2*m+1:2*m+n+2)
Fv = y(2*m+n+3)
Fl = y(2*m+n+4)
!Catalyst constraint
theta0 = 1
theta = 1 - sum(thetai)
call Mixthermo(m,P,x,yy, fix, fiy, phix, phiy, Ki, Zx, Zy) !Routine will yield the fugacities and fugacity coefficients
call rxns(m,yy, qi, ff, fix, fiy, kr, Ke, thetai,theta, t, rate, a )
r5 = rate(5:n+3)
r6 = rate(n+4:m) !59 olefinic rates (C2= - C20=)
r7 = rate(m+1:3*n+1) !59 paraffic rates for C2 - c20
!Liquid and Vapour densities
rhoL = P/(Zx*R*Temp)
rhoV = P/(Zy*R*Temp)
!=========================================================================
!Transient reactor equations
!Total balances
delta(1) = Vliq*rhol*yprime(1) + Vgas*rhov*yprime(m+1) - (Fin(1) - FV*yy(1) - FL*x(1) - rate(1)*mcat)
!CO
delta(2) = Vliq*rhol*yprime(2) + Vgas*rhov*yprime(m+2) - (Fin(2) - FV*yy(2) - FL*x(2) - rate(2)*mcat) !H2
delta(3) = Vliq*rhol*yprime(3) + Vgas*rhov*yprime(m+3) - (Fin(3) - FV*yy(3) - FL*x(3) + rate(1)*mcat)
!water
delta(4) = Vliq*rhol*yprime(4) + Vgas*rhov*yprime(m+4) - (Fin(4) - FV*yy(4) - FL*x(4) + rate(4)*mcat)
!methane
!Paraffins (C2 - Cn)
delta(5:n+3) = Vliq*rhol*yprime(5:n+3) + Vgas*rhov*yprime(m+5:m+n+3) - (Fin(5:n+3) - FV*yy(5:n+3) -
FL*x(5:n+3) + r7*mcat)
!Olefins (C2= - Cn=)
delta(n+4:m) = Vliq*rhol*yprime(n+4:m) + Vgas*rhov*yprime(m+n+4:2*m) - (Fin(n+4:m) - FV*yy(n+4:m)
- FL*x(n+4:m) + r6*mcat)
!=========================================================================

!Equilibrium equations
delta(m+1:2*m) = yy - Ki*x
!=========================================================================
!Adsorption reactions
delta(2*m+1) = (-4*rate(1)+2*rate(2)-rate(3)-rate(4)+sum(r6)-sum(r7)) *Mcat/Ncat - yprime(2*m+1) !HT
delta(2*m+2) = (rate(1)-rate(3)-sum(r5))*mcat/Ncat - yprime(2*m+2) !CH2T
delta(2*m+3) = (rate(3)-rate(4)-r5(1))*mcat/Ncat- yprime(2*m+3) !Ch3T
delta(2*m+4:2*m+n+1) = (r5(1:n-2) - r5(2:n-1)-r6(1:n-2)-r7(1:n-2))*mcat/Ncat - yprime(2*m+4:2*m+n+1)
!C2T - C59T*mcat
delta(2*m+n+2) = (r5(n-1) - r6(n-1) - r7(n-1))*mcat/Ncat - yprime(2*m+n+2)

!Summation equations
delta(2*m+n+3) = 1-sum(x)
delta(2*m+n+4) = 1- sum(yy)
end subroutine
```

```
    subroutine rxns(m,x, qi, ff, fix, fiy, kr, Ke, thetai, theta, t, rate,a )
integer:: m
integer, parameter:: n = 60
double precision:: x(m), qi(m), rate(3*n+1), ff(m), fix(m), fiy(m), kr(7),Ke(7), kr6rev
double precision:: a(m), thetai(m), aole(n-1), apar(n)
double precision:: theta, alpha, COT, HT, CH2T, CnT(n)
rate = 0.
a = 0.
alpha = 2
!=============================================================================
!Defining the activities
a = fix/ff
apar = a(4:n+3)
aole = a(n+4:m)
!=============================================================================
!Defining the fraction intermediates
HT = thetai(1)
CH2T = thetai(2)
CnT = thetai(3:n+2)
!=============================================================================
kr(2) = kr(1) /70
kr(3) = kr(1)*2.42d2
kr(4) = kr(1)*2.18d3
kr(5) = kr(4)*5000 /(7000.12)
kr(6) = kr(1)* 4
kr6rev = kr(1)*0.67d-6
kr(7) = kr(1)*9.71d1
!kr(7) = kr(6)*10
rate(1) = kr(1)*(a(1)*HT) ! - thetai(1)/Ke(1)) !CO adsorption reaction
rate(2) = kr(2)*(a(2)*theta**2) ! - HT**2/Ke(2)) !H2 adsorption reaction
rate(3) = kr(3)*(ch2T*HT) ! - CnT(1)*theta/Ke(3)) !Ch3T formation: Chain intiation
rate(4) = kr(4)*(CnT(1)*HT) ! - apar(1)*theta**2/Ke(4)) !Methanation reaction
rate(5:n+3)= kr(5)*(CH2T*CnT(1:n-1)) ! - CnT(2:n)*theta/Ke(5)) !Chain growth
rate(n+4:m) = kr(6)*CnT(2:n) !- kr6rev*aole*HT !Olefin formation rate
rate(m+1:3*n+1) = kr(7)*(CnT(2:n)*HT) ! - apar(2:n)*theta**2/Ke(7)) ! Paraffin formation rate
rate = rate*(1-exp(-alpha*t))*(1+0.25*sin(0*t))
!At time t = 0 there's no rate, and with increasing time, the rate increases
end subroutine
```

Mixture-thermodynamics subroutines

```
subroutine Mixthermo(m, P,x,y, fix, fiy, phix, phiy,Ki, Zx, Zy) !Routine will yield the fugacities and fugacity
coefficients
implicit none
!=============================================================================
integer:: i, m
integer, parameter:: n = 60, comp = 122
real*8:: x(m), y(m), xx(m), yy(m), a(m),b(m), fix(m),fiy(m)
double precision:: P, Tc1(m), Pc1(m), w1(m)
```

```
character*15:: name1(m)
real*8 :: amx,bmx,amy,bmy
!=====================================================================
!Thermodynamic variables on call
double precision:: Ki(m), phix(m), phiy(m), Zx, Zy
!=====================================================================
!Common variables
double precision:: ff(122), Temp, Tc(122), Pc(122), w(122), Z(122)
character*15:: name(122)
common ff, Temp, Tc, Pc, w, name, Z
!=====================================================================
Tc1(1:comp) = Tc(1:comp)
Pc1(1:comp) = Pc(1:comp)
w1(1:comp) = w(1:comp)
name1(1:comp) = name(1:comp)
call PRconstants(m,Temp,P,Tc1,Pc1,w1,a,b) !To get vectors a and b for each component
call mixing(m,x,Temp,P,a,b,amx,bmx)
call mixing(m,y,Temp,P,a,b,amy,bmy)
call solveZ(m,x,P,Temp,amx,bmx,Zx,'L')
call solveZ(m,y,P,Temp,amy,bmy,Zy,'V')
call solvePhi(m,Temp,P,x,a,b,zx,amx,bmx,phix)
call solvePhi(m,Temp,P,y,a,b,zy,amy,bmy,phiy)
fix = phix*x*P
fiy = phiy*y*P
Ki = phix/phiy
end subroutine
```

Subroutine **PRconstants** is shown in Appendix C.

```
subroutine mixing(n,z,T,P,a,b,am,bm)
implicit none
integer :: n,i,j
real*8, dimension (n) :: a,b,z
real*8 :: am,bm,T,P
!constants
!vectors
am=0.
do i=1,n
am=am+sum(z(i)*z(:)*sqrt(a(i)*a(:)))
enddo
bm=0.
bm=sum(z(:)*b(:))
return
end


    subroutine solveZ(n,zf,P,T,am,bm,Z,phase)
!using a damped newton method
!the rpoly route seems to be the best
use dflib
implicit none
integer :: i,j,n
character(1) :: phase
```

```
real(8), dimension (n) :: zf
real*8 :: am,bm,Z,R,sqrt2,sigma,eta,omega,psi,zcc,RT,beta,qm,T,P,znew
real*8 :: f,fd,df,dz,temp
!Variables required for rpoly
integer, parameter:: degree = 3
real*8, dimension(4) :: op
LOGICAL FAIL
DOUBLE PRECISION ZEROR(3), ZEROI(3), Z1, z1y , ee
!constants
R=8.314d0
sqrt2=sqrt(2.d0)
sigma=1.d0+sqrt2
eta=1.d0-sqrt2
omega=0.0778d0
psi=0.45724d0
Zcc=0.30740d0
RT=R*T
beta=bm*P/RT
qm=am/(bm*RT)
ee = eta
op(1) = -1
op(2) = (1+beta*(1-ee-sigma))
op(3) = ((ee+sigma-ee*sigma)*beta**2 + (ee-qm+sigma)*beta
op(4) = ee*sigma*beta*beta**2 + (ee*sigma+qm)*beta**2
call RPOLY(OP,DEGREE,ZEROR,ZEROI,FAIL)
!remove the imaginary roots
do i = 1,3
if (abs(zeroi(i)).gt.2.d-16) then
! write (64,*) 'imaginary roots'
! write (64,*) i,zeror(i), zeroi(i)
zeror(i)=0.d0
zeroi(i)=0.d0
endif
enddo
!find the max and min values
z1y=maxVAL (zeror, MASK=zeror .gt. 0.0)
z1=minVAL (zeror, MASK=zeror .gt. 0.0)
!call SORTQQ (loc(zeror), 10,SRTINTEGER2)
!write(65,*) ' '
!write(65,*) 'Sorted real roots'
!do i = 1,3
!write(65,*) i, zeror(i)
!enddo
if ((phase.eq.'V').or.(phase.eq.'v')) then
write(64,*)'zv=',z1y,(z.lt.beta)
z = z1y
if (z.gt.1.d0) then
z = 0.99999d0
endif
```

```
endif
if ((phase.eq.'L').or.(phase.eq.'l')) then
write(64,*)'zl=',z1,(z.lt.beta)
z=z1
if (z.lt.beta) then
z = 1.00001d0*beta
endif
endif
return
end

subroutine solvePhi(n,T,P,zf,a,b,z,am,bm,phi)
!following Smith and vanNess 7th edition
implicit none
integer :: n
real*8 :: T,P,z,am,bm
integer :: i
real*8 :: R,sqrt2,sigma,eta,omega,psi,Zcc,RT,Beta,qm,Ci
character(10) :: phase
real*8, dimension(n) :: a,b,ap,qp,zf,phi
!constants
R=8.314d0
sqrt2=sqrt(2.d0)
sigma=1.d0+sqrt2
eta=1.d0-sqrt2
omega=0.0778d0
psi=0.45724d0
Zcc=0.30740d0
RT=R*T
beta=bm*P/RT
qm=am/(bm*RT)
!vectors
do i=1,n

ap(i)=2.d0*sum(zf(:)*sqrt(a(i)*a(:)))-am
enddo
Ci=1.d0/(sigma-eta)*log((z+sigma*beta)/(z+eta*beta))
qp=qm*(1.d0+ap/am-b/bm)
phi=exp(b/bm*(z-1.d0)-log(z-beta)-qp*Ci)
!write(*,*) 'error=', z-beta
return
end
```

D.2 Transient single-phase model (no VLE)

```
subroutine pres(P,x0, ygas0, L, V, Ki,comp, zx, zy)
use dflib
implicit none
```

```
!Ddaspk variables
integer, parameter:: m =122, n=60 , neq = 2*m+n+3, maxord = 5
integer, parameter:: liw=5000000, lrw= 5000000
integer:: idid, iwork(liw), ipar(20), info(30), nt, i, j, comp

double precision:: dt,t0, tf, y(neq), yprime(neq), rtol, atol, rwork(lrw), rpar(20), senpar(20), tout, tend
external withoutvle, jac, psol, Gres, ares, kres, tres
!=======================================================================
!Variables from flash start-up double precision:: Vgas0, Vliq0, ygas0(comp), x0(comp), L, V, Ni(m), ygas(m),
xi(m), yi(m), zi1(n), zi2(n-1), zio(m), zio1(n), zio2(n-1)
double precision:: x(m), F
double precision:: P,R , Vgas, Vliq, conversion
logical(4) :: hello
character*12,allocatable :: dash(:),ddash(:)
!=======================================================================
!Thermodynamic block
double precision:: Ki(m), Zx, Zy
!=======================================================================
!General Common block
double precision:: ff(122), Temp, Tc(122), Pc(122), w(122), Z(122)
character*15:: name(122)
common ff, Temp, Tc, Pc, w, name, Z
!=======================================================================
!Thermodynamic variables
double precision:: fix(122), fiy(122), phix(122), phiy(122), theta, rhol, rhov, rho(122), rate(181), a(122)
common /fugacities/ fix, fiy, phix, phiy, theta,rhol, rhov, rho, rate, a
allocate(dash(neq+1),ddash(neq+1))
!=======================================================================
!Ddaspk variables
rtol = 0.5d-6
atol = 0.5d-6
info =0
info(16) = 1
do i = 1,m
iwork(40+i) = 1 !differential !First m equations are differential
iwork(40+i+m) =-1 !This is the equilibrium equation
iwork(40+i+m+n+2) = 1 !This is the dqi/dt equation
end do
iwork(40+2*m+n+3) = -1
!iwork(40+3*m+2) = -1
F = 1000
!=======================================================================
!integration range
t0=0.d0
tend = 1.d6
nt=100!No of points
dt=log(tend)/nt
!=======================================================================
dash(:)='————————'
```

```
ddash(:)='============'
write(31,'(a1,200(a12))')",(ddash(i),i=1,m+1)
write(31,'(a1,200(a12))')", 'time', (name(i),i=1,m)
write(35,'(a1,200(a12))')",(ddash(i),i=1,m+1)
write(35,'(a1,200(a12))')", 'time', (name(i),i=1,m)
write(36,'(a1,200(a12))')",(ddash(i),i=1,n+3)
write(36,'(a1,200(a12))')", 'time', (name(i),i=1,m)
write(37,'(a1,200(a12))')",(ddash(i),i=1,2)
write(37,'(a1,200(a12))')", 'time', 'flow'
write(32,'(a1,200(a12))')",(ddash(i),i=1,m+1)
write(33,'(a1,200(a12))')",(ddash(i),i=1,m+1)
write(34,'(a1,200(a12))')",(ddash(i),i=1,2+1)
!=============================================================================
R = 8.314
rho = P/(Z*R*Temp) !Molar density in mol/m3
Vliq = 0.5
Vgas = 0.5
!=============================================================================
rhol = P/(Zx*R*Temp)
rhov = P/(Zy*R*Temp)
write(*,*) 'initial rhol=', rhol
write(*,*) 'initial rhov=', rhov
!Initially
x=0.
ygas = 0.
x(1:comp) = x0
ygas(1:comp) = ygas0
y = 0.d0
yprime = 0.d0
z = (L*x0 + V*ygas0)/F
Ni = ygas0*rhov*Vgas + x0*rhol*Vliq
zio = Ni/sum(Ni)
zio1 = zio(4:n+3)
zio2 = zio(n+4:m)
z = zio
Ni = z*(Vliq+Vgas)*500
write(39,'(i3,1pe12.3e3)')1,zio1(1)
do j=2,n-1
write(39,'(i3,1pe12.3e3)')j,zio1(j)
end do
do j = 1,n-2
write(40,'(i3,1pe12.3e3)')j+1,zio2(j)
end do
y(1:m) = Ni
y(m+1:2*m) = z
!=============================================================================
!Calculating the no. of moles of H2 originally in the reactor
do i = 1,nt+1
Tout= 1.d-3+exp(dt*(i-1))-1.d0
```

```
!Tout=dble(i-1)*dt+1.d-3
call DDASPK (withoutvle, NEQ, t0, Y, YPRIME, TOUT, INFO, RTOL,ATOL,IDID, RWORK, LRW, IWORK,
LIW, RPAR, IPAR, JAC, PSOL,SENPAR, GRES, KRES, TRES, ARES) !pause
write(31,'(300(1pe12.3e3))')tout,(y(j), j = 1,m) !Displaying the No. of moles
write(35,'(300(1pe12.3e3))')tout,(y(j), j = m+1,2*m) !Displaying the mol fractions zi
write(36,'(300(1pe12.3e3))')tout,(y(j), j = 2*m+1,2*m+n+2) !These are the theta values
write(37,'(300(1pe12.3e3))')tout, y(neq) !This is the flowrate out
write(55,'(300(1pe12.3e3))')tout,(a(j), j = 1,m) !Displaying the activities
write(*,*) 'theta=', theta
!=====================================================================
Ni = y(1:m)
z = y(m+1:2*m)
zi1 = z(4:n+3) !Paraffin mol fraction
zi2 = z(n+4:m) !lefin mole fraction
write(53,'(1pe12.3e3,1pe12.3e3,1pe12.3e3)') tout, y(m+1)*y(neq), y(m+2)*y(neq)
!Writing for the surface plot; mol fraction plot for paraffins
write(11,'(1pe12.3e3,i3,1pe12.3e3)')tout,1,y(4)
do j=2,n-1
write(11,'(1pe12.3e3,i3,1pe12.3e3)')tout,j,j*y(3+j)
end do
write(11,'(a20)')' '
write(11,'(a20)')' '
!=====================================================================
!Writing for the surface plot; mol fraction plot for olefins
write(12,'(1pe12.3e3,i3,1pe12.3e3)')tout,1,y(4)
do j=2,n-1
write(12,'(1pe12.3e3,i3,1pe12.3e3)')tout,j,j*y(n+2+j)
end do
write(12,'(a20)')' '
write(12,'(a20)')' '
!Plotting the ratio of the C10 formation rate :
write(52,'(1pe12.3e3,1pe12.3e3)') tout, rate(n+13)/rate(m+9)
enddo
!=====================================================================
!ASF plot for paraffins
write(15,'(i3,1pe12.3e3)')1,zi1(1)
do j=2,n
write(15,'(i3,1pe12.3e3)')j,zi1(j)
end do
do j = 1,n-1
write(16,'(i3,1pe12.3e3)')j+1,zi2(j)
end do
!=====================================================================
write(31,'(a1,200(a12))')",(dash(i),i=1,neq+1)
write(35,'(a1,200(a12))')",(dash(i),i=1,m+1)
write(36,'(a1,200(a12))')",(dash(i),i=1,m+1)
write(37,'(a1,200(a12))')",(dash(i),i=1,2)
!=====================================================================
conversion = (500 - y(m+1)*y(neq))/500 !On the basis of vapour flow out of the reactor
```

```
write(*,*) 'CO Conversion=', conversion
hello = SYSTEMQQ('BandK.bat')
end subroutine


    subroutine withoutvle(t, y, yprime, cj, delta, ires, ipar) !, senpar)
implicit none
integer, parameter:: m =122, n=60, neq = 2*m+n+3
integer:: i
!=======================================================================
!Ddaspk variables
integer ires, ipar(20)
double precision:: senpar(20), rpar(20)
double precision:: cj, t, y(neq), delta(neq), yprime(neq)
!=======================================================================
!variables
double precision:: FV, FL, qi(m), yy(m), x(m), Ki(m), Fin(m), Fin0(m), zi(m), psi(m), Ni(m)
double precision:: Vgas, Vliq, kr(7), Ke(7), r5(n-1), r6(n-1), r7(n-1)
double precision:: FCOin, alpha, R, P, Zx, Zy
!=======================================================================
!catalyst properties
double precision:: mcat, ncat, catloading ,theta0, thetai(n+2)
!=======================================================================
!Common Variables
double precision:: ff(122), Temp, Tc(122), Pc(122), w(122), Z(122)
character*15:: name(122)
common ff, Temp, Tc, Pc, w, name, Z
!=======================================================================
!Thermodynamic variables
double precision:: fix(122), fiy(122), phix(122), phiy(122), theta, rhol, rhov, rho(122), rate(181), a(122)
common /fugacities/ fix, fiy, phix, phiy, theta,rhol, rhov, rho, rate, a

!=======================================================================
!Start-up common block
double precision:: ki0(m)
common /startup/ ki0
!=======================================================================
!Input variables
R = 8.314d0
P = 101325*20.d0
alpha = 2
ires = 0
```

```
Fin = 0
Fin0 = 0
!Inlet flows
Fin0(1) = 500.d0 !mol/s
Fin0(2) = 2*Fin0(1) !mol/s
Fin0(n+3) = Fin0(1) /10000
Fin = Fin0*(1-exp(-alpha*t))*(1+0.25*sin(0*t))
!Fixed liquid and vapour volumes
Vliq = 0.5 !m3
Vgas = 0.5 !m3
!Catalyst properties
catloading = 4.d5
mcat = catloading*(Vliq+Vgas)
Ncat = mcat/58.93
!Reaction rate constants
kr = 1
Ke = 0.8
!Defining the variables
Ni = y(1:m)
zi = y(m+1:2*m)
thetai = y(2*m+1:2*m+n+2)
Fv = y(2*m+n+3)
!Catalyst constraint
theta0 = 1
theta = 1 - sum(thetai)
call rxns(m,zi, qi, ff, fix, fiy, kr, Ke, thetai,theta, t, rate, a )
r5 = rate(5:n+3)
r6 = rate(n+4:m) !59 olefinic rates (C2= - C20=)
r7 = rate(m+1:3*n+1) !59 paraffic rates for C2 - c20
rhol = 500
!=========================================================================
!Transient reactor equations
!Total balances
delta(1) = yprime(1) - (Fin(1) - FV*zi(1) - rate(1)*mcat) !CO
delta(2) = yprime(2) - (Fin(2) - FV*zi(2) - rate(2)*mcat) !H2
delta(3) = yprime(3) - (Fin(3) - FV*zi(3) + rate(1)*mcat) !water
delta(4) = yprime(4) - (Fin(4) - FV*zi(4) + rate(4)*mcat) !methane
!Paraffins (C2 - Cn)
delta(5:n+3) = yprime(5:n+3) - (Fin(5:n+3) - FV*zi(5:n+3) + r7*mcat) !r7
!Olefins (C2= - Cn=)
```

```
delta(n+4:m) = yprime(n+4:m) - (Fin(n+4:m) - FV*zi(n+4:m) + r6*mcat) !r6
!=======================================================================
!Molar eqns equations
delta(m+1:2*m) = Ni - zi*(Vliq+Vgas)*rhol
!=======================================================================
!Adsorption reactions
delta(2*m+1) = (-4*rate(1)+2*rate(2)-rate(3)-rate(4)+sum(r6)-sum(r7)) *Mcat/Ncat - yprime(2*m+1) !HT
delta(2*m+2) = (rate(1)-rate(3)-sum(r5))*mcat/Ncat - yprime(2*m+2) !CH2T
delta(2*m+3) = (rate(3)-rate(4)-r5(1))*mcat/Ncat- yprime(2*m+3) !Ch3T
delta(2*m+4:2*m+n+1) = (r5(1:n-2) - r5(2:n-1)-r6(1:n-2)-r7(1:n-2))*mcat/Ncat - yprime(2*m+4:2*m+n+1)
!C2T - C59T*mcat
delta(2*m+n+2) = (r5(n-1) - r6(n-1) - r7(n-1))*mcat/Ncat - yprime(2*m+n+2)
!Summation equations
delta(2*m+n+3) = 1-sum(zi)
!write(*,*) y(2*m+1)*Ncat
end subroutine
```

The subroutine rxns is identical as that for the Transient model with VLE, with a slight modification to the activity, according to equation 3.21.

Appendix E

Isothermal Flash results

Table E.1: K_i, x_i and y_i values for the species in the FTS system after the isothermal flash calculation

Component	$\mathbf{K_i}$	$\mathbf{x_i}$	$\mathbf{y_i}$
CO	2.310E+01	4.331E-03	1.000E-01
H_2	3.466E+01	2.886E-03	1.000E-01
Water	2.871E+00	3.484E-02	1.000E-01
Paraffins			
C_1	1.514E+01	6.938E-03	1.050E-01
C_2	7.476E+00	9.834E-03	7.352E-02
C_3	4.684E+00	1.099E-02	5.146E-02
C_4	2.975E+00	1.211E-02	3.602E-02
C_5	1.949E+00	1.293E-02	2.521E-02
C_6	1.299E+00	1.359E-02	1.765E-02
C_7	8.776E-01	1.408E-02	1.235E-02
C_8	5.972E-01	1.448E-02	8.645E-03
C_9	4.088E-01	1.480E-02	6.050E-03
C_{10}	2.804E-01	1.510E-02	4.234E-03
C_{11}	1.938E-01	1.529E-02	2.962E-03
C_{12}	1.346E-01	1.539E-02	2.072E-03
C_{13}	9.424E-02	1.537E-02	1.449E-03
C_{14}	6.581E-02	1.539E-02	1.013E-03
C_{15}	4.624E-02	1.530E-02	7.074E-04
C_{16}	3.277E-02	1.507E-02	4.938E-04
C_{17}	2.275E-02	1.513E-02	3.442E-04
C_{18}	1.644E-02	1.458E-02	2.396E-04
C_{19}	1.178E-02	1.413E-02	1.665E-04
C_{20}	8.206E-03	1.404E-02	1.152E-04

continued on next pg

Table E.1: *continued*

Component	$\mathbf{K_i}$	$\mathbf{x_i}$	$\mathbf{y_i}$
C_{21}	5.452E-03	1.451E-02	7.912E-05
C_{22}	3.799E-03	1.423E-02	5.407E-05
C_{23}	2.633E-03	1.389E-02	3.658E-05
C_{24}	1.824E-03	1.339E-02	2.442E-05
C_{25}	1.262E-03	1.270E-02	1.602E-05
C_{26}	8.721E-04	1.179E-02	1.028E-05
C_{27}	6.011E-04	1.067E-02	6.415E-06
C_{28}	4.125E-04	9.387E-03	3.872E-06
C_{29}	2.835E-04	7.969E-03	2.259E-06
C_{30}	1.942E-04	6.542E-03	1.270E-06
C_{31}	1.331E-04	5.194E-03	6.911E-07
C_{32}	9.101E-05	4.005E-03	3.645E-07
C_{33}	6.234E-05	3.012E-03	1.878E-07
C_{34}	4.255E-05	2.223E-03	9.457E-08
C_{35}	2.903E-05	1.616E-03	4.690E-08
C_{36}	1.981E-05	1.161E-03	2.301E-08
C_{37}	1.353E-05	8.282E-04	1.121E-08
C_{38}	9.251E-06	5.872E-04	5.432E-09
C_{39}	6.315E-06	4.147E-04	2.619E-09
C_{40}	4.320E-06	2.921E-04	1.262E-09
C_{41}	2.952E-06	2.053E-04	6.060E-10
C_{42}	2.015E-06	1.441E-04	2.905E-10
C_{43}	1.380E-06	1.011E-04	1.395E-10
C_{44}	9.451E-07	7.086E-05	6.696E-11
C_{45}	6.471E-07	4.965E-05	3.213E-11
C_{46}	4.432E-07	3.477E-05	1.541E-11
C_{47}	3.036E-07	2.435E-05	7.394E-12
C_{48}	2.089E-07	1.705E-05	3.563E-12
C_{49}	1.434E-07	1.194E-05	1.711E-12
C_{50}	9.845E-08	8.358E-06	8.229E-13
C_{51}	6.768E-08	5.851E-06	3.960E-13
C_{52}	4.659E-08	4.096E-06	1.909E-13
C_{53}	3.212E-08	2.867E-06	9.210E-14
C_{54}	2.218E-08	2.007E-06	4.452E-14
C_{55}	1.528E-08	1.405E-06	2.147E-14
C_{56}	1.059E-08	9.836E-07	1.041E-14
C_{57}	7.320E-09	6.885E-07	5.040E-15

continued on next pg

Table E.1: *continued*

Component	$\mathbf{K_i}$	$\mathbf{x_i}$	$\mathbf{y_i}$
C_{58}	5.050E-09	4.820E-07	2.434E-15
C_{59}	3.507E-09	3.374E-07	1.183E-15
C_{60}	2.431E-09	2.362E-07	5.740E-16
Olefins			
$C_{2=}$	8.725E+00	1.204E-02	1.050E-01
$C_{3=}$	4.968E+00	1.480E-02	7.352E-02
$C_{4=}$	3.174E+00	1.622E-02	5.146E-02
$C_{5=}$	2.086E+00	1.726E-02	3.602E-02
$C_{6=}$	1.390E+00	1.814E-02	2.521E-02
$C_{7=}$	9.411E-01	1.875E-02	1.765E-02
$C_{8=}$	7.129E-01	1.733E-02	1.235E-02
$C_{9=}$	4.251E-01	2.033E-02	8.643E-03
$C_{10=}$	2.966E-01	2.039E-02	6.048E-03
$C_{11=}$	2.042E-01	2.072E-02	4.232E-03
$C_{12=}$	1.417E-01	2.089E-02	2.960E-03
$C_{13=}$	9.882E-02	2.095E-02	2.070E-03
$C_{14=}$	6.880E-02	2.103E-02	1.447E-03
$C_{15=}$	4.799E-02	2.106E-02	1.011E-03
$C_{16=}$	3.383E-02	2.086E-02	7.056E-04
$C_{17=}$	2.423E-02	2.031E-02	4.921E-04
$C_{18=}$	1.721E-02	1.991E-02	3.426E-04
$C_{19=}$	1.193E-02	1.994E-02	2.379E-04
$C_{20=}$	8.451E-03	1.949E-02	1.647E-04
$C_{21=}$	5.671E-03	1.998E-02	1.133E-04
$C_{22=}$	3.940E-03	1.966E-02	7.746E-05
$C_{23=}$	2.735E-03	1.919E-02	5.247E-05
$C_{24=}$	1.895E-03	1.852E-02	3.509E-05
$C_{25=}$	1.312E-03	1.759E-02	2.307E-05
$C_{26=}$	9.055E-04	1.638E-02	1.483E-05
$C_{27=}$	6.255E-04	1.485E-02	9.291E-06
$C_{28=}$	4.316E-04	1.307E-02	5.642E-06
$C_{29=}$	2.970E-04	1.114E-02	3.308E-06
$C_{30=}$	2.050E-04	9.155E-03	1.877E-06
$C_{31=}$	1.412E-04	7.289E-03	1.029E-06
$C_{32=}$	9.722E-05	5.637E-03	5.480E-07
$C_{33=}$	6.688E-05	4.253E-03	2.845E-07
$C_{34=}$	4.614E-05	3.144E-03	1.451E-07

continued on next pg

Table E.1: *continued*

Component	$\mathbf{K_i}$	$\mathbf{x_i}$	$\mathbf{y_i}$
$C_{35=}$	3.176E-05	2.290E-03	7.274E-08
$C_{36=}$	2.194E-05	1.649E-03	3.618E-08
$C_{37=}$	1.513E-05	1.178E-03	1.782E-08
$C_{38=}$	1.042E-05	8.359E-04	8.710E-09
$C_{39=}$	7.212E-06	5.908E-04	4.261E-09
$C_{40=}$	4.987E-06	4.164E-04	2.077E-09
$C_{41=}$	3.447E-06	2.929E-04	1.009E-09
$C_{42=}$	2.381E-06	2.057E-04	4.897E-10
$C_{43=}$	1.650E-06	1.443E-04	2.380E-10
$C_{44=}$	1.143E-06	1.012E-04	1.156E-10
$C_{45=}$	7.947E-07	7.089E-05	5.634E-11
$C_{46=}$	5.509E-07	4.966E-05	2.736E-11
$C_{47=}$	3.820E-07	3.478E-05	1.329E-11
$C_{48=}$	2.660E-07	2.436E-05	6.479E-12
$C_{49=}$	1.847E-07	1.705E-05	3.150E-12
$C_{50=}$	1.289E-07	1.194E-05	1.539E-12
$C_{51=}$	8.968E-08	8.359E-06	7.496E-13
$C_{52=}$	6.247E-08	5.851E-06	3.655E-13
$C_{53=}$	4.374E-08	4.096E-06	1.792E-13
$C_{54=}$	3.044E-08	2.867E-06	8.729E-14
$C_{55=}$	2.130E-08	2.007E-06	4.275E-14
$C_{56=}$	1.493E-08	1.405E-06	2.097E-14
$C_{57=}$	1.044E-08	9.836E-07	1.027E-14
$C_{58=}$	7.314E-09	6.885E-07	5.036E-15
$C_{59=}$	5.114E-09	4.820E-07	2.465E-15
$C_{60=}$	3.583E-09	3.374E-07	1.209E-15

Appendix F

Equilibrium *K-value* as a function of carbon number

The equilibrium constant, *K-value* plays a big part in causing the deviations from classical ASF distribution. Figure F.1 exhibits the *K-value* as a function of carbon number for paraffins and olefins. The *K-values* for the olefins and paraffins are identical, as K-value is a function

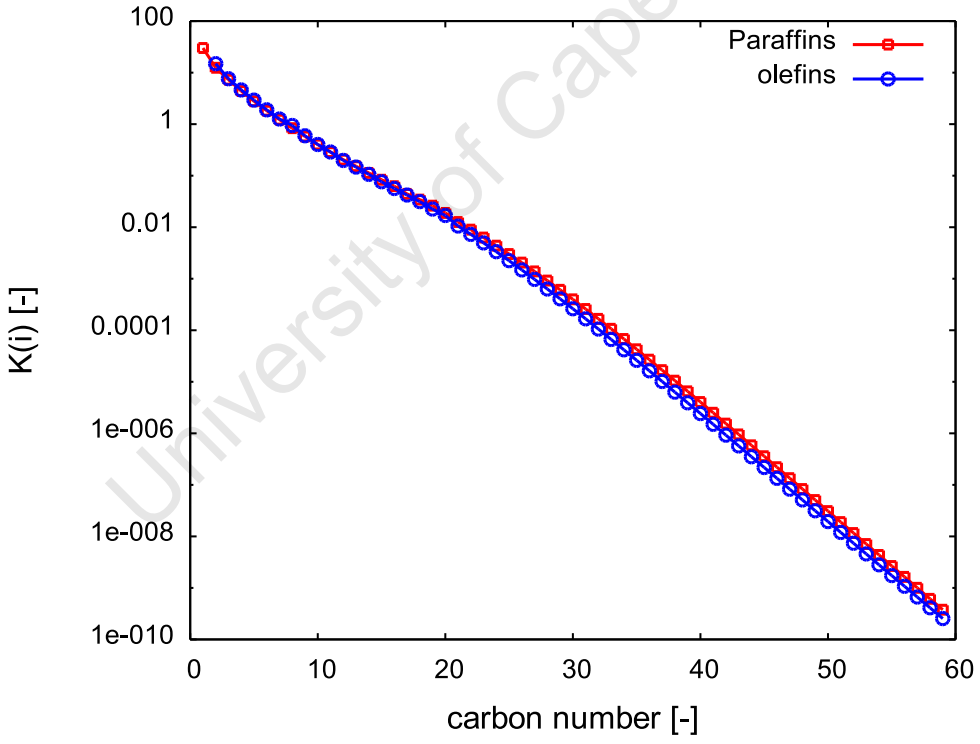

Figure F.1: *K-value* as a function of carbon number for the 2-phase model

of the carbon number, and not the molecular structure. It can therefore be concluded that even though the kinetics are similar in both models, VLE causes a significant distribution that differs from the two-phase model.

Appendix G

Hydrocarbon liquid fraction at steady state

Table G.1 gives the liquid fraction data as a function of carbon number.

Table G.1: Hydrocarbon liquid fraction (ψ) vs. of Carbon number C_N

C_N	**Paraffins**	**Olefins**
1	9.491E-002	-
2	2.024E-001	1.744E-001
3	3.015E-001	2.925E-001
4	4.182E-001	4.057E-001
5	5.306E-001	5.182E-001
6	6.335E-001	6.243E-001
7	7.205E-001	7.144E-001
8	7.903E-001	7.699E-001
9	8.453E-001	8.413E-001
10	8.867E-001	8.865E-001
11	9.165E-001	9.162E-001
12	9.390E-001	9.410E-001
13	9.538E-001	9.555E-001
14	9.653E-001	9.674E-001
15	9.742E-001	9.764E-001
16	9.805E-001	9.824E-001
17	9.861E-001	9.868E-001
18	9.892E-001	9.901E-001
19	9.917E-001	9.929E-001
20	9.940E-001	9.947E-001
21	9.960E-001	9.967E-001

continued on next pg

Table G.1: *continued*

C_N	**Paraffins**	**Olefins**
22	9.972E-001	9.977E-001
23	9.980E-001	9.984E-001
24	9.986E-001	9.989E-001
25	9.990E-001	9.993E-001
26	9.993E-001	9.995E-001
27	9.996E-001	9.997E-001
28	9.997E-001	9.998E-001
29	9.998E-001	9.999E-001
30	9.999E-001	9.999E-001
31	9.999E-001	9.999E-001
32	9.999E-001	1.000E+000
33	1.000E+000	1.000E+000
34	1.000E+000	1.000E+000
35	1.000E+000	1.000E+000
36	1.000E+000	1.000E+000
37	1.000E+000	1.000E+000
38	1.000E+000	1.000E+000
39	1.000E+000	1.000E+000
40	1.000E+000	1.000E+000
41	1.000E+000	1.000E+000
42	1.000E+000	1.000E+000
43	1.000E+000	1.000E+000
44	1.000E+000	1.000E+000
45	1.000E+000	1.000E+000
46	1.000E+000	1.000E+000
47	1.000E+000	1.000E+000
48	1.000E+000	1.000E+000
49	1.000E+000	1.000E+000
50	1.000E+000	1.000E+000
51	1.000E+000	1.000E+000
52	1.000E+000	1.000E+000
53	1.000E+000	1.000E+000
54	1.000E+000	1.000E+000
55	1.000E+000	1.000E+000
56	1.000E+000	1.000E+000
57	1.000E+000	1.000E+000
58	1.000E+000	1.000E+000

continued on next pg

Table G.1: *continued*

$\mathbf{C}_N$	**Paraffins**	**Olefins**
59	1.000E+000	1.000E+000
60	1.000E+000	1.000E+000